


**The formation of Earth's early felsic continental crust  
by water-present eclogite melting**

by

Angelique Laurie

*Dissertation presented for the degree of Doctor of  
Earth Sciences at  
Stellenbosch University*

The image shows the official crest of Stellenbosch University, which is a shield-shaped emblem with various heraldic symbols, including a crown on top and a banner at the bottom. The crest is rendered in a semi-transparent, light-colored style, positioned behind the text of the dissertation title.

Supervisor: Prof. Gary Stevens

Faculty of Science

March 2013

## **DECLARATION**

By submitting this dissertation electronically, I declare that the entirety of the work contained therein is my own, original work, that I am the sole author thereof (save to the extent explicitly otherwise stated), that reproduction and publication thereof by Stellenbosch University will not infringe any third party rights and that I have not previously in its entirety or in part submitted it for obtaining any qualification.

(Angelique Laurie)

March 2013

Copyright © 2015 University of Stellenbosch

All rights reserved

## ABSTRACT

The sodic and leucocratic Tonalite, Trondhjemite and Granodiorite (TTG) granitoid series of rocks characterise Paleo- to Meso- Archaean felsic continental crust, yet are uncommon in the post-Archaean rock record. Consequently, petrogenetic studies on these rocks provide valuable insight into the creation and evolution of Earth's early continental crust. The high-pressure (HP)-type of Archaean TTG magmas are particularly important in this regard as their geochemistry requires that they are formed by high-pressure melting of a garnet-rich eclogitic source. This has been interpreted as evidence for the formation of these magmas by anatexis of the upper portions of slabs within Archaean subduction zones. In general, TTG magmas have been assumed to arise through fluid-absent partial melting of metamafic source rocks. Therefore, very little experimental data on fluid-present eclogite melting to produce Archaean TTG exist, despite the fact that water drives magmatism in modern arcs. Consequently, this study experimentally investigates the role of fluid-present partial melting of eclogite-facies metabasaltic rock in the production of Paleo- to Meso-Archaean HP-type TTG melts. Experiments are conducted between 1.6 GPa and 3.0 GPa and 700 °C and 900 °C using natural and synthetic eclogite, and gel starting materials of low-K<sub>2</sub>O basaltic composition. Partial melting of the natural and synthetic eclogite occurred between 850 °C and 870 °C at pressures above 1.8 GPa, and the melting reaction is characterised by the breakdown of sodic clinopyroxene, quartz and water:  $Qtz + Cpx_1 + H_2O \pm Grt_1 = Melt + Cpx_2 \pm Grt_2$ . The experimental melts have the compositions of sodic peraluminous trondhjemites and have compositions that are similar to the major, trace and rare earth element composition of HP-type Archaean TTG. This study suggests that fluid-present eclogite melting is a viable

petrogenetic model for this component of Paleo- to Meso-Archaean TTG crust. The nature of the wet low-K<sub>2</sub>O eclogite-facies metamafic rock solidus has been experimentally defined and inflects towards higher temperatures at the position of the plagioclase-out reaction. Therefore, the results indicate that a crystalline starting material is necessary to define this solidus to avoid metastable melting beyond temperatures of the Pl + H<sub>2</sub>O + Qtz solidus at pressures above plagioclase stability. Furthermore, this study uses numerical and metamorphic models to demonstrate that for reasonable Archaean mantle wedge temperatures within a potential Archaean subduction zone, the bulk of the water produced by metamorphic reactions within the slabs is captured by an anatectic zone near the slab surface. Therefore, this geodynamic model may account for HP-type Archaean TTG production and additionally provides constraints for likely Archaean subduction. The shape of the relevant fluid-present solidus is similar to the shape of the pressure-temperature paths followed by upper levels of the proposed Archaean subducting slab, which makes water-fluxed slab anatexis is very dependant on the temperature in the mantle wedge. I propose that cooling of the upper mantle by only a small amount during the late Archaean ended fluid-present melting of the slab. This allowed slab water to migrate into the wedge and produce intermediate composition magmatism which has since been associated with subduction zones.

**Keywords:** *Archaean, continental crust, trondhjemite, fluid-present eclogite melting.*

## OPSOMMING

Die reeks natruimhoudende en leukokraties Tonaliet, Trondhjemit en Granodioriet (TTG) felsiese stollingsgesteentes is kenmerkend in die Paleo- tot Meso-Argeïkum felsiese kontinentale kors, maar is ongewoon in die post-Argeïese rots rekord. Gevolglik, petrogenetiese studies op hierdie rotse verskaf waardevolle insig in die skepping en evolusie van die aarde se vroeë kontinentale kors. Die hoë-druk (HD)-tipe van die Argeïkum TTG magmas is veral belangrik in hierdie verband as hulle geochemie vereis dat hulle gevorm word deur hoë druk smelting van 'n granaat-ryk eklogitiese bron. Dit word interpreteer as bewys vir die vorming van hierdie magmas deur smelting van die boonste gedeeltes van die blaaië in Argeïese subduksie sones. TTG magmas in die algemeen, is veronderstel om op te staan deur middel van water-afwesig gedeeltelike smelting van metamafiese bron rotse. Daarom bestaan baie min eksperimentele data op water-teenwoordig eklogiet smelting om Argeïkum TTG te produseer, ten spyte van die feit dat water magmatisme dryf in moderne boë. Gevolglik is hierdie studie 'n eksperimentele ondersoek in die rol van water-teenwoordig gedeeltelike smelting van eklogiet-fasies metamafiese rots in die produksie van Paleo- tot Meso-Argeïkum HD-tipe TTG smelte. Eksperimente word uitgevoer tussen 1.6 GPa en 3.0 GPa en 700 °C en 900 °C met behulp van natuurlike en sintetiese eklogiet, en gel begin materiaal van lae-K<sub>2</sub>O basaltiese samestelling. Gedeeltelike smelting van die natuurlike en sintetiese eklogiet het plaasgevind tussen 850 °C en 870 °C te druk bo 1.8 GPa, en die smeltings reaksie is gekenmerk deur die afbreek van natruimhoudende klinopirokseen, kwarts en water:  $Qtz + Cpx_1 + H_2O \pm Grt_1 = Smelt + Cpx_2 \pm Grt_2$ . Die eksperimentele smelte het die komposisies van natruimhoudende trondhjemites en is soortgelyk aan die hoof-, spoor- en

seldsame aard element samestelling van HD-tipe Argeïkum TTG. Hierdie studie dui daarop dat water-teenwoordig eklogiet smelting 'n lewensvatbare petrogenetiese model is vir hierdie komponent van Paleo- tot Meso-Argeïkum TTG kors. Die aard van die nat lae-K<sub>2</sub>O eklogiet-fasies metamafiese rock solidus is eksperimenteel gedefinieër en beweeg na hoër temperature by die posisie van die plagioklaas-out reaksie. Daarom dui die resultate daarop dat 'n kristallyne materiaal nodig is om hierdie solidus te definieër en metastabiele smelting buite temperature van die Pl + H<sub>2</sub>O + Qtz solidus druk bo plagioklaas stabiliteit te vermy. Verder maak hierdie studie gebruik van numeriese en metamorfiese modelle om aan te dui dat die grootste deel van die water geproduseer deur metamorfiese reaksies binne die blaaie bestaan vir redelike Argeïkum mantel wig temperature binne 'n potensiële Argeïkum subduksie sone, en word opgevang deur 'n smelting sone naby die blad oppervlak. Daarom kan hierdie geodinamies model rekenskap gee vir HD-tipe Argeïkum TTG produksie en dit bied ook die beperkinge vir waarskynlik Argeïese subduksie. Die vorm van die betrokke water-teenwoordig solidus is soortgelyk aan die vorm van die druk-temperatuur paaie gevolg deur die boonste vlakke van die voorgestelde Argeïkum subderende blad, wat water-vloeiing blad smeltingbaie afhanklik maak van die temperatuur in die mantel wig. Ons stel voor dat afkoeling van die boonste mantel met slegs 'n klein hoeveelheid gedurende die laat Argeïese, die water-vloeiing smelting van die blad beëindig. Dit het toegelaat dat die blad water in die wig migreer en intermediêre samestelling magmatisme produseer wat sedert geassosieer word met subduksie sones.

***Sleutelwoorde:***  *Argeïkum, kontinentale kors, trondhjemet, water-teenwoordig eklogiet smelting.*

## ACKNOWLEDGEMENTS

The last eight years at Stellenbosch University, within the Department of Earth Sciences, have been life altering. Although Stellenbosch University is an academic institution, and I have been here to study, my time here has meant so much more to me. It has enriched my life with friendships, opportunity, adventure and passion. I have every person in this department to acknowledge and thank for their contributions, whether small or big, to my amazing experience here at Stellenbosch. Thank you.

I would like to give special mention to the following people: My fellow classmates (honours class of 2008) who know me as Timba or Zebra - Thanks for all the great laughs, adventures and memories. All of my undergraduate and honours lecturers - I have so much respect and admiration for each of you. Thank you for your enthusiasm and thank you for inspiring me. Tannie Loxie, my Geology mom - Thank you for your smiles and all the effort that you always put into making sure things run smoothly. George - Thank you for always being so helpful! Madelaine, Riana and Esme - Thank you for your time assisting me during my analytical acquisitions. Jeanne and Cynthia, my student mentors - Thank you for your wonderful friendships, for all the wonderful memories spent together and thank you for being there to support me through every up and down. Gary - I am indebted to you for providing me with this opportunity to do research and for all that you have done for me over the years. Thank you for all the time and effort that you spent with me, teaching me an array of new skills and sharing your knowledge on experimental petrology and geology as a whole. Thank you for guiding my written work, helping me to improve my public speaking skills and speak

slower during presentations (Tee Tee Gee). Thank you for the opportunity to be involved in scientific thinking and discussion and for providing me with the opportunity to accompany you and the rest of the research group on field trips and to conferences. I have cherished every experience. I am truly grateful for all that you have done for me and I feel very privileged to have had you as a supervisor and mentor.

I want to thank all of my best mates for all the good times and encouragement throughout the years, as well as my family (Tash, Charles, Berdine, Berns, Mom and Dad) for their support and love and for always believing in me. I love you all very much. Thank you Bernard for just being you. You have been through everything with me. I am so lucky to have you in my life. Lastly, I would like to thank my Mom and Dad so much for providing me with the opportunity to go to university and the privilege to choose to pursue what I am passionate about.



---

**TABLE OF CONTENTS**

	<i>Page</i>
<b>Declaration</b>	<b>i</b>
<b>Abstract</b>	<b>ii</b>
<b>Opsomming</b>	<b>iv</b>
<b>Acknowledgements</b>	<b>vi</b>
<b>Table of Contents</b>	<b>viii</b>
<b>List of Figures</b>	<b>xi</b>
<b>List of Tables</b>	<b>xiv</b>
<b>Chapter 1: Introduction</b>	<b>1</b>
<b>Chapter 2: Water-present eclogite melting to produce Earth's early felsic crust</b>	<b>16</b>
Abstract	17
1. Introduction	17
2. Experimental procedure and analytical techniques	18
2.1. <i>Experimental starting material</i>	18
2.2. <i>Experimental set-up and procedure</i>	19
2.3. <i>Analytical techniques</i>	22
3. Experimental results and interpretation	23
3.1. <i>Mineral compositions and phase relations</i>	23
3.1.1. <i>Approach to equilibrium</i>	24
3.1.2. <i>Oxygen fugacity</i>	24
3.2. <i>Experimental glass compositions and melting reactions</i>	24

---

3.2.1. Major element composition of the glasses	24
3.2.2. Melting reaction	24
3.2.3. Systematic variation in experimental glass composition with pressure	26
3.2.4. Trace element composition of the glasses	26
3.2.5. Trace element modelling	27
4. Comparison of experimental glasses with HP-type Archaean TTG	27
5. Conclusion	27
Acknowledgements	27
Appendix A	28
References	28
<b>Chapter 3: The end of continental growth by TTG magmatism</b>	<b>30</b>
Abstract	31
Introduction	31
Modelling	32
<i>Modelling set-up</i>	32
<i>Results</i>	32
Slab dehydration	33
Discussion	35
Implications	35
Acknowledgements	35
References	36
<b>Chapter 4: The water-saturated low-K<sub>2</sub>O eclogite solidus: Implications for the generation of Earth's early felsic continental crust</b>	<b>38</b>
Abstract	39

---

---

Introduction	39
Experimental and analytical techniques	41
<i>The starting materials</i>	42
<i>The natural eclogite starting material</i>	43
<i>The basaltic composition gel starting material</i>	43
<i>The synthetic eclogite starting material</i>	48
<i>Experimental set-up and procedure</i>	48
<i>Analytical techniques</i>	48
Experimental results	49
<i>Detection of melt</i>	49
<i>Results of experiments using a natural eclogite starting material</i>	49
<i>Results of experiments using a gel starting material</i>	53
<i>Results of experiments using a synthetic eclogite starting material</i>	54
Discussion	54
<i>Comparison of experimental results produced using gel and     crystalline starting materials at <math>\pm 2.1</math> GPa</i>	54
<i>Comparison of experimental results produced using crystalline     starting materials at <math>\pm 2.1</math> GPa</i>	55
Interpretation	55
Implications	56
Acknowledgements	58
References	58
<b>Chapter 5: Conclusion</b>	<b>60</b>

---

---

## LIST OF FIGURES

	<i>page</i>
<b>Chapter 1: Introduction</b>	
<b>Fig. 1.</b> Photographs illustrating an Archaean grey gneiss complex and an Archaean tonalite-trondhjemite-granodiorite (TTG) granitoid.	2
<b>Fig. 2.</b> A global map indicating the distribution of Archaean provinces.	3
<b>Fig. 3</b> Binary and ternary diagrams indicating the characteristic major-, trace- and rare-earth-element composition of high- $\text{Al}_2\text{O}_3$ (high and medium pressure) type Archaean TTG granitoids; low- $\text{Al}_2\text{O}_3$ (low-pressure) type (LP) TTG Archaean TTG granitoids; post-Archaean and calc-alkaline I-type granitoids.	6
<b>Fig. 4:</b> A diagram illustrating the effects that the source composition, the depth at which partial melting occurs, and the resultant residual mineralogy's have on melt geochemistry, which produce the various TTG types.	7
<b>Fig. 5:</b> Schematic diagram comparing a typical post-Archaean arc and a hypothetical Archaean arc.	10
<b>Chapter 2:</b>	
<b>Fig. 1.</b> Starting material bulk rock composition.	21
<b>Fig. 2.</b> Backscatter electron (BSE) images of partially melted experimental run products.	23
<b>Fig. 3.</b> The major and trace element chemistry of the experimental glasses.	25

---

**Chapter 3:**

- Fig. 1.** The major and trace element chemistry of experimental glasses compared with the compositions of high-pressure (HP)-type Archaean TTG. 32
- Fig. 2.** Modelled pressure-temperature ( $P$ - $T$ ) paths followed by the upper portion of subducting slabs. 33
- Fig. 3.** A comparison between Archaean and present-day fast subduction of young slabs. 34

**Chapter 4**

- Fig. 1.** Na<sub>2</sub>O-K<sub>2</sub>O-CaO ternary diagram. 40
- Fig. 2.**  $P$ - $T$  diagram illustrating previously defined solidi. 41
- Fig. 3.** Backscatter electron (BSE) images of experimental run products. 51
- Fig. 4.** A  $P$ - $T$  diagram which illustrates the experimental results and conditions of this study. 52
- Fig. 5.** Na<sub>2</sub>O-K<sub>2</sub>O-CaO ternary geochemical diagram representing the experimental melt. 53
- Fig. 6.** Na-Ca-Mg-Fe tetrahedron geochemical diagram comparing experimental run products. 55
- Fig. 7.** Comparison of Archaean and present-day subduction scenarios. 57

**Chapter 5:**

- Fig. 1.** Schematic diagrams depicting proposed geodynamic scenarios for the formation of high, medium and low-pressure TTG granitoids during the Archaean and  $P$ - $T$  diagrams indicating the  $P$ - $T$

evolution of the metamafic source rock during the corresponding  
geodynamic scenario. 61

**Fig. 2.** A schematic diagram illustrating the tectonic model proposed by  
this study. 64

---

## LIST OF TABLES

	<i>Page</i>
<b>Chapter 1:</b>	
<b>Table 1.</b> Distribution of the geochemical rock types identified within the globally preserved Archaean grey gneiss complexes.	5
<b>Chapter 2:</b>	
<b>Table 1.</b> Experimental run conditions and experimental products.	18
<b>Table 2.</b> Major element geochemistry of the starting material and averaged normalised anhydrous experimental glass major element compositions.	19
<b>Table 3.</b> Trace element geochemistry DSE4 starting material and averaged experimental glass compositions.	20
<b>Table 4.</b> Garnet compositions from DSE4 starting material and experimental run products.	21
<b>Table 5.</b> Clinopyroxene compositions from DSE4 starting material and experimental run products.	22
<b>Table 6.</b> Calculated phase proportions by major element least squared mass balance for the 2.2 GPa – 880 °C and the 2.9 GPa – 870 °C experimental run products.	24
<b>Table 7.</b> Trace element modelling results and comparison of calculated melt compositions with measured experimental glass compositions.	26
<b>Appendix A.</b> Accuracy and precision of EDS and WDS analyses from the University of Stellenbosch SEM configuration.	28

**Chapter 4:**

<b>Table 1.</b> Experimental run conditions and experimental products.	40
<b>Table 2.</b> Major element bulk rock geochemistry of the starting materials.	41
<b>Table 3.</b> Garnet compositions from DSE4 starting materials and experimental run products.	42
<b>Table 4.</b> Clinopyroxene compositions from DSE4 starting materials and experimental run products.	44
<b>Table 5.</b> Averaged normalised anhydrous experimental glass and precipitate major element compositions.	48



## CHAPTER 1

### Introduction

The nature of the geological processes that controlled the growth and evolution of Earth's early continental crust remains the subject of intense on-going scientific debate (e.g. De Wit, 1998; Hamilton, 1998; Collins *et al.*, 1998; Collins and Van Kranendonk, 1999; Kisters *et al.*, 2003; Moyen *et al.*, 2006; Condie and Pease, 2008). The Paleo- to Meso-Archaean continental crust is dominated by grey gneiss complexes that are made up of several components of which granitoids form the majority (Fig. 1, Table 1). Archaean granitoids are characterised by a group of sodic granitoids collectively called the Tonalite–Trondhjemite–Granodiorite (TTG) suite (Jahn *et al.*, 1981; Drummond and Defant, 1990; Martin, 1994; Condie, 1981; Martin, 1994; Windley, 1995). These granitoids constitute approximately 75% of Archaean granitoids within grey gneiss complexes (Moyen, 2011). Although sodic granitoids, similar to Archaean TTG granitoids, occur within the post-Archaean rock record, they are very uncommon and volumetrically insignificant. This indicates a dramatic change towards the end of the Archaean Eon that caused a transition in the composition of felsic continental growth products from sodic TTG to more Ca- and K-rich calc-alkaline I-type granitoids (e.g. Shirey and Hanson, 1984). This represents a first order secular change in felsic magmatism on Earth (Moyen, 2011).

Geochemical studies indicate that Archaean TTG granitoids reflect the composition of melt that was extracted from the source, and that they do not represent a significantly evolved magma (e.g. Clemens *et al.*, 2006). Thus, the geochemical signature of these granitoids reflects the composition and metamorphic mineral assemblage of the source rock from

---

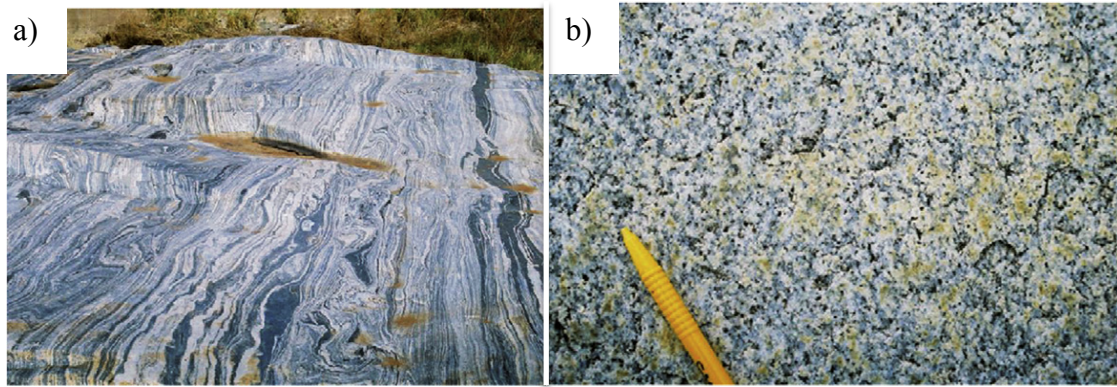


**Fig. 1:** Photographs illustrating a) an Archaean grey gneiss complex and b) an Archaean tonalite-trondhjemite-granodiorite (TTG) granitoid. Archaean granitoids, which are characterised by the sodic TTG granitoid suite, constitute the largest proportion of Archaean grey gneiss complexes.

which the TTG melt was extracted. The mineral assemblage of the source in turn implicates the pressure at which the TTG melt was generated. Consequently, genetic models for Archaean TTG are based upon the geochemical signatures of the ancient preserved TTG crust (Fig. 2). Due to the fragmented and limited rock record of this ancient crust worldwide, experimental petrology is an invaluable tool to investigate and evaluate TTG petrogenetic models. Furthermore petrogenetic models set constraints which enable deductions to be made about possible geodynamic scenarios for TTG genesis. Therefore, it is the interpretation of TTG geochemistry that shapes our understanding of Archaean crust generation. Consequently, the geochemistry of Archaean TTG underpins what is known about the origin of Earth's early felsic continental crust.

The mineralogy of Archaean TTG granitoids is dominated by plagioclase (typically oligoclase) with quartz typically being the second most abundant mineral and occasionally small amounts of K-feldspar may exist. The ferro-magnesian phases include biotite (nearly always) and hornblende (commonly). Accessory minerals are typically epidote, allanite, sphene, zircon, magnetite, and ilmenite (Moyen and Stevens, 2006). Most Archaean felsic granitoids plot in the tonalite and trondhjemite fields, with a smaller number falling in the

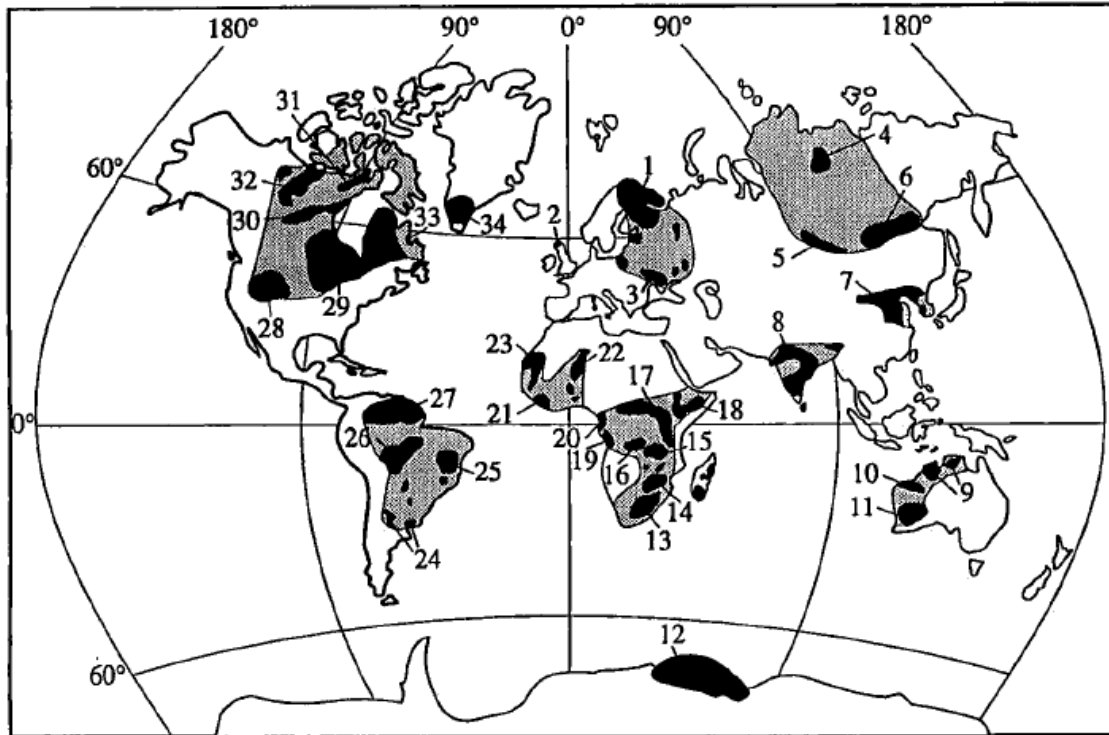


**Fig. 2:** Global distribution of Archaean provinces (after Condie, 1981). The exposed Archaean terranes are in black, and the areas underlain by Archaean rocks are in grey. (1) Baltic Shield; (2) Scottish Shield; (3) Ukrainian Shield; (4) Anabar Shield; (5) Baikal, Sayan and Yenisei fold belts; (6) Aldan Shield; (7) Sino-Korean, Tarim and Yangtze cratons; (8) Indian Shield; (9) Litchfield, Rul Jungle and Nanambu Complexes; (10) Pilbara block; (11) Yilgarn block; (12) Napier Complex; (13) Kaapvaal Craton; (14) Zimbabwe Craton; (15) Zambian Block; (16) Kasai' Craton; (17) Central Africa Craton; (18) Ethiopian Block; (19) Chaillu Craton; (20) Cameroon N'tem Complex; (21) Man Shield; (22) Tuareg Shield; (23) Reguibat Shield; (24) Rio de la Plata and Luis Alves Massifs; (25) SBo Francisco Craton; (26) Guapore Craton; (27) Guiana Shield; (28) Wyoming Province; (29) Superior Province; (30) Kaminak Group; (31) Committe Bay Block; (32) Slave Province; (33) Labrador Shield; (34) Greenland Shield.

granodiorite field of the O'Connor (1965) normative An-Ab-Or triangular classification for quartz-bearing plutonic rocks (Fig. 3). The clustering of points around the triple junction of the three compositional fields is typical of juvenile Archaean continental crust irrespective of geographic location and age (Barker and Arth, 1976; Condie, 1981). This leads to the commonly given name of TTG (Tonalite, Trondhjemite, Granodiorite) association (Jahn *et al.*, 1981; Martin *et al.*, 1983).

Barker and Arth (1976) characterised Archaean granitoids with trondhjemitic affinities to be either high-aluminum (i.e.,  $Al_2O_3 > 15\%$  at  $SiO_2 = 70\%$ ) or low-aluminum (i.e.,  $Al_2O_3 <$

15 % at  $\text{SiO}_2 = 70$  wt.%) and subdivided Archaean granitoids into high- and low- $\text{Al}_2\text{O}_3$  groups. Most Archaean felsic granitoids belong to the high- $\text{Al}_2\text{O}_3$  group (Table 1). Consequently in the early work on these rocks (e.g. Arth and Hanson, 1972; Barker and Arth, 1976), the TTG suite was also defined as being high in  $\text{Al}_2\text{O}_3$ . Although no formal definition for TTG exists, the generally accepted definition for high- $\text{Al}_2\text{O}_3$  TTG granitoids (e.g. Drummond and Defant, 1990) is that TTG granitoids are silica-rich ( $\text{SiO}_2 \approx 64$  wt.% average) and sodic ( $3.0 \text{ wt.}\% < \text{Na}_2\text{O} < 7.0 \text{ wt.}\%$  (Drummond and Defant, 1990). These rocks are characterised by high Na: Ca and Na: K ratios ( $\text{Na}_2\text{O}/\text{CaO} > 1.0$  and  $\text{Na}_2\text{O}/\text{K}_2\text{O} > 2.0$ ) and consequently they plot near the Na corner of Or-Ab-An feldspar ternary plots, well off the calc-alkaline trend (Martin, 1994) (mineral abbreviations throughout the thesis are as recommended by Kretz (1983)) (Fig. 3). TTG granitoids are relatively leucocratic ( $\text{FeO} + \text{MgO} + \text{MnO} + \text{TiO}_2 < 5 \text{ wt.}\%$ ), with an average Mg# (molecular  $100 \times (\text{Mg}/\text{Mg} + \text{Fe})$ ) of 43 (Moyen, 2011). Their trace element patterns are similar to typical “arc” rocks (i.e., calc-alkaline series, with a primitive mantle normalised trace element pattern showing distinct negative HFSE anomalies including Nb–Ta and Ti and commonly a positive Pb anomaly), except for elevated Sr and Eu and low Yb and Y contents, which results in strongly fractionated REE (La/Yb up to 150) patterns, no pronounced Eu anomaly, and high Sr/Y ratios (Moyen, 2011).

The low- $\text{Al}_2\text{O}_3$  group of Barker and Arth (1976) has elevated HREE and low Sr, Sr/Y and La/Yb, and therefore does not match all the requirements of the original TTG definition; however, whether or not low- $\text{Al}_2\text{O}_3$  Archaean granitoids should be included in the TTG suite is a matter of debate (Moyen, 2011; Willbold *et al.*, 2010; Feng and Kerrich, 1992; Whalen *et al.*, 2002) and is outside the scope of this study.

**Table 1:** Distribution of the geochemical rock types identified within preserved global Archaean grey gneiss complexes compiled from the database of Moyen (2011).

Archaean Grey Gneiss					%			
Non granitoids ( <i>leucosomes/restites, metasediments, amphibolites..</i> )					30			
Granitoids	70 %	Potassic	10 %		10			
		Misc.	15 %		10			
		Sodic TTG	75 %	High Al <sub>2</sub> O <sub>3</sub>	80 %	High pressure	20 %	10
						Medium Pressure	60 %	30
		Low Al <sub>2</sub> O <sub>3</sub>	20 %	Low Pressure	20 %	10		

The characteristic geochemistry of the high-Al<sub>2</sub>O<sub>3</sub> type Archaean TTG granitoids (Barker and Arth, 1976) (Fig. 3) indicates that these rocks form by partial melting of a slightly enriched MORB composition source at pressures sufficient to stabilise at least 15% garnet in the residuum (Moyen *et al.*, 2006; Martin and Sigmarsson, 2007). Furthermore, the high Sr contents and low Nb/Ta ratios of these rocks indicate an absence of plagioclase in the source and the presence of rutile in the residuum respectively (Zamora, 2000; Martin and Moyen, 2002; Foley *et al.*, 2002; Schmidt *et al.*, 2004). Thus, a high-pressure metabasaltic source is indicated (Barker and Arth, 1976; Drummond and Defant, 1990; Martin, 1987, 1994; Rapp *et al.*, 2003). Despite general consensus on this point, considerable controversy still surrounds the details of TTG magma origins, as there is considerable debate concerning the depth of melting, the mineralogy of the source, and the geological scenarios relevant to the formation of the magmas (Foley *et al.*, 2002; Rapp *et al.*, 2003; Bédard, 2006).

Explicitly or not, most studies discussing the origin of the Archaean TTG series regard it as one single, unique rock type for which there should be only one tectonic site of formation. However, detailed regional TTG studies from specific Archaean terranes around the world have found TTG plutons with clearly different geochemical features within the same terrane (Moyen, 2011), for instance in the Zimbabwe craton (Luais and Hawkesworth, 1994), the

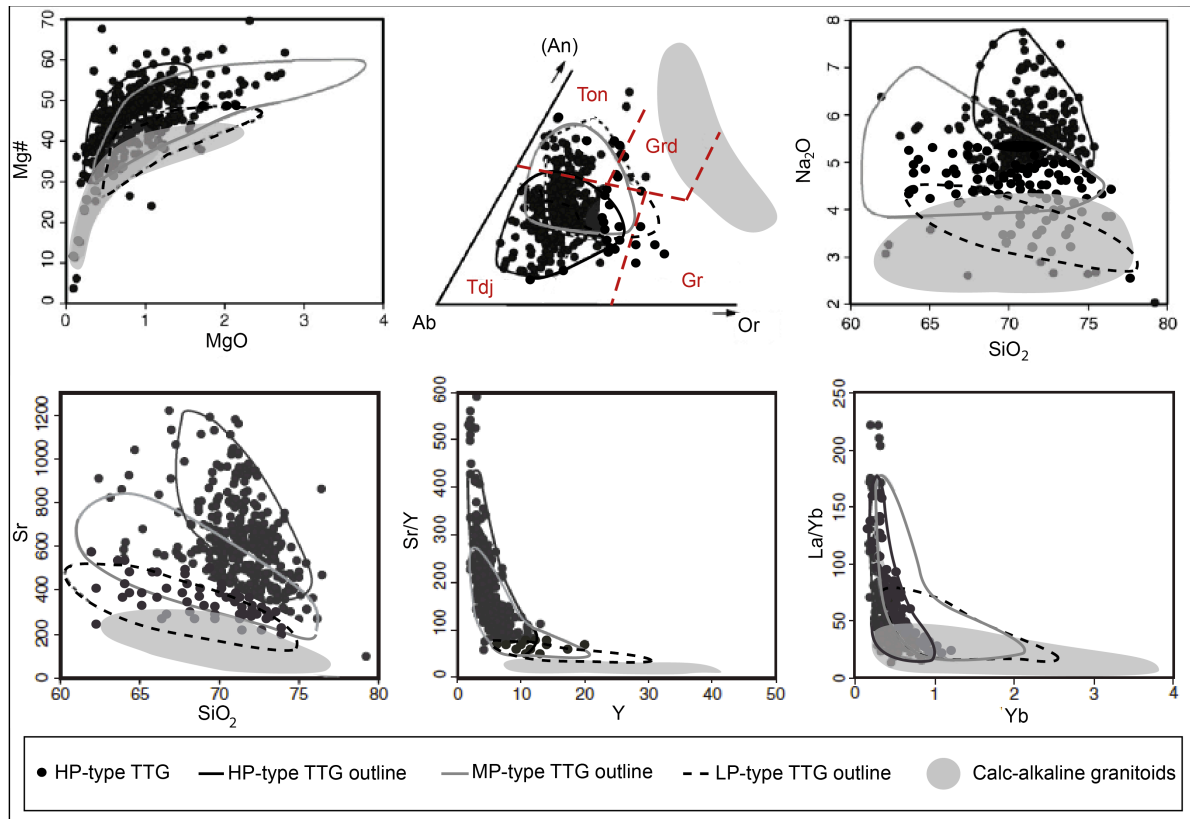


**Fig. 3:** Binary and ternary diagrams indicating the characteristic major-, trace- and rare-earth-element composition of the high-pressure (HP) variety of the high- $\text{Al}_2\text{O}_3$  type Archaean tonalite-trondhjemite-granodiorite (TTG) granitoids; the medium-pressure (MP) variety of the high- $\text{Al}_2\text{O}_3$  type TTG; the low-pressure (LP) variety of TTG (which can also be described as low- $\text{Al}_2\text{O}_3$ ); and calc-alkaline I-type granitoids which represent post-Archaean felsic continental crust (Moyen, 2011). MgO vs. Mg# (molecular Mg/Mg + Fe x 100), showing the leucocratic character of the HP group (lower MgO), although the HP-type has typically higher Mg# than the other TTG groups and calc-alkaline granitoids. Ab-An-Or O'Connor (1965) feldspar ternary diagram illustrates the sodic nature of TTG compared with more calcic and potassic calc-alkaline I-type granitoids. The HP-type TTG granitoids are more trondhjemitic compared to the more tonalitic MP- and LP-type TTGs. The  $\text{SiO}_2$  vs.  $\text{Na}_2\text{O}$  and  $\text{SiO}_2$  vs. Sr Harker-type diagram illustrates the different trends occupied by the various TTG groups and I-type granitoids. In the Sr/Y vs. Y diagram, the combined lower Y and higher Sr of the HP-type TTG result in a position closer to the “left” axis of the diagram and the same observation applies in the La/Yb vs. Yb diagram.

Western Superior Province (Whalen *et al.*, 2004), the Barberton granite–greenstone terrane (Yearron, 2003; Clemens *et al.*, 2006; Moyen *et al.*, 2007), the Pilbara (Champion and Smithies, 2007) or the Karelian and Kola cratons of Finland (Halla *et al.*, 2009). Therefore, the idea of one TTG series is at odds with most regional studies. Moyen (2011) investigated the variation geochemical features of a global database of TTG granitoid compositions and interpreted the geochemical data to reflect various depths of melting with corresponding

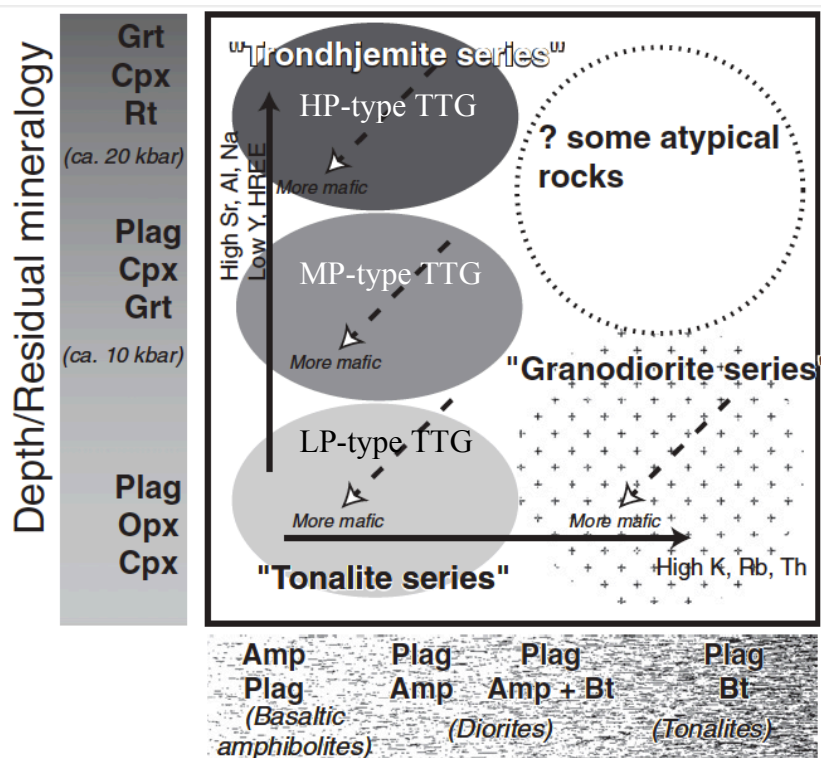


**Fig. 4:** A diagram illustrating the effects that the source composition, the depth at which partial melting occurs, and the resultant residual mineralogy have on melt geochemistry which produce the various TTG types and other LILE-rich granitoids which form part of the Archaean grey gneiss complexes (modified from Moyen, 2011). The evolution towards a progressively enriched source (X-axis) forms LILE-rich granitoids; the evolution towards higher depth of melting (Y-axis) generates granitoids richer in Na and Sr, poorer in HREE.

variable source mineral assemblages (Fig. 4). Consequently, Moyen (2011) categorised high- $\text{Al}_2\text{O}_3$  type TTG into high-pressure (HP) and medium-pressure (MP) types and classified the low- $\text{Al}_2\text{O}_3$  type “TTG” to be synonymous to a low-pressure (LP) type “TTG”. This PhD thesis focuses on the genesis of the HP-type Archaean TTG granitoids, which are characterised by elevated  $\text{Al}_2\text{O}_3$ ,  $\text{Na}_2\text{O}$ , Sr; and low Y, Yb, Ta and Nb; and are also somewhat more leucocratic (with lower MgO and higher  $\text{SiO}_2$ ) compared to the medium-pressure variety (Fig. 2). The high Sr content (typically > 300 ppm) and low Nb-Ta ratios (typically < 7 ppm Nb, < 0.5 ppm Ta) are respectively interpreted to indicate an absence of plagioclase and the presence of rutile, in the residuum from which the magmas separated (Martin and Moyen, 2002; Schmidt *et al.*, 2004). Consequently, HP-type TTG magmas are interpreted to

arise by high-pressure melting of an eclogite-facies metabasaltic source rock (Barker and Arth, 1976; Moyen, 2011) which will leave a Grt + Cpx + Rt residuum, compared to the MP-TTG which are interpreted to arise by the partial melting of an garnet-bearing amphibolite-facies metabasaltic source (Moyen, 2011; Foley *et al.*, 2002). HP-type Archaean TTG compositions are also characterised by high Ni and Cr contents and high Mg numbers compared with other leucocratic magmas. This characteristic has been interpreted to indicate that the magmas interacted with mantle material prior to emplacement (Martin and Moyen, 2002) despite the challenges to magma survival posed by such a process. However, there is a paucity of experimental studies which have analysed experimental melts for a full range of major, trace and rare earth elements, including Ni and Cr, on which to evaluate the origin of such trace-element signatures. Analysing experimental glasses, that represent quenched partial melts, for trace element compositions is; however, exceptionally challenging, as glasses are very rarely crystal-free. Laser ablation-ICP-MS, which is the best technique by which to acquire a full range of trace and REE in such glasses, requires relatively large volumes of crystal-free glass.

Fertility for granitoid magma production, at reasonable temperatures, requires H<sub>2</sub>O in the source (Clemens, 1984; Tuttle and Bowen, 1958; Wyllie and Tuttle, 1961). This, coupled with the high pressure of partial melting that is required by the absence of plagioclase, as well as the presence of rutile and a high garnet fraction in the source, may indicate that HP-type TTG magmas form by anatexis of the upper portions of Archaean subducting slabs, within relatively hot Archaean subduction zones which has previously been proposed for high-Al<sub>2</sub>O<sub>3</sub> type TTG in general (Condie, 1981; Rapp *et al.*, 2003; Smithies and Champion, 2000; Smithies *et al.*, 2003), as a consequence of higher Archaean mantle temperatures than exist on Earth at present (Rudnick, 1995; Albarède, 1998; Prelevic and Foley, 2007). Alternative



genetic models exist for high- $\text{Al}_2\text{O}_3$  type TTG, most of which propose formation sites that are unrelated to plate boundaries (e.g. Bédard, 2006; Davies, 1992; Rudnick, 1995). One set of models sees TTG magmas arising through partial melting at the base of an over-thickened basaltic plateau in an intra-plate setting (e.g. Smithies, 2000; Zegers and van Keken, 2001) while other authors suggests that TTG granitoids form by the melting of thick oceanic crust which is followed by repeated events of partially melting the delaminated eclogitised lower crust (Bedard, 2006). However, these models, proposed for TTG in general, struggle to meet the depth requirement for HP-type TTG as well as the necessity that the source be continuously re-fertilised, which is implied by construction of TTG plutons over protracted time periods (e.g. Kisters *et al.*, 2010).

Since the end of the Archaean Eon, the dominant continental-crust-forming processes are reasonably well understood and calc-alkaline magmatism associated with subduction settings remains a prominent site for continental crust formation. This process is considered to begin with slab-derived fluids that flux partial melting of peridotite in the mantle wedge. Therefore, fluid drives this process of arc magmatism within Phanerozoic subduction zones (e.g. Schmidt *et al.*, 1998; Connolly *et al.*, 2002) (Fig. 5). Consequently, understanding the role of water-rich fluid within Archaean subduction zones may provide considerable insight into the genesis of HP-type TTG magmas. However, in general, the generation of high- $\text{Al}_2\text{O}_3$  TTG magmas has been considered to occur through fluid-absent melting of amphibole, and a substantial body of experimental data relevant to this process exists (see Moyen and Stevens (2006) for review). Although, this premise that only fluid-absent melting processes are relevant to TTG genesis is certainly wrong for the HP-type variety. The reason for this is that HP-type TTG chemistry indicates their formation by the anatexis of subducting eclogite-facies basaltic crust, yet firstly, the melting of relatively anhydrous eclogite by fluid-absent

melting is unlikely; and secondly, there is little evidence for fluid-fluxed mantle wedge melting coincident with HP-type TTG production from the Paleo- to Meso-Archaean rock record, such as the concurrent emplacement of intermediate magmas with TTG granitoids. Thus, the question becomes: If HP-type TTG magmas arise as a consequence of fluid-absent slab melting, then what became of the likely considerable volume of metamorphic water released during the pre-anatectic history of the slab?

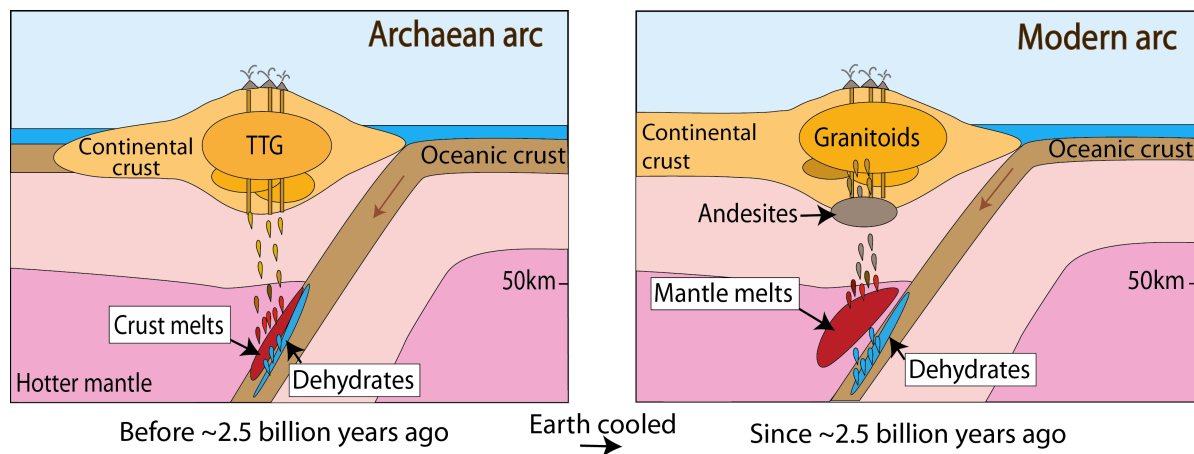


**Fig. 5:** Schematic diagram comparing a typical post-Archaean arc and a hypothetical Archaean arc. Within the post-Archaean arc magmas with a calc-alkaline affinity are produced by a process that begins with fluid-saturated partial melting of peridotite in the mantle wedge that is induced by the ascent of slab derived water-rich fluids or melts (Grove *et al.* 2006). The resultant initially near fluid-saturated mantle melts rise through the mantle wedge, equilibrating with hotter and dryer mantle, to ultimately produce the basalts and andesites that characterise this setting. The re-melting of juvenile continental crust of intermediate average composition, consisting largely of andesite and related volcanoclastic sedimentary material, produces the calc-alkaline I-type series granitoids associated with arcs (e.g. Gill 1981; Hildreth *et al.* 1987; Miller and Harris 1989). As a consequence of a hotter Archaean mantle, the upper portions of Archaean slabs may undergo fluid-fluxed melting as fluids from the lower portions within the slab are released by prograde dehydration reactions and migrate upwards.

Fluid-present melting of the slab to produce TTG magmas represents an attractive alternative hypothesis. However, this model has previously been disregarded because of the very low porosities of high-grade metamorphic rocks (Peacock *et al.*, 2005). Drummond and Defant (1990) proposed that metamorphic fluid given off by the interiors of Archaean subducting

slabs might have induced fluid-fluxed anatexis of the overlying upper layers in the slab (Fig. 5). The thermal structure of subducting slabs seems to support this hypothesis, as the upper portion of the slab is the hottest, due to the thermal effect of the overlying mantle wedge (e.g. Peacock *et al.*, 2005; van Keken *et al.*, 2002). However, limited experimental work investigating fluid-present melting processes in appropriate metabasaltic sources has been conducted at the high pressures relevant to HP-type Archaean TTG magma formation. Thus, there is a paucity of information on which the fluid-saturated slab-melting hypothesis can be evaluated.

In light of this, the current PhD thesis has attempted to contribute to the state of knowledge on the formation and evolution of the Earth's early continental crust. This was done by experimentally investigating the petrogenesis of Paleo- to Meso- Archaean HP-type trondhjemitic crust by fluid-present eclogite partial melting of a low-K metabasaltic rock (at 1.6 - 3.0 GPa and 700 - 900 °C), and unravelling the potential geodynamic and crustal evolutionary implications by modelling the likely Archaean subduction scenarios that may have satisfied this scenario. Additionally, this PhD study has experimentally investigated the relevant low-K<sub>2</sub>O metabasaltic solidus and discusses its possible implications for late Archaean continental crustal evolution.

The thesis is presented as a compilation of two published papers and one submitted manuscript that were generated during the course of this PhD study. These are presented as individual chapters dealing with various aspects of HP-type Archaean TTG generation, and can be summarised as follows:

(1) The first paper presents the experimental findings of fluid-present eclogite partial melting between 1.9 and 3.0 GPa and 870 - 900 °C. The major, trace and rare Earth element compositions of the experimental glasses (quenched melts) are measured using SEM-EDS, SEM-WDS and LA-ICP-MS. The experimental glasses have the compositions of peraluminous trondhjemites and have similar major-, trace- and rare-earth-element signatures to Archaean HP-type TTG granitoids. The implications of the proposed petrogenetic model for Archaean HP-type TTG are discussed.

(2) The second paper is an investigation into the geodynamic implications for HP-type TTG formation via water-present eclogite melting. The possibility of HP-type TTG being produced by fluid-fluxed slab anatexis within a potential Archaean subduction zone is explored using metamorphic and numerical modelling.

(3) The third manuscript experimentally investigates the onset of partial melting of rocks with a low-K<sub>2</sub>O metabasaltic composition between 700 and 900 °C within the pressure range between 1.6 and 3.0 GPa. The effect of using different starting materials, including natural eclogite, synthetic eclogite and gel starting materials, at the relevant conditions is critically evaluated. The results of experiments define the nature of the eclogite-facies fluid-present solidus between 1.8 and 3.0 GPa. Knowledge of the location of this solidus is necessary to evaluate the formation of HP-type Archaean TTG by the petrogenetic and geodynamic models proposed by this study. However, this solidus has previously not been experimentally defined within this pressure interval. The solidus has implications for the understanding of the mechanism that caused the geochemical shift in the compositions of new additions to continental crust, from sodic TTG to intermediate composition andesites and diorites, towards the end of the Archaean Eon.

**References:**

- Albarède, F., 1998. The growth of continental crust. *Tectonophysics*, 196:1-14.
- Arth, J.G., Hanson, G.N., 1972. Quartz-diorites derived by partial melting of eclogite or amphibolite at mantle depth. *Contribution to Mineralogy and Petrology* 37, 164–174.
- Barker, F., Arth, J.G., 1976. Generation of trondhjemite-tonalite liquids and Archaean bimodal trondhjemite-basalt suites. *Geology* 4, 596–600.
- Bédard, J., 2006. A catalytic delamination-driven model for coupled genesis of Archaean crust and sub-continental lithospheric mantle. *Geochimica Cosmochimica Acta* 70, 1188–1214.
- Champion, D.C. and Smithies, R.H., 2007. Geochemistry of Paleoproterozoic granites of the East Pilbara Terrane, Pilbara Craton, Western Australia: implications for early Archean crustal growth. In: Van Kranendonk, M.J., Smithies, R.H., Bennett, V. (Eds.), *Earth's Oldest Rocks. Developments in Precambrian Geology*. Elsevier, pp. 369–410.
- Clemens, J.D., 1984. Water contents of silicic to intermediate magmas. *Lithos* 17, 273–287.
- Clemens, J.D., Yearron, L.M., Stevens, G., 2006. Barberton (South Africa) TTG magmas: geochemical and experimental constraints on source-rock petrology, pressure of formation and tectonic setting. *Precambrian Research* 151, 53–78.
- Collins, W.J., Van Kradendonk, M.J., and Teyssier, C., 1998. Partial convective overturn of the Archaean crust in the eastern part of the Pilbara Craton, Western Australia: 2. Driving mechanisms and tectonic implications: *Journal of Structural Geology*, v. 20, p. 1405–1424.
- Collins, W.J. and Van Kradendonk, M.J., 1999. Model for the development of kyanite during partial convective overturn of Archaean granite-greenstone terranes: the Pilbara Craton, Australia: *Journal of Metamorphic Geology*, v. 17, p. 145-156.
- Condie, K.C., 1981. *Archaean Greenstone Belts*. Elsevier, Amsterdam, pp 434
- Condie, K.C., and Pease, V., 2008, When did plate tectonic begin on planet Earth?: The Geological society of America, Special Paper, v.440, p. 294.
- Connolly, J.A.D. and Petrini, K. 2002. An automated strategy for calculation of phase diagram sections and retrieval of rock properties as a function of physical conditions. *J. Metamorph. Geol.*, 20, 697-708.
- Davies, G.F., 1992. On the emergence of plate tectonics. *Geology* 20 (11), 963–966.
- De Wit, M.J., 1998. On Archaean granites, greenstones, cratons and tectonics: does the evidence demand a verdict?: *Precambrian Research*, v. 91, p. 181–226.
- Drummond, M.S. and Defant, M.J., 1990. A model from trondhjemite-tonalite-dacite genesis and crustal growth via slab melting: Archean to modern comparisons. *J. Geophys. Res.*, 95, 21503-21521.
- Feng, R. and Kerrich, R., 1992. Geochemical evolution of granitoids from the Archean Abitibi southern volcanic zone and the Pontiac subprovince, Superior Province, Canada: implications for tectonic history and source regions. *Chemical Geology* 98, 23–70.
- Foley, S.F., Tiepolo, M. and Vannucci, R., 2002. Growth of early continental crust controlled by melting of amphibolite in subduction zones. *Nature*, 417, 837-840.
- Gill, J.B., 1981. *Orogenic Andesites and Plate Tectonics*. Springer-Verlag, Berlin, pp. 390.
- Grove, T.L., Chatterjee, N., Parman, S.W., Médard, E., 2006. The influence of H<sub>2</sub>O on mantle wedge melting. *Earth and Planetary Science Letters* 249, 74–89.
- Halla, J., Van Hunen, J., Heilimo, E. and Hölttä, P., 2009. Geochemical and numerical constraints on Neoproterozoic plate tectonics. *Precambrian Research* 174, 155–162.

- Hamilton, W.B., 1998, Archaean magmatism and deformation were not products of plate tectonics: *Precambrian Research*, v. 91, p. 143–179.
- Hildreth, W. and Moorbath, S., 1987. Crustal contributions to arc magmatism in the Andes of Central Chile. *Contrib. Min. Pet.* 98(4):455-489.
- Jahn, B.M., Glikson, A.Y., Peucat, J.J. and Hickman, A.H., 1981. REE geochemistry and isotopic data of Archaean silicic volcanics and granitoids from the Pilbara Block, western Australia: implications for the early crustal evolution. *Geochim. Cosmochim. Acta*, 45, 1633–1652.
- Kisters, A.F.M., Stevens, G., Dziggel, A., Armstrong, R.A., 2003. Extensional detachment faulting and core-complex formation in the southern Barberton granite–greenstone terrain, South Africa: evidence for a 3.2 Ga orogenic collapse. *Precambrian Research* 127, 355–378.
- Kisters, A.F.M., Belcher, R., Poujol, M. and Dziggel, A., 2010. Continental growth and convergence-related arc plutonism in the Mesoarchaean: evidence from the Barberton granitoid-greenstone terrain, South Africa. *Precambrian. Res.*, 178, 15-26.
- Kretz, 1983. Symbols for rock-forming minerals. *Am. Min.* 68:277-279.
- Luais, B. and Hawkesworth, C., 1994. The generation of continental crust: an integrated study of crust-forming processes in the Archaean of Zimbabwe. *Journal of Petrology* 35 (1), 43.
- Martin, H., 1987. Petrogenesis of Archaean trondhjemites, tonalites and granodiorites from eastern Finland; major and trace element geochemistry. *Journal of Petrology* 28 (5), 921–953.
- Martin, H., 1994. The Archean grey gneisses and the genesis of the continental crust in Archean crustal evolution. In: (Condie, K. C. eds) Elsevier, Amsterdam, 205-259.
- Martin, H. and Moyen, J-F., 2002. Secular changes in TTG composition as markers of the progressive cooling of the Earth. *Geology*, 30 (4), 319-322.
- Martin, E., Sigmarsson, O., 2007. Crustal thermal state and origin of silicic magma in Iceland: the case of Torfajökull, Ljósufjöll and Snæfellsjökull volcanoes. *Contributions to Mineralogy and Petrology* 153, 593–605.
- Miller, J.F. and Harris, N.B.W., 1989. Evolution of continental crust in the Central Andes; constraints from Nd isotope systematics. *Geology* 17(7) : 615-617.
- Moyen, J-F., Stevens, G. and Kisters, A., 2006. Record of mid-Archaean subduction from metamorphism in the Barberton terrain, South Africa. *Nature*, 442, 559–562.
- Moyen, J-F. and Stevens, G., 2006. Experimental constraints on TTG petrogenesis: Implications for Archean geodynamics. In: (Benn, K., et al. eds) Archean geodynamics and environments. AGU Geophys. Monogr., 164, 149–175.
- Moyen, J.-F., Stevens, G., Kisters, A.F.M. and Belcher, R.W., 2007. TTG plutons of the Barberton granitoid-greenstone terrain, South Africa. In: Van Kranendonk, M.J., Smithies, R.H., Bennett, V. (Eds.), *Earth's Oldest rocks. Developments in Precambrian geology*. Elsevier, pp. 606–668.
- Moyen, J-F., 2011. The composite Archaean grey gneisses: petrological significance, and evidence for a non-unique tectonic setting for Archaean crustal growth. *Lithos*, 123, 21-36.
- O'Connor, A.C., 1965. A classification for quartz-rich igneous rocks based on feldspar ratios. *US Geol. Surv. Prof. Paper*, 525B, 79-8.
- Peacock, S.M., van Keken, P.E., Holloway, S.D., Hacker, B.R., Abers, G.A. and Ferguson, R.L., 2005. Thermal structure of the Costa Rica–Nicaragua subduction zone. *Phys. Earth Planet In.*, 149, 187–200.
- Prelevic, D. and Foley, S.F., 2007. Accretion of arc-oceanic lithospheric mantle in the Mediterranean: Evidence from extremely high-Mg olivines and Cr-rich spinel inclusions in lamproites. *Earth Planet. Sc. Lett.*, 256 (1-2), 120-135.
- Rapp, R.P., Shimizu, N. and Norman, M.D., 2003. Growth of early continental crust by partial melting of eclogite. *Nature*, 425, 605-609.

- Rudnick, R.L., 1995. Making continental crust. *Nature*, 378, 571-578.
- Schmidt, M.W. and Poli, S., 1998. Experimentally based water budgets for dehydrating slabs and consequences for arc magma generation. *Earth Planet. Sc. Lett.* 163, 361–379.
- Schmidt, M.W., Dardon, A., Chazot, G. and Vannucci, R., 2004. The dependence of Nb and Ta rutile-melt partitioning on melt composition and Nb/Ta fractionation during subduction processes. *Earth. Planet. Sc. Lett.*, 226, 415-432.
- Shirey, S.B. and Hanson, G.N., 1984. Mantle-derived Archaean monzodiorites and trachyandesites. *Nature*, 310, 222–224.
- Smithies, R.H., 2000. The Archaean tonalite-trondhjemitic-granodiorite (TTG) series is not an analogue of Cenozoic adakite. *Earth and Planetary Science Letters* 182, 115–125.
- Smithies, R.H. and Champion, D.C., 2000. The Archean high-Mg diorite suite: links to tonalite–trondhjemitic–granodiorite magmatism and implications for early Archean crustal growth. *J. Petrol.*, 41, 1653–1671.
- Smithies, R.H., Champion, D.C. and Cassidy, K.F., 2003. Formation of Earth's early Archaean continental crust. *Precambrian Res.*, 127(1-3), 89-101.
- Tuttle, O.F., Bowen, N.L., 1958. Origin of granite in the light of experimental studies in the system  $\text{NaAlSi}_3\text{O}_8 - \text{KAlSi}_3\text{O}_8 - \text{SiO}_2 - \text{H}_2\text{O}$ . *Geological Society of American Memoirs* 74.
- van Keken, P.E., Kiefer, B. and Peacock, S.M., 2002. High-resolution models of subduction zones: Implications for mineral dehydration reactions and the transport of water into the deep mantle: *Geochem. Geophys. Geosys.*, 3, 1056, doi:10.1029/2001GC000256.
- Whalen, J.B., Percival, J.A., McNicoll, V.J. and Longstaffe, F.J., 2002. A mainly crustal origin for tonalitic granitoid rocks, Superior Province, Canada: Implications for late Archean tectonomagmatic processes. *Journal of Petrology* 43 (8), 1551–1570.
- Whalen, J.B., McNicoll, V.J., Galley, A. and Longstaffe, F.J., 2004. Tectonic and metallogenic importance of an Archean composite high-Al low-Al tonalite suite, Western Superior Province, Canada. *Precambrian Research* 132 (3), 275–301.
- Willbold, M., Hegner, E., Stracke, A. and Rocholl, A., 2009. Continental geochemical signatures in dacites from Iceland and implications for models of early Archaean crust formation. *Earth and Planetary Science Letters* 279, 44–52.
- Windley, B.F., 1995. *The Evolving continents*. John Wiley and sons, Chester. 526 pp.
- Wyllie, P.J. and Tuttle, O.F., 1961. Experimental Investigation of silicate systems containing two volatile components, Part II. The effects of  $\text{NH}_3$  and HF, in addition to  $\text{H}_2\text{O}$ , on the melting temperatures of albite and granite. *American Journal of Science* 259, 128–143.
- Yearron, L.M., 2003. Archaean granite petrogenesis and implications for the evolution of the Barberton Mountain Land, South Africa. Unpub. PhD thesis Thesis, Kingston University, Kingston, UK, 315 pp.
- Zamora, D., 2000. Fusion de la croûte océanique subductée: approche expérimentale et géochimique, Thèse d'université thesis, Université Blaise-Pascal, Clermont-Ferrand.
- Zegers, T. and van Keken, P.E., 2001. Middle Archean continent formation by crustal delamination. *Geology*, 29, 1083-1086.

## CHAPTER 2

### **Water-present eclogite melting to produce Earth's early felsic crust**

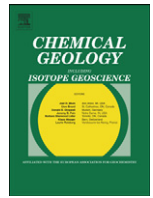
#### *A presentation of the published research paper*

This research paper is published in *Chemical Geology*. I am the first author and Prof. Gary Stevens is the co-author.

This research paper investigates the role of high-pressure fluid-present melting of an eclogite-facies starting material, in the production of Paleo- to Meso-Archaean HP-type TTG melts by conducting fluid-saturated partial melting experiments with a natural eclogite-facies metabasaltic starting material between 1.9 and 3.0 GPa and 850 and 900 °C. The research paper details the analyses of the major- and trace- element compositions of experimental glasses produced by water-present melting of a natural eclogite assemblage and uses geochemical modelling to better understand the glass geochemistry and melting behaviour.

All aspects of the sample preparation, experiments, data acquisitions, calculation and geochemical modelling and were led by me under the supervision of Prof. Gary Stevens. I did all of the written work and created all the diagrams. Prof. Gary Stevens conceptualized the research idea and participated in the writing as a typical second author. Dr Esme Spicer, who was the XRF laboratory manager at Stellenbosch University, analysed the whole-rock composition of the starting material using XRF. Acquisition of the trace and REE of the whole rock and experimental glasses using LA-ICP MS was done equitably between myself and Riana Rossouw, who is the ICP MS laboratory manager at Stellenbosch University.





Research paper

# Water-present eclogite melting to produce Earth's early felsic crust

Angelique Laurie\*, Gary Stevens

Centre for Crustal Petrology, Department of Earth Science, University of Stellenbosch, Stellenbosch, Private Bag X1, Matieland 7602, South Africa

## ARTICLE INFO

### Article history:

Received 19 June 2011

Received in revised form 30 April 2012

Accepted 3 May 2012

Available online 9 May 2012

Editor: K. Mezger

### Keywords:

Archaean

Continental crust

Trondhjemite

Eclogite

Water-present melting

## ABSTRACT

The geochemistry of well preserved Archaean Tonalite–Trondhjemite–Granodiorite (TTG) rocks, such as the trondhjemites of the Meso-Archaean Barberton granitoid–greenstone terrain in South Africa, provides insight into the origins of Earth's early felsic continental crust. This is particularly well demonstrated by the high pressure (HP)-type of Archaean TTG magmas, where the geochemistry requires that they are formed by high-pressure melting of a garnet-rich eclogitic source. This has consequently been interpreted as evidence for the formation of these magmas by anatexis of the upper portions of slabs within Archaean subduction zones. Most of the experimental data relevant to TTG genesis has been generated by studies of fluid-absent melting of metabasaltic sources. However, water drives arc magmatism within Phanerozoic subduction zones and thus, understanding the behaviour of water in Archaean subduction zones, may have considerable value for understanding the genesis of HP-type Paleo- to Meso-Archaean trondhjemites. Consequently, this study investigates the role of high-pressure water-present melting of an eclogite-facies starting material, in the production of Paleo- to Meso-Archaean HP-type TTG melts. Water-saturated partial melting experiments were conducted between 1.9 and 3.0 GPa; and, 870 °C and 900 °C. The melting reaction is characterised by the breakdown of the jadeite molecule in the clinopyroxene, together with quartz and water, to form melt in conjunction with a less sodic clinopyroxene:  $Qtz + Cpx_1 + Grt_1 + H_2O = Melt + Cpx_2 + Grt_2$  and produced melt compositions that, if allowance is made for the low Mg# and almost K<sub>2</sub>O-free character of the starting material, are an excellent major element match with HP-type TTG compositions. In two of the experimental run products, melt segregated efficiently from residual crystals, allowing for the measurement of a full range of trace elements, via Laser Ablation Inductively Coupled Plasma Mass Spectroscopy (LA-ICP-MS). The experimental glasses produced are Light Rare Earth Element (LREE) (24–44 ppm La; 50–86 ppm Ce) and Zr (101–228 ppm) enriched; and Heavy Rare Earth Element (HREE) (0.4 ppm Yb; 50.9 La/Yb<sub>n</sub>), Y (2.2–3.2 ppm; 82–142 Sr/Y), Sm (2.1–4.3 ppm; 40.9–50.8 Zr/Sm) and Nb (1.7–2.8 ppm) depleted compared to the DSE4 starting material. Thus, the REE element compositions of the experimental glasses are also similar to HP-type TTG compositions, and in more particular they are strikingly similar to Meso-Archaean Barberton trondhjemites. Additionally, we propose that due to Cpx being a major reactant, Ni and Cr contents (4–29 ppm Ni and 43 ppm Cr) of the glasses which were analysed for these elements, are within the compositional range displayed by HP-type Archaean TTG. This study suggests that the geochemistry of HP-type Archaean trondhjemites may reflect high pressure water-present partial melting of an eclogite facies metabasaltic source. Consequently, we propose that water-present melting of an eclogitic source is a viable mechanism for the genesis of this component of Paleo- to Meso-Archaean TTG crust.

© 2012 Elsevier B.V. All rights reserved.

## 1. Introduction

The geochemistry of the Archaean Tonalite–Trondhjemite–Granodiorite (TTG) series of granitoids (Barker and Arth, 1976; Moyen, 2011) underpins almost everything we know about the origins of Earth's Paleo- to Meso-Archaean continental crust. These rocks are characterised by high Na:Ca and Na:K ratios and a strongly leucocratic character. Consequently, they plot near the Na corner of

Or:Ab:An ternary plots, well off the calc-alkaline trend (Martin, 1994), and are interpreted to reflect melting of low K<sub>2</sub>O metabasaltic source rocks (Martin and Sigmarsson, 2007). Despite general consensus on this point, considerable controversy still surrounds the details of TTG magma origins, as there is considerable debate concerning the depth of melting, the mineralogy of the source; and the geological scenarios relevant to the formation of the magmas (Foley et al., 2002; Rapp et al., 2003; Bédard, 2006). Moyen (2011) investigated the details of the complex range of chemistry exhibited by TTG granitoids and showed that various depths of melting, to produce TTG, can explain this range. Subsequently, Moyen (2011) proposed that such magmas could have formed in a range of different

\* Corresponding author. Tel.: +27 21 808 3127; fax: +27 21 808 3129.  
E-mail address: [alaurie@sun.ac.za](mailto:alaurie@sun.ac.za) (A. Laurie).

genetic settings and categorised TTG into low (LP) (<1.5 GPa), medium (MP) (1.5–2.0 GPa) and high pressure (HP) (>2.0 GPa) subtypes. Therefore, this suggests the need for more focused investigation into the genesis of the particular subtypes of these granitoids.

HP-type TTG are predominantly trondhjemitic and make up approximately 20% of Archaean TTG granitoids (Moyen, 2011). The chemical characteristics of HP-type TTG granitoids include high Sr content (typically >300 ppm) and low Nb–Ta ratios (typically <7 ppm Nb, <0.5 ppm Ta) which are respectively interpreted to indicate an absence of plagioclase and the presence of rutile, in the residuum from which the magmas separated (Foley et al., 2002; Martin and Moyen, 2002; Schmidt et al., 2004). Similarly, low Yb (typically <1 ppm) and a subsequent high La/Yb ratio (ave. 56) is interpreted to reflect a substantial fraction of garnet (>15%) in the residuum (Rapp et al., 2003; Moyen and Stevens, 2006). Consequently, these magmas are interpreted to arise by high pressure melting of an eclogitic source rock (Barker and Arth, 1976; Moyen, 2011) of MORB-like composition (Moyen and Stevens, 2006). HP-type Archaean TTG compositions are also characterised by high Ni and Cr contents and high Mg#s compared with other leucocratic magmas. Despite the challenges to magma survival posed by the process, this characteristic has been interpreted to indicate that the magmas interacted with mantle material prior to emplacement (Martin and Moyen, 2002).

Fertility for granitoid magma production, at reasonable temperatures, requires water in the source (Tuttle and Bowen, 1958; Wyllie and Tuttle, 1961; Clemens, 1984). This, coupled with the high pressure of partial melting that is required by the absence of plagioclase, as well as the presence of rutile and an abundant garnet fraction in the source, possibly indicate that HP-type TTG magmas form by anatexis of the upper portions of slabs within Archaean subduction zones (Condie, 1981; Martin, 1994, 1999; Smithies and Champion, 2000; Foley et al., 2002; Rapp et al., 2003; Smithies et al., 2003). Alternative models exist, most of which propose formation sites which are unrelated to plate boundaries (e.g. Davies, 1992; Rudnick, 1995; Bédard, 2006). However, these models struggle to meet the depth requirement for HP-type TTG genesis or the necessity that the source be continuously re-fertilised which is implied by construction of TTG plutons over protracted time periods (e.g. Kisters et al., 2010). Additionally, suitably hydrated metamafic source rocks are available in the anatectic zone associated with subduction zones over a protracted time period. This is much less likely, if not impossible, to occur within the context of underplated basalts. Consequently, the broadest consensus supports the hypothesis that these magmas are a consequence of slab melting. Perhaps the most convincing evidence supporting this concept are the 3.2 Ga syntectonic trondhjemitic from the Barberton granitoid–greenstone terrain (BGGT), in South Africa, which were emplaced over 60 Myr during a Meso–Archaean subduction event (Moyen et al., 2006; Kisters et al., 2010).

Water drives arc magmatism within Phanerozoic subduction zones (e.g. Schmidt and Poli, 1998; Connolly and Pettrini, 2002). Consequently, understanding the role of water in Archaean subduction zones, beyond the requirement that it was sufficiently available to make the source fertile for melt generation, may provide considerable insight into the genesis of HP-type TTG magmas. In general, the generation of high- $Al_2O_3$  (which includes MP and HP-type) TTG magmas by partial melting of the subducting oceanic crust, has been considered to occur through fluid-absent melting of amphibole and a substantial body of experimental data relevant to this process exists (see Moyen and Stevens (2006) for review). However, this basic premise that only fluid-absent melting conditions are relevant is very likely wrong. Indeed, the reason for this, as argued above, is that the genesis of HP-type TTG magmas requires a hydrated source, and TTG chemistry is consistent with their formation via the anatexis of subducting basaltic crust, yet there is little evidence for mantle wedge melting coincident with HP-type TTG production from the Paleo- to Meso–Archaean rock record. Thus, the question becomes: If HP-type TTG magma arises as a consequence of fluid-absent

slab melting, what became of the likely considerable volume of metamorphic water released during the pre-anatectic history of the slab? This was recognised by Drummond and Defant (1990), who proposed that this metamorphic water would have induced fluid-present anatexis of the upper layers in the slab. The thermal structure of subducting slabs seems to support this hypothesis well, as the upper portion is the hottest due to the thermal effect of the overlying mantle wedge (e.g. van Keken et al., 2002; Peacock et al., 2005). Typically the source region of metamorphic fluids is limited to the upper 3 km of the slab, due to substantial hydration, through sea-floor alteration, mostly in ridge systems, prior to subduction (Alt and Teagle, 2000; Dick, 2000). Although modern slabs typically do not melt, higher Archaean mantle temperatures may have served to make upper-slab-surface-fluid-present melting a common feature during the Paleo- and Meso–Archaean Eon. Consequently, progressive mantle cooling eventually resulted in the subsequent “turning off” of this process towards the end of the Archaean Eon. However, limited experimental work investigating water-present melting processes in metabasaltic sources has been conducted at the high pressures relevant for HP-type TTG magma formation, resulting in a paucity of information on which the water-saturated slab melting hypothesis can be evaluated. Consequently, this study aims to investigate the major and trace element compositions of the experimental glasses produced by water-present melting of a natural eclogite assemblage and will compare the resultant experimental glasses to HP-type Archaean TTG and 3.2 Ga Barberton trondhjemitic.

## 2. Experimental procedure and analytical techniques

Water-present partial melting experiments were conducted between 1.9 and 3.0 GPa and 870 °C and 900 °C. Table 1 summarises the experimental run conditions and the experimental results.

### 2.1. Experimental starting material

As these experiments set-out to investigate the water-saturated partial melting of eclogite, an essentially K-free eclogite facies rock of MORB-like composition (DSE4) (Tables 2 and 3) was used as the starting material. This somewhat unconventional choice of starting material comes with both advantages and disadvantages over more conventional choices, such as glasses, gels, or lower metamorphic grade metabasaltic rock powders. The advantages are that the likelihood of meta-stable melting of plagioclase + quartz +  $H_2O$  will be avoided during heating of

**Table 1**  
Experimental run conditions and experimental products.

Exp. run	Starting material	P (GPa)	Dev.	T (°C)	Dev.	Duration (days)	$H_2O^a$ (wt.%)	Assemblage <sup>b</sup>
	DSE4							Grt, Cpx, Rt, (Ilm), (Am), (Plag), Qtz
1		1.9	0.0	870	1	7	21	Grt, Cpx, (Rt), Ilm, glass, vapour
2		1.9	0.1	900	1	7	20	Grt, Cpx, Rt, (Ilm), glass, vapour
3		2.2	0.1	880	1	7	19	Grt, Cpx, Rt, (Ilm), glass, vapour
4		2.6	0.1	870	1	7	25	Grt, Cpx, Rt, glass, vapour
5		2.9	0.1	870	1	7	29	Grt, Cpx, Rt, glass, vapour
6		3.0	0.1	870	1	7	32	Grt, Cpx, Rt, glass, vapour

<sup>a</sup>  $H_2O$  represents the weight percentage of distilled water added to the experimental capsule before the capsule was sealed. Therefore the values are maximum concentrations.

<sup>b</sup> Phases in brackets occur as relict phases; Grt—garnet; Cpx—clinopyroxene; Rt—rutile; Ilm—ilmenite; Am—amphibole; Plag—plagioclase; Qtz—quartz.

**Table 2**

Major element geochemistry of the starting material and averaged normalised anhydrous experimental glass major element compositions. The average compositions for high pressure-type Archaean TTG (Moyen, 2011) and the average 3.2 Ga Trondhjemite compositions from the Barberton granitoid greenstone terrain (BGGT), South Africa (Clemens et al., 2006), are provided for comparison to the experimental glass composition. The compositions of C-F2b (Smithies et al., 2009) and average global MORB (Winter, 2001 (BVTP Table 1.2.5.2)) are provided for comparison with this study's starting material (DSE4—Dabie Shan eclogite). C-F2b is an Eastern Pilbara (Coucal Fm) basalt considered to represent an Archaean basaltic crustal composition. Bulk rock analysis for DSE4 was done via XRF and glass analyses were done using SEM-EDS with a cryostage.

	DSE4	C-F2b	Ave. MORB	Ave. glass compositions						HP-type	3.2 Ga								
				1.9		2.2		2.6		2.9		3.0		Archaean	BGGT				
P (GPa)				1.9	1.9	2.2	2.6	2.9	3.0			TTG	Tdj						
T (°C)				870	900	880	870	870	870	Ave.	Ave.								
N				3	3	3	3	3	3	265	42								
wt.%				$\sigma$	$\sigma$	$\sigma$	$\sigma$	$\sigma$	$\sigma$	$\sigma$	$\sigma$	$\sigma$	$\sigma$						
SiO <sub>2</sub>	50.0	46.5	50.5	74.7	0.9	74.4	0.7	75.2	0.6	75.3	0.2	75.3	0.8	75.1	0.4	70.9	2.5	71.2	2.0
TiO <sub>2</sub>	2.5	2.0	1.6	0.1	0.0	0.3	0.5	0.5	0.1	0.4	0.1	0.4	0.2	0.2	0.3	0.3	0.1	0.2	0.1
Al <sub>2</sub> O <sub>3</sub>	12.8	15.0	15.3	14.7	0.7	14.7	0.6	14.6	0.5	14.1	0.7	14.0	0.2	14.1	0.3	15.5	1.0	15.8	0.7
FeO <sup>a</sup>	16.2	13.8	10.5	2.0	0.6	2.4	0.7	2.2	0.1	2.4	0.0	2.3	0.2	2.1	0.2	1.9	0.9	1.9	0.6
MgO	5.7	7.2	7.5	0.4	0.4	0.5	0.6	0.3	0.1	0.2	0.3	0.2	0.1	0.3	0.4	0.8	0.5	0.8	0.3
MnO	0.3	0.2	0.0	0.1	0.4	0.0	0.0	0.0	0.0	0.0	0.0	0.0	0.0	0.0	0.0	0.1	0.0	0.0	0.0
CaO	9.6	9.2	11.5	2.4	0.1	2.7	0.4	2.2	0.1	2.3	0.1	2.2	0.4	2.3	0.6	2.8	1.0	2.5	0.6
Na <sub>2</sub> O	2.0	2.3	2.6	5.4	0.8	4.9	1.5	4.9	0.1	5.3	0.1	5.4	0.7	5.9	0.9	5.2	0.9	5.4	0.8
K <sub>2</sub> O	0.01	0.9	0.2	0.1	0.2	0.1	0.2	0.1	0.0	0.2	0.0	0.1	0.2	0.1	0.2	1.6	0.7	1.3	0.3
P <sub>2</sub> O <sub>5</sub>	0.3	0.1	0.1	0.0	0.1	0.0	0.0	0.0	0.1	0.0	0.0	0.0	0.0	0.0	0.1	0.1	0.1	0.1	0.0
Total	99.5	97.2	99.8	100		100		100		100		100		100		99.3		99.7	
H <sub>2</sub> O <sup>b</sup>				15.9	2.1	15.9	0.6	16.1	0.5	16.9	0.8	18.9	1.1	18.6	0.9				
Na <sub>2</sub> O/CaO				2.2		1.8		2.2		2.3		2.4		2.5		2.4		2.3	
K <sub>2</sub> O/Na <sub>2</sub> O				0.02		0.02		0.02		0.03		0.02		0.01		0.3		0.2	
Ferro <sup>c</sup>				2.7		3.2		3.0		3.0		2.8		2.5		3.0		2.9	
Mg# <sup>d</sup>	38.5	48.2	56.0	25.8		25.7		21.3		15.7		15.6		18.7		43.8		42.9	
A/NK				1.7		1.8		1.8		1.6		1.6		1.5		1.5		1.5	
A/CNK				1.1		1.1		1.2		1.1		1.1		1.0		1.0		1.1	

$\sigma$ —standard deviation.

<sup>a</sup> All Fe is expressed as FeO.

<sup>b</sup> H<sub>2</sub>O contents deduced from totals.

<sup>c</sup> Ferro = TiO<sub>2</sub> + FeO + MgO + MnO.

<sup>d</sup> Mg# = 100 \* Mg / (Mg + Fe<sup>2+</sup> + Fe<sup>3+</sup>).

the experiment and that the experiment will not need to grow a large garnet fraction in order to equilibrate, which can significantly affect melt major and trace element compositions. In experiments which use gels or glasses as the starting material, substantial amounts of garnet must grow in the presence of melt in order to reach high garnet proportions expected at the experimental pressure. Due to vastly different diffusion rates for HREE (Skora et al., 2006) in garnet compared to melt (Chakraborty et al., 1995) and the potentially different rates of garnet and melt formation in the charge, these experimental garnets will be zoned in terms of HREE and consequently contain domains that are not in equilibrium with the melt (Ayres et al., 1997; Carbone and Canil, 2001). We anticipate that this will produce melts enriched in HREE relative to melts in equilibrium with a large garnet fraction with uniformly high HREE. Our experimental design ensures that an appropriate garnet with a uniform distribution of abundant HREE is able to coexist with melt.

A disadvantage is that the large garnet fraction will result in sluggish diffusion under conditions where the mode of garnet is less, or the equilibrium composition of garnet significantly different, to those which characterise the equilibrium assemblage at the run conditions (Carlson, 2006). However, the garnet proportion in DSE4 (~35%) is well matched with the fact that conventional metamorphic modelling suggests garnet proportions of more than 30% are common in MORB compositions within the pressure range of the experiments (Deer et al., 1997). Furthermore, Moyen and Stevens (2006) calculated that a minimum of 15% garnet proportion in the residuum is required to produce the HREE-depleted signature that is typical of high-Al<sub>2</sub>O<sub>3</sub> TTG compositions.

The decision to use a natural basaltic eclogite starting material has consequences for the range of rock compositions available. Suitable material exists only in collisional zones where metamorphosed oceanic crust has been exhumed and this means that compositions are relatively

low in K<sub>2</sub>O concentration and Mg# are low relative to proposed Archaean oceanic crustal compositions (Moyen and Stevens, 2006). The bulk compositions of average N-MORB (Hofmann, 1988; Winter, 2001) and of a basaltic rock from the Pilbara Craton (Coucal Formation (C-F2b)) interpreted to be a plausible source rock composition for some TTG granitoids on the Pilbara craton (Smithies et al., 2009), are given in Tables 2 and 3 for comparison, and displayed in Fig. 1.

DSE4 is characterised by the peak metamorphic mineral assemblage: (~40%) Omp + (~35%) Grt + (~12%) Qtz + (~5%) Rt + (~1%) Aln + (~1%) Ap + (tr) Phg + (tr) Zrn (mineral abbreviations as recommended by Kretz (1983)). Representative garnet and clinopyroxene compositions from DSE4 are provided in Table 4 and Table 5. The clinopyroxene is omphacitic and the garnet is almandine-rich (59.3–60.8% alm; 19.5–21.8% grs; 16.7–19.6% prp; and 1.1% sps) (Table 4). Retrograde ilmenite occurs around relict rutile grains and the ilmenite has a Fe<sub>2</sub>O<sub>3</sub> content consistent with 2% hematite in the solid solution ( $X_{\text{hem}} = 0.5\text{Fe}^{3+} / (\text{Ti} + 0.5\text{Fe}^{3+} + \text{Fe}^{2+}) = 0.02$ ). Minor retrograde symplectitic coronas of amphibole and clinopyroxene intergrowths, with subordinate albitic plagioclase have formed at the expense of garnet and omphacite during decompression. The clinopyroxene crystals of the intergrowths are augitic and less sodic (4.0–2.5 wt.% Na<sub>2</sub>O) than the peak metamorphic omphacite (Table 5). There are two distinct amphibole compositions within the symplectite (magnesianhornblende (2.8 wt.% Na<sub>2</sub>O; 5.4 wt.% Al<sub>2</sub>O<sub>3</sub>); and magnesianhastingsite (1.5 wt.% Na<sub>2</sub>O; 12.5 wt.% Al<sub>2</sub>O<sub>3</sub>). These retrograde intergrowths constitute only a small fraction of the rock (~5%), thus, plagioclase is present in almost negligible amounts.

## 2.2. Experimental set-up and procedure

The experiments were conducted using a Holloway design, non-end-loaded, 12.5 mm piston cylinder apparatus for experiments at





**Table 5**  
Clinopyroxene compositions from DSE4 starting material and experimental run products. Clinopyroxene formulas calculated to 6 oxygen.

P (GPa)	Starting material					Experimental run products											
	10		1		4	1.9		1.9		2.2		2.6		2.9		3.0	
T (°C)	10		1		4	870		900		880		870		870		870	
N	10		1		4	5		5		1		5		1		5	
wt.%	Omp	$\sigma$	Cpx1	Cpx2	$\sigma$	Ave.	$\sigma$	Ave.	$\sigma$	Rep.	Ave.	$\sigma$	Rep.	Ave.	$\sigma$		
SiO <sub>2</sub>	56.3	0.0	54.2	54.4	0.7	53.6	0.0	53.5	0.1	53.2	52.5	0.1	54.8	53.5	0.1		
TiO <sub>2</sub>	0.0	0.0	0.0	0.0	0.0	0.3	0.0	0.2	0.1	0.4	0.2	0.1	0.0	0.0	0.0		
Al <sub>2</sub> O <sub>3</sub>	7.5	0.0	5.1	2.6	0.0	2.0	0.0	1.9	0.0	2.7	1.3	0.0	2.1	1.9	0.0		
Cr <sub>2</sub> O <sub>3</sub>	0.0	0.0	0.0	0.0	0.0	0.2	0.1	0.0	0.0	0.0	0.0	0.0	0.0	0.0	0.0		
Fe <sub>2</sub> O <sub>3</sub>	3.6	0.3	1.7	1.2	2.3	0.0	0.0	0.0	0.0	0.0	0.5	0.0	0.1	0.0	0.0		
FeO	4.8	0.3	7.9	9.9	0.1	11.0	0.0	11.5	1.0	12.6	15.2	0.4	9.6	11.5	1.0		
MnO	0.0	0.0	0.0	0.0	0.0	0.0	0.0	0.0	0.0	0.0	0.0	0.0	0.0	0.0	0.0		
MgO	8.9	0.0	9.8	11.0	0.0	13.1	1.0	12.9	0.0	11.0	11.1	0.2	12.3	12.9	0.0		
CaO	13.6	0.1	17.8	18.6	0.2	18.8	0.8	19.3	0.1	18.3	18.6	0.0	20.4	19.3	0.1		
Na <sub>2</sub> O	6.3	0.1	3.6	2.5	0.0	1.0	0.0	0.8	0.0	1.6	0.9	0.0	1.7	0.8	0.0		
K <sub>2</sub> O	0.0	0.0	0.0	0.0	0.0	0.0	0.0	0.0	0.0	0.0	0.0	0.0	0.0	0.0	0.0		
Totals	100.9		100.1	100.2		99.9		100.0		99.8	100.3		101.0	99.8			
Si	2.0	0.0	12.0	2.0	0.0	2.0	0.0	2.0	0.0	2.0	2.0	0.0	2.0	2.0	0.0		
Ti	0.0	0.0	0.0	0.0	0.0	0.0	0.0	0.0	0.0	0.0	0.0	0.0	0.0	0.0	0.0		
Al	0.3	0.0	0.2	0.1	0.0	0.1	0.0	0.1	0.0	0.1	0.1	0.0	0.1	0.1	0.0		
Cr	0.0	0.0	0.0	0.0	0.0	0.0	0.0	0.0	0.0	0.0	0.0	0.0	0.0	0.0	0.0		
Fe <sup>3+</sup> <sup>a</sup>	0.1	0.0	0.1	0.0	0.0	0.0	0.0	0.0	0.0	0.0	0.0	0.0	0.0	0.0	0.0		
Fe <sup>2+</sup>	0.1	0.0	0.2	0.3	0.0	0.3	0.0	0.4	0.0	0.4	0.5	0.0	0.3	0.4	0.0		
Mn	0.0	0.0	0.0	0.0	0.0	0.0	0.0	0.0	0.0	0.0	0.0	0.0	0.0	0.0	0.0		
Mg	0.5	0.0	0.5	0.4	0.1	0.7	0.0	0.7	0.0	0.6	0.6	0.0	0.7	0.7	0.0		
Ca	0.5	0.0	0.7	0.7	0.0	0.7	0.0	0.8	0.0	0.7	0.8	0.0	0.8	0.8	0.0		
Na	0.4	0.0	0.3	0.2	0.0	0.1	0.0	0.1	0.0	0.1	0.1	0.0	0.1	0.1	0.0		
K	0.0	0.0	0.0	0.0	0.0	0.0	0.0	0.0	0.0	0.0	0.0	0.0	0.0	0.0	0.0		
Sum	4.0		4.0	4.0		4.0		4.0		4.0	4.0		4.0	4.0			
Mg# <sup>b</sup>	71.4		65.0	57.1		68.0		66.6		60.9	55.9		69.3	66.6			
Class <sup>c</sup>	Omp		Aug	Aug		Aug		Aug		Aug	Aug		Aug	Aug			

<sup>a</sup> Fe<sup>3+</sup> calculated using method from Droop (1987).<sup>b</sup> Mg# = 100 \* Mg / (Mg + Fe<sup>2+</sup> + Fe<sup>3+</sup>).<sup>c</sup> Class—Classification. Omp—omphacite; Aug—augite.

the presence of excess water vapour and thus water saturation during the experiment. Diffusive loss of hydrogen from the capsules during the experiments was monitored, by measuring the hematite component in ilmenite, as this has implications for the water content, and this is discussed in Section 3.1.2.

### 2.3. Analytical techniques

The minerals in the starting material, as well as the minerals and glasses in the experimental run products, were analysed by quantitative energy-dispersive X-ray spectroscopy (EDS) and wavelength-dispersive X-ray spectroscopy (WDS) using a Zeiss EVO MA 15 Scanning Electron Microscope (SEM) (Tables 2, 4, 5 and Appendix A Table A1). Major elements were determined via EDS using an Oxford Instruments® X-Max 20 mm<sup>2</sup> detector and Oxford INCA software. Sr concentration in the glasses was selectively quantified via WDS analysis using Oxford Instrument® Wave Dispersive X-ray Spectrometer and Oxford INCA software. Beam conditions during the quantitative analyses were 20 kV and approximately 1.0A, with a working distance of 8.5 mm and a specimen beam current of ~20.00 nA. For mineral and glass analyses counting time was 15 s live-time. Natural mineral standards were used for standardisation and verification of the analyses. The system is designed to perform high-resolution imaging concurrently with quantitative analysis, with errors ranging from ±0.6 to 0.1 wt.% on the major elements using EDS and ±0.01 to 0.03 wt.% on major and trace elements using WDS (Appendix A Table A1). During analyses of the glasses a cryogenic stage was used to cool the sample to below -180 °C. This counteracts the migration-related counting losses on the light elements, especially Na<sub>2</sub>O, that make quantitative analyses of hydrous aluminous silicate glasses problematic (e.g. Vielzeuf and Clemens, 1992). Further details

of the techniques used for mineral and glass analyses are described by Diener et al. (2005), Moyen and Stevens (2006), and Spicer et al. (2004).

Trace element and rare earth element (REE) compositions of the starting rock, and the experimental glasses, from experiments that produced sufficiently large volumes of crystal-free glass to allow for analysis, were determined using a Laser Ablation Inductively Coupled Plasma Mass Spectroscopy (LA-ICP-MS) at Stellenbosch University. For experimental glasses, in situ sampling on polished sections was performed using a 30 µm or 55 µm ablation spot generated by a New Wave 213 nm Nd-YAG Laser coupled to an Agilent 7500ce ICP-MS. Ablation was performed in a He atmosphere with 0.9 L/min in the He carrier gas. The He was mixed with Ar (0.95 L He + 1 L Ar) with a flow rate of 0.9 L/min introduction into the ICP. Operating conditions for the laser were 3 Hz frequency, ~8 J/cm<sup>3</sup> fluence and 20 s counting time, for 30 µm spot size analyses; and 15 Hz frequency, ~5 J/cm<sup>3</sup> fluence and 40 s counting time, for the 55 µm spot size analyses. Trace elements were quantified using a 2-point calibration with a gas blank and NIST-612 glass control standard and measured experimental glass (via EDS) SiO<sub>2</sub> contents were used as an internal standard. Accuracy and reproducibility of multiple analyses were established via the analysis of the secondary standard BHVO 2G, a USGS natural basaltic glass standard. Results were better than 5% relative for most elements in concentrations > 50 ppm and better than 10% relative for elements in concentration < 50 ppm. Data was processed using Glitter (v 4.4.2) software and averages determined from sigma 1 errors and trace element values defined by the software are reported (Table 3). Data was acquired in time resolved mode (Longerich et al., 1996), which allowed potential contamination from mineral inclusions or fractures to be identified and excluded

from the analysis. Additionally, concentrations of Ti, Sr and Ca were used to identify such crystal contamination, as the concentrations of these elements in the glasses were determined by SEM EDS and WDS analysis prior to the LA-ICP-MS investigation. The much higher spatial resolution of the electron beam technique allows for many more analytical spots and easy avoidance of inclusions. Multiple analytical sessions were conducted for each sample during which several 30  $\mu\text{m}$  spot analyses were performed, averaged, and presented in Table 3 for each session. After each such session the sample was ground down (typically by approximately 100 to 50  $\mu\text{m}$ ) and repolished to prepare the surface for further analysis. Thus, the various analytical sessions for each run product represent average experimental glass compositions for different depths within quenched melt pools of the specific sample. This strategy was followed to increase the number of average experimental glass compositions that could be determined per sample. The 30  $\mu\text{m}$  spot size was found to be optimum for producing accurate data with very little contamination; but Yb and Cr were compromised because at this spot size the concentrations of these elements in the glass are close to the limits of detection. The 2.9 GPa–870 °C run product has the largest quenched melt pools and enabled an analytical session during which analyses were obtained using the 55  $\mu\text{m}$  laser spot size. In this case, the elements were divided into 2 groups (REE and non

REE) and each group was analysed with separate spot analysis in order to obtain better quantitative results by increasing the counts per element.

### 3. Experimental results and interpretation

#### 3.1. Mineral compositions and phase relations

Garnet and clinopyroxene were the dominant minerals coexisting with melt at the conditions of the experiments and in all run products quartz was consumed (Fig. 2). Garnet and clinopyroxene compositional details are provided in Tables 4 and 5. The clinopyroxene produced during the experimental runs is less sodic (0.8–1.5 wt.% Na<sub>2</sub>O) and aluminous, and more calcic and MgO rich compared with the clinopyroxene in the starting material. Small remnant cores of un-reacted clinopyroxene (6.3 wt.% Na<sub>2</sub>O) make up a small proportion of the run products. In areas where melt pooled, small euhedral crystals of clinopyroxene appear within the experimental glass (quenched melt) (Fig. 2). Euhedral facets of new garnet are formed on the crushed garnet crystals of the starting material which indicates the production of new garnet as a consequence of melting. The new garnet growth is more difficult to visualise in BSE images than the clinopyroxene, because in most experiments it is very similar in composition to the garnet of the

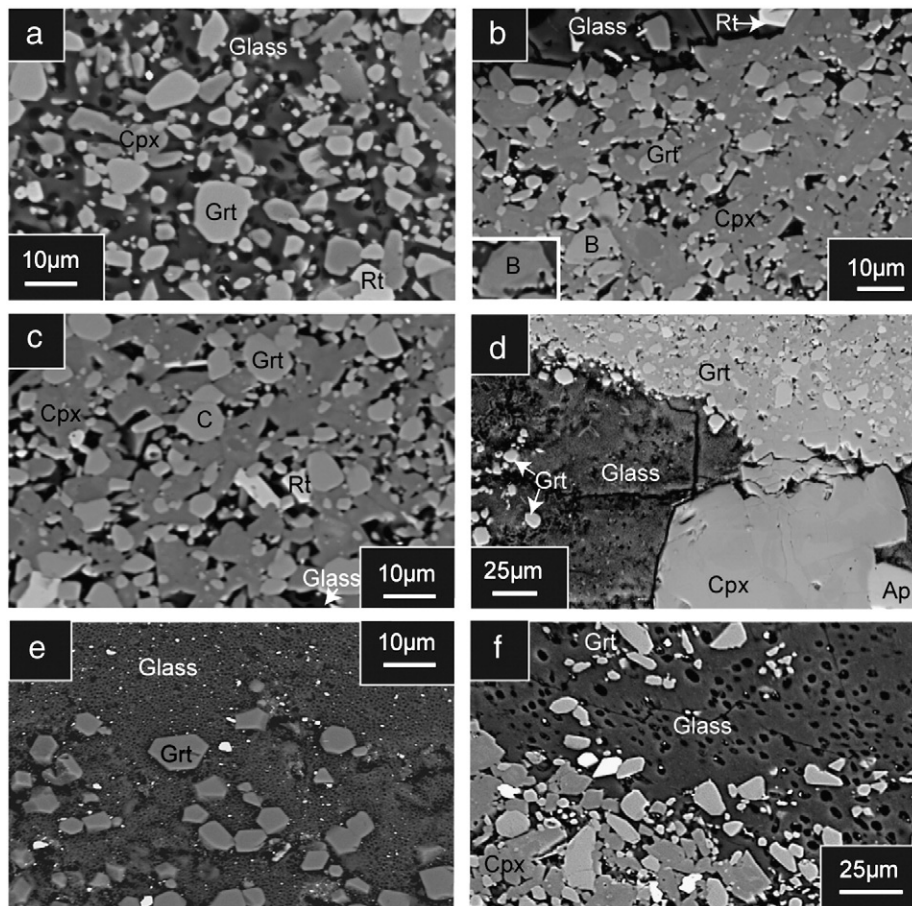


**Fig. 2.** Back-scatter electron (BSE) images of partially melted experimental run products. Melt segregation resulted in crystal-rich domains (a) coexisting with, and adjacent to, domains of nearly crystal-free (e) experimental glass (b, d, e and g). Typical glass textures are illustrated in b,d-f, and particularly well in image e where the contrast of the image has been lowered. Crystal-rich domains are dominated by garnet and clinopyroxene. Abundant faceted crystals indicate that significant crystal growth occurred. Garnet crystals have new garnet rims which have higher Mg#s and can be clearly seen in the inset image B which has been adjusted by increasing the contrast and decreasing the brightness (b). Small euhedral garnet crystals grew, particularly in melt-rich domains (f), and they are chemically identical to the garnet rims which grew within the groundmass. On several occasions large new clinopyroxene crystals grew within melt-rich domains (d) and have the same chemical composition as the groundmass clinopyroxene. Clinopyroxene is characterised by few scattered dark relict Na-rich cores surrounded by extensive newly crystallised lighter clinopyroxene crystals. New clinopyroxene is irregularly zoned and mostly the BSE brightest (i.e. most Na-poor) clinopyroxene is in contact with the experimental glass. In image d, one lone apatite crystal grew in the melt which was the only apatite crystal in the charge. Grt—garnet; Cpx—clinopyroxene; Rt—rutile; Ap—apatite.

starting material, suggesting that the strategy used to select the starting material was sound (see discussion in Section 2.1). The compositional contrast between starting material and neofomed garnet is greatest in experiments above 2.6 GPa and in these experiments the new garnet growth appears slightly darker than the cores in BSE images due to higher Mg# and slightly lower CaO compared to garnet in the starting material (Fig. 2b). The Mg# of the new garnet increases with increasing pressure of the experimental run and slightly with increased temperature runs. Additionally, small euhedral garnet crystals have formed within the experimental glass. Textures consistent with garnet breakdown are evident in run products of experiments below 2.6 GPa, and garnet rims are less extensive and crystals are subhedral. This indicates that in these experiments the equilibrium garnet mode was somewhat less than the garnet fraction in the starting material. However, new garnet rims and faceted garnet crystals adjacent to subhedral garnet crystals do occur in these run products. Rutile was the stable titaniferous phase above 1.9 GPa, despite the persistence of relict ilmenite cores up to 2.2 GPa. At 1.9 GPa, where ilmenite was stable, ilmenite occasionally grows around small relict rutile cores. Where ilmenite occurs, its hematite component ( $X_{\text{hem}} = 0.5\text{Fe}^{3+} / (\text{Ti} + 0.5\text{Fe}^{3+} + \text{Fe}^{2+})$ ) ranges from 0.015 to 0.022 which is less than or similar to the  $X_{\text{hem}}$  component of the ilmenite in the starting material. Apatite occurred as an accessory phase at 2.9 GPa (Fig. 2d). Phase proportions in the run products were determined by least squared mixing calculation using the phase and starting material major element compositions (Table 6). The calculated mineral proportions are consistent with visual estimates of the phase proportions from BSE images of the run products.

Large domains of experimental glass indicate that melt segregated efficiently from residual crystals during many of the experimental runs (Fig. 2). In all experimental run products the experimental glass accumulated adjacent to the gold capsule walls in all directions. The good degree of melt segregation exhibited by these experiments is promoted by the water-saturated nature of the experiments, and the capsule design which presents two crimped ends, largely devoid of starting material powder, into which the melt could wick. The textures produced are similar to the melt segregation textures produced by Grove et al. (2006), in water-present partial melting experiments involving peridotite. EDS analyses of interstitial and segregated melt indicate that there is no systematic major element chemical variation in melt composition with degree of segregation (Table 2). The fact that melt has segregated efficiently in these experiments provided the unique opportunity to analyse the major element compositions of the experimental glasses, as well as of a full range of trace and RE elements in the experimental glasses, without having to use crushed crystalline materials as melt traps (e.g. Hermann et al., 2006).

### 3.1.1. Approach to equilibrium

The run products are characterised by features that appear to demonstrate a reasonable approach to equilibrium, even in refractory minerals. For example, rutile is favoured over ilmenite as pressure increases; and garnet mode and Mg# increase as a function of pressure. New mineral compositions respond in a systematic way to pressure. The persistence of small remnant clinopyroxene and garnet cores indicate that perfect equilibration was not attained; however, these features are common in almost all near-solidus partial melting experimental studies that use mineral mixtures as starting materials (Tepley et al., 2000).

### 3.1.2. Oxygen fugacity

The oxygen fugacity within the experimental charge is an important parameter to control, as hydrogen loss from the capsule would affect the amount of water available for melting. This could not have been a major problem for these experiments as in all cases quartz was the limiting reagent in the melting reactions, as reflected by the absence of quartz in the run products and the weight loss on

**Table 6**

Calculated phase proportions by major element least squared mass balance for the 2.2 GPa–880 °C and the 2.9 GPa–870 °C experimental run products.

P (GPa)	22	29
T (°C)	880	870
Melt	0.19	0.21
Grt	0.40	0.45
Omp	0.11	0.05
Cpx	0.26	0.25
Cpx total	0.36	0.31
Rt	0.01	0.02
Ilm	0.03	
Zr		0.00
Ap		0.01
Sum	1.00	1.00
SSR	0.01	0.34

SSD—sum of squared residuals. Grt—garnet; Cpx—clinopyroxene; Rt—rutile; Ilm—ilmenite; Qtz—quartz; Omp—omphacite; Zr—zircon; Ap—apatite.

piercing and drying of the capsules. The hematite content of ilmenite is a sensitive indicator of reduction–oxidation state within the capsule that can be used as a monitor of oxygen fugacity change during experimental studies of partial melting (e.g. Spicer et al., 2004). All experiments which produced ilmenite have a  $X_{\text{hem}}$  in ilmenite which is very similar to the  $X_{\text{hem}}$  composition of the ilmenite in the starting material. Additionally the  $X_{\text{hem}}$  composition of ilmenite in the “normal” experiments is the same as those where the capsule was compacted within boron nitride powder. Additionally, no other significantly Fe<sup>3+</sup>-bearing minerals are produced. Thus, it is concluded that no appreciable hydrogen loss from the capsule has occurred, which is interpreted as reflecting the fact that the graphite furnace produces an inherently reducing environment (e.g. Médard et al., 2008).

## 3.2. Experimental glass compositions and melting reactions

### 3.2.1. Major element composition of the glasses

The experimental glasses have the compositions of peraluminous trondhjemites (1.8–2.5 Na<sub>2</sub>O:CaO) (1.45–1.83 A/NK; 1.01–1.21 A/CNK) (Fig. 3) (Table 2). They are very silica-rich (74.4–75.3 wt.% SiO<sub>2</sub>; 3.3 wt.% > MgO + FeO + TiO<sub>2</sub> + MnO). They have very low K<sub>2</sub>O (0.1–0.2 wt.% K<sub>2</sub>O) and MgO contents (0.2–0.5 wt.% MgO) and consequently the glasses also have low K<sub>2</sub>O:Na<sub>2</sub>O ratios (0.01–0.03) and Mg#s (15.6–25.8 Mg/(Mg + Fe)); however, this merely reflects the composition of the starting material, which has a very low K<sub>2</sub>O content (<0.1 wt.%) and Mg#(38.5), as discussed in Section 2.1. The experimental glass compositions presented in Table 2 are anhydrous equivalent compositions normalised to 100 wt.% total. The water content in the experimental glass, as estimated from the pre-normalisation wt.% total of the analyses, increases with pressure from 12.9 wt.% H<sub>2</sub>O at 1.9 GPa and 870 °C, to 19.9 wt.% H<sub>2</sub>O at 3.0 GPa and 870 °C. The water content of the glasses is high, as expected for leucocratic melts at high pressure (Sykes et al., 1992).

### 3.2.2. Melting reaction

The textural and mineral chemical evidence documented above suggest that clinopyroxene and quartz are the principle mineral reactants in the wet melting of eclogite. Specifically, the jadeite molecule in clinopyroxene is consumed with quartz, water (2.5–4 wt.% H<sub>2</sub>O), minor garnet and trace amounts of rutile, to produce a trondhjemitic melt. A relatively larger volume of sodium-poor clinopyroxene is produced as the principal solid product of this incongruent melting reaction. In these water saturated experiments quartz was the limiting reagent in the melting reaction. At 2.9 GPa–



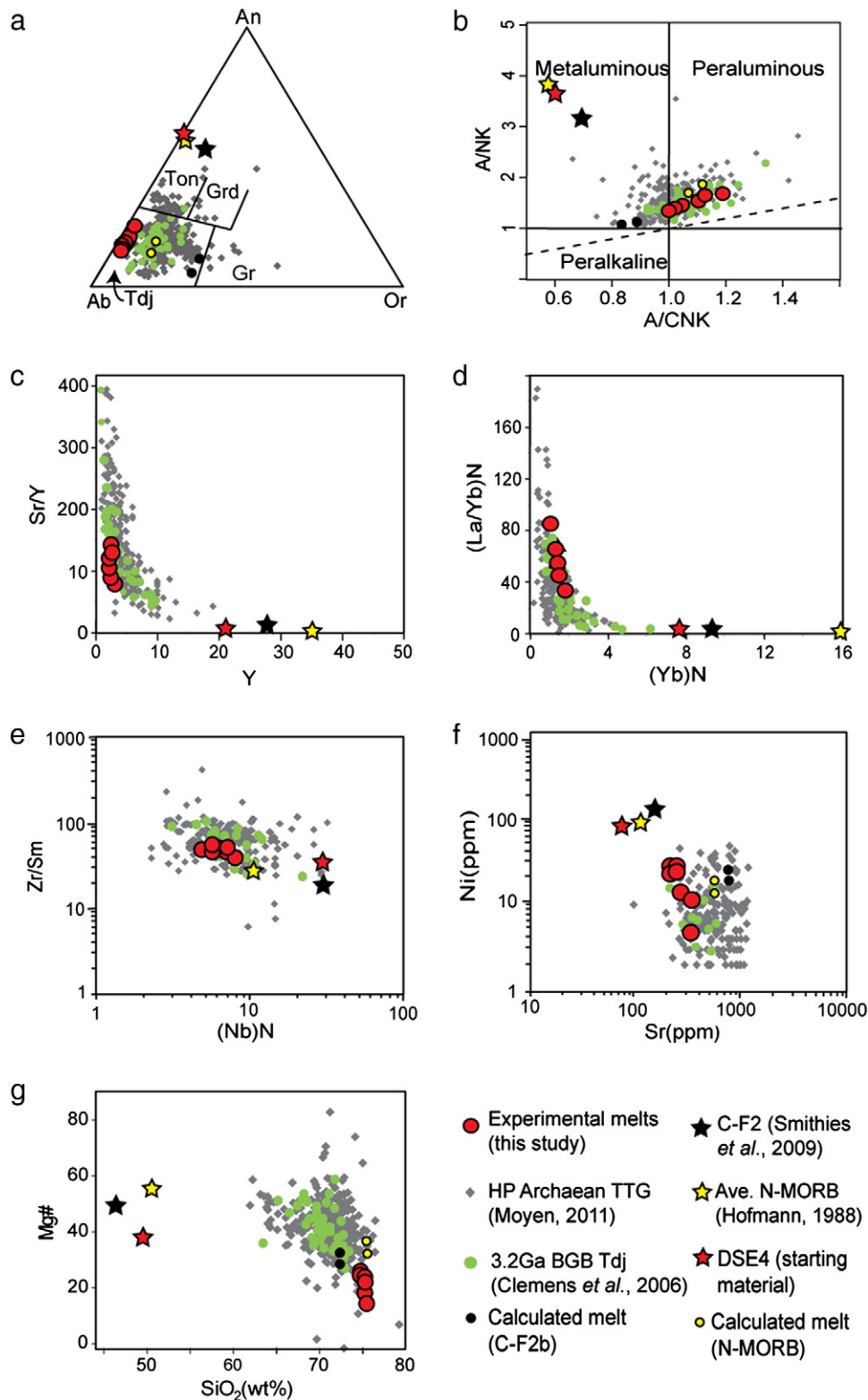


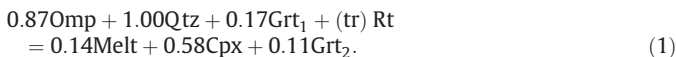
**Fig. 3.** The major and trace element chemistry of the experimental glasses. Red circles represent the experimental glasses produced by this study. The gray symbols represent the high pressure (HP)-type Archaean TTG defined by *Moyen (2011)*. The green circles represent the 3.2 Ga syntectonic trondhjemites of the Barberton granitoid–greenstone terrain (BGGT), South Africa (*Clemens et al., 2006*). The red star represents the composition of starting material DSE4 used in this study, and for comparison, the black star represents the composition of *Smithies et al. (2009)* Pilbara basalt (C-F2b) which represents an Archaean basaltic composition; and the yellow star represents an average N-MORB composition (*Hofmann, 1988*). The yellow and black circles represent the calculated experimental glass compositions for the 2.9 GPa–870 °C run and the 2.2 GPa–880 °C run using the N-MORB starting composition and the C-F2b starting composition respectively. a) The Ab (albite)–An (anorthite)–Or (orthoclase) ternary feldspar diagram (*O'Connor, 1965*) with the granitoid fields defined by *Barker (1979)*. Gr–granite; Tdj–trondhjemite; Ton–tonalite; Grd–granodiorite. b) The *Shand (1943)* A/NK vs. A/CNK diagram. c–f) Measured trace element analyses of the 2.2 GPa–880 °C and 2.9 GPa–870 °C run product glasses. c) Sr/Y vs. Y. d)  $(La/Yb)_N$  vs.  $(Yb)_N$ . The red circles in this diagram represent the spot analyses from session 2.9E (Table 3), where a 55  $\mu\text{m}$  spot was used. Smaller spot sizes were unable to accurately measure Yb. e) Zr/Sm vs.  $(Nb)_N$ . f) Ni vs. Sr. The Archaean TTG data were filtered to remove the anomalously high Ni concentration data ( $>200$  ppm Ni). g) Mg# vs.  $\text{SiO}_2$ .

**Table 7**  
Trace element modelling results and comparison of calculated melt compositions with measured experimental glass compositions. The bulk distribution coefficient ( $D$ ) is calculated for each element using the partition coefficients ( $KD^{min/liq}_{elm}$ ) and the weight fraction of mineral (min) in the rock ( $W_{min}$ ) (see Table 6) via equation:  $D_{elm} = \sum W_{min} KD^{min/liq}_{elm}$ . The concentration of the trace elements in the melt ( $C_L$ ) are calculated using the calculated bulk distribution coefficient and the batch melting equation (Shaw, 1970):  $C_L = C_0 / (D_{elm}(1 - F) + F)$ . Where  $C_0$  is the concentration of the original assemblage before melting, and  $F$  is the weight fraction of the melt produced.

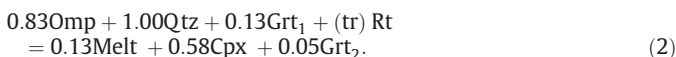
	P (GPa)		2.2											2.9				
	T (°C)		880											870				
	$C_0$	$K_D$	D							Ave. glass	$C_L$	$r$	$\%r$	D	Ave. glass	$C_L$	$r$	$\%r$
	DSE4	Grt	Cpx	Rt	Ap	Zr	Ilm		N=6	Calc.				N=33	Calc.			
Ni	90.1	4.8	7.3	0.0	0.4	0.0	6.8	3.5	8.2	26.7	21.6	364.9	3.0	25.2	34.2	10.0	39.8	
Sr	74.8	0.0	0.0	0.0	1.4	20.0	0.0	0.0	346.1	355.2	9.1	102.6	0.0	238.4	306.5	68.1	28.6	
Y	20.9	14.1	0.6	0.0	17.5	80.0	0.4	7.4	2.6	3.4	0.9	133.6	8.4	2.4	3.1	0.6	26.6	
Zr	94.3	0.5	0.1	3.7	16.0	130.0	2.3	0.5	230.4	165.4	65.0	71.8	0.7	110.1	122.3	12.2	11.0	
Nb	9.2	0.0	0.0	42.8	0.1	50.0	3.0	0.8	1.9	10.0	8.1	527.1	1.7	2.3	5.8	3.5	154.6	
La	7.3	0.0	0.0	0.0	1.2	26.6	0.0	0.0	43.7	34.2	9.5	78.3	0.0	25.2	29.7	4.5	17.8	
Ce	18.2	0.1	0.1	0.0	1.5	23.5	0.0	0.1	86.0	78.3	7.7	91.1	0.1	52.5	68.3	15.8	30.1	
Pr	2.7	0.2	0.1	0.0	17.0	20.0	0.0	0.1		9.2			0.4	5.9	5.5	0.4	6.6	
Nd	9.3	0.2	0.1	0.0	19.0	21.7	0.0	0.2		28.8			0.4	21.4	17.1	4.3	20.0	
Sm	2.5	1.4	0.3	0.1	20.0	17.7	0.0	0.8	4.4	2.9	1.5	66.4	1.2	2.3	2.2	0.1	4.3	
Gd	3.0	4.8	0.4	0.0	20.0	15.0	0.0	2.6	1.8	1.3	0.5	73.4	3.1	1.1	1.1	0.0	2.8	
Tb	0.5	7.8	0.5	0.0	19.0	37.3	0.0	4.1		0.1			4.8	0.2	0.1	0.1	37.9	
Dy	3.4	11.5	0.6	0.0	18.0	60.0	0.0	6.0	0.7	0.7	0.0	95.9	6.9	0.6	0.6	0.0	0.3	
Ho	0.7	15.3	0.6	0.0	16.8	120.0	0.0	7.9		0.1			9.1	0.2	0.1	0.1	52.5	
Er	2.0	18.8	0.6	0.0	15.5	200.0	0.1	9.7		0.3			11.0	0.4	0.2	0.2	42.7	
Tm	0.3	21.5	0.6	0.0	14.2	300.0	0.1	11.1		0.0			12.5	0.1	0.0	0.1	70.3	
Yb	1.9	23.2	0.6	0.0	13.0	490.0	0.1	11.9		0.2			13.5	0.4	0.2	0.2	56.8	
Yb <sub>n</sub>										0.8			1.6		0.7			
La/Yb <sub>n</sub>										121.3			42.6		116.3			
Nb <sub>n</sub>									5.4	28.6			6.5		16.6			
Sr/Y									135.7	104.2			98.7		100.2			
Zr/Sm									52.4	56.6			47.3		54.9			

$r$ —residual.  $\%r$ —percentage of the absolute value of the residual (difference between the calculated value and the measured average glass analysis) out of the average measured glass value; Yb<sub>n</sub>—Yb normalised to chondrite; La/Yb<sub>n</sub>—ratio of chondrite normalised La and chondrite normalised Yb.

870 °C the melting reaction is characterised by the reaction (anhydrous and using a 16 oxygen melt molecule, a 12 oxygen Grt molecule; and a 6 oxygen Cpx molecule):



At 2.2 GPa–880 °C the melting reaction (anhydrous) is characterised by:



### 3.2.3. Systematic variation in experimental glass composition with pressure

The experimental glass compositions vary systematically with pressure. The alkali content of the experimental glasses increases as a function of pressure, which is consistent with the pressure effect described by Moyen and Stevens (2006). However, Moyen and Stevens (2006) propose TTG magmas to predominantly arise through fluid-absent melting of amphibole and attribute the increased alkali contents with smaller melt proportions which developed at higher pressures due to the pressure control on water solubility in the melt. In these experiments melt production is not limited by water availability but by that of quartz, and melt proportions increased slightly with pressure. This may be due to the grossular content in garnet increasing as a function of pressure, and as a result Ca partitions between clinopyroxene and garnet, and SiO<sub>2</sub> is released to increase the melt volume slightly and produce more sodic melts and higher melt fractions at higher pressures. Least squared mixing calculations indicate approximately 19 wt.% melt is produced at 2.2 GPa–880 °C and 21 wt.% melt is produced at 2.9 GPa–870 °C (Table 6). Al<sub>2</sub>O<sub>3</sub> contents and Mg number of the experimental glasses decrease slightly with increasing pressure as garnet becomes more stable. Consequently, an increase of Na<sub>2</sub>O and decrease of Al<sub>2</sub>O<sub>3</sub> contents of the experimental

glasses with increasing pressure of the experimental conditions, result in a diminution of A/CNK ratios of the glasses.

### 3.2.4. Trace element composition of the glasses

Analysis of experimental glass via LA-ICP-MS is difficult, and consequently most studies of this type do not report measured REE and trace element data from experimental glasses. This analytical difficulty is due to two main reasons: 1) Low concentrations must be detected (e.g. HREE), therefore spots of at least 30 μm are typically required for a quantitative analysis; and, 2) quenched melt pools of sufficient size are rare in typical experimental run products, and then the number of pools which are crystal-free to ensure an uncontaminated analysis are virtually non-existent. Consequently, few experimental studies of partial melting have measured trace element compositions of TTG experimental glasses (e.g. Rapp et al., 2010; Foley et al., 2002; Rapp et al., 2003). The same difficulties present themselves in this study and consequently, successful trace element analyses were only performed on the experimental glasses produced in the 2.2 GPa–880 °C and the 2.9 GPa–870 °C experiments, as they were the only run products with large enough melt pools for analyses via LA-ICP-MS. The trace element compositions of the experimental glasses are provided in Table 3 and are characterised by high Zr and Sr; and low Nb and Sm, compared to the source material (Fig. 3d, e, f). They have highly fractionated REE patterns due to high LREE and low HREE, and subsequent high Zr/Sm, Sr/Y and La/Yb ratios compared to the source material.

As explained in Section 2.3, each of the two run products in which sizeable melt pools formed were analysed several times as we sectioned through the sample. The compositional variation between spot analyses in a given analytical session is considered to be insignificant for individual analytical sessions on both the 2.9 GPa–870 °C and 2.2 GPa–880 °C glasses, as the standard deviation from the average composition, for each session, is less than the standard deviation of the measured BHVO standard from the certified composition for the standard (Table 3).

Exceptions to this are Ni, Sm and Gd; however, Sm and Gd occur in abundances less than 2.1 ppm and have standard deviations less than 15%. Compositional variation between the average glass compositions from the two 2.2 GPa–880 °C sessions is less than 15% standard deviation for all the elements, except for Ni. Similarly, compositional variation between average glass compositions from the five 2.9 GPa–870 °C sessions is less than 20% standard deviation for all elements with abundances more than 2 ppm, except for Ni. The above observations indicate that the melt is to some degree heterogeneous in terms of Ni, Cr concentration, and to a significantly lesser extent in terms of Sm and Gd. For example, Ni concentration in 2.2 GPa–880 °C averaged at  $4.3 \pm 0.7$  ppm in analytical session A. In session B, which sampled about 1 mm lower within the run product, Ni concentration averaged at  $12 \pm 6.2$  ppm. Similar figures for 2.9 GPa–870 °C where there were 5 separate analytical sessions are as follows:  $24 \pm 12.8$  ppm;  $25.3 \pm 12.7$  ppm;  $28.7 \pm 4.9$  ppm;  $21.2 \pm 4.7$  ppm;  $28.5 \pm 21.9$  ppm. We interpret this data to reflect a significantly higher concentration of Ni in the melt that existed within 2.9 GPa–870 °C, compared with that in 2.2 GPa–880 °C, as well as the fact that the Ni concentration in the latter melt was not completely homogenous. Thus, the composition of the 2.2 GPa–880 °C glass is richer in Sr, Zr, La, Ce and Sm; and poorer in Ni, compared to the 2.9 GPa–870 °C glass.

### 3.2.5. Trace element modelling

Geochemical modelling of trace element compositions of the glasses ( $C_L$ ) was performed using the composition of the starting material DSE4 ( $C_0$ ); the equilibrium phase proportions which were calculated via least squared mixing calculations (Table 6); and partition coefficients from Bédard (2006) ( $KD^{min/liq}_{elm}$ ; min-mineral, liq-liquid, elm-element). The aim of this modelling is to compare the measured trace element composition of the glasses (Table 7) with the modelled compositions and predict the concentration of elements which were not analysed. The modelling results (Table 7, Fig. 3) indicate that the trace element composition, particularly the enrichment in Sr and LREE, of the experimental glass produced at 2.2 GPa–880 °C compared to the glass produced at 2.9 GPa–870 °C run, can be explained by the presence of small amounts of apatite and zircon in the residuum of the 2.9 GPa–870 °C experimental run product whilst not in the residuum of the 2.2 GPa experimental run product, and by the slightly smaller melt fraction of the 2.2 GPa–880 °C ( $\pm 19$  wt.%) run product compared to the 2.9 GPa–870 °C ( $\pm 21$  wt.%).

## 4. Comparison of experimental glasses with HP-type Archaean TTG

Numerous aspects of the compositions of TTG granitoids have been interpreted to have petrogenetic significance. In the case of HP-type TTGs in particular, their Na<sub>2</sub>O-rich character has been interpreted to reflect a metabasaltic source; their high HREE contents have been interpreted to reflect a high abundance of garnet in the residuum, which is consistent with a formation pressure above 2.0 GPa; their negative Nb anomaly is interpreted to reflect rutile in the residuum, which supports a similarly high pressure in the source (see Moyen and Stevens (2006) for a review on the about listed indicators); and their high Ni and Cr contents, as well as high Mg#s are interpreted to reflect interaction with the mantle wedge during magma ascent (Martin and Moyen, 2002).

Consequently, it is constructive to compare the experimental glasses in this study to a global database of HP-type Archaean TTGs from Moyen (2011). Additionally, the glasses are compared to a database of well preserved syntectonic Meso-Archaean trondhjemites of the Barberton granitoid–greenstone terrain (BGGT), South Africa (Clemens et al., 2006) which provide convincing evidence supporting HP-type TTG formation by anatexis of the upper portions of slabs within Archaean subduction zones (Moyen et al., 2006).

However, in doing so, the nature of the DSE4 source material allows two prominent points of departure to be predicted as mentioned in Section 2.1. The starting material is essentially K<sub>2</sub>O-free, thus, melt compositions will be depleted in K<sub>2</sub>O relative to HP-type Archaean TTG which are proposed to have arisen via the melting of relatively enriched mafic rock compositions (Moyen and Stevens, 2006; Smithies et al., 2009). Similarly, the low Mg# of DSE4 relative to proposed TTG source rock compositions (C-F2b) and N-MORB (Table 2) will ensure low Mg# in the melt. Similar arguments can be presented for Sr concentrations in DSE4, which also differ somewhat from proposed TTG source rocks. These differences are completely source composition imposed and no inference on petrogenetic process should be made on these grounds. Consequently, melt compositions were modelled using a proposed likely TTG source composition (C-F2b) and N-MORB composition (Tables 2 and 3). The results are illustrated on Fig. 3 and the compositions of the melt with regard to Mg#, K<sub>2</sub>O, Sr are consistent with HP-type Archaean TTG trends.

With the exception of the above mentioned chemical parameters, the experimental glasses produced by this study have similar major and trace element compositions and ratios to HP-type Archaean TTG values and in more particular the glasses are similar to 3.2 Ga Barberton trondhjemites (Fig. 3) (Tables 2 and 3). The experimental glasses also have high Ni and Cr contents (4–12 ppm Ni in the 2.2 GPa–880 °C; 14–29 ppm Ni and 43 ppm Cr in the 2.9 GPa–870 °C glass) for leucocratic melts and the compositions are within the chemical range displayed by HP-type Archaean TTG (1–48 ppm Ni, 10 ppm ave. Ni; 1–143 ppm Cr, 21 ppm ave. Cr) and 3.2 Barberton trondhjemites (7–56 ppm Ni, 34 ppm ave. Ni; 8–75 ppm Cr, 37 ppm ave. Cr) (Fig. 3f). Despite the limited number of Ni and Cr analyses obtained for the experimental glasses, the characteristically high Ni and Cr measurements of the glasses may indicate that the high Ni and Cr signature of HP-type Archaean TTG may be source-controlled and be a result of melting Ni- and Cr-bearing omphacite. Consequently, these results potentially challenge the notion that this aspect of TTG geochemistry indicates mantle interaction with the TTG magma prior to emplacement.

## 5. Conclusion

The experimental glasses produced in this experimental study via high pressure (1.9–3.0 GPa) water-present partial melting of an eclogite-facies metabasalt (DSE4) have a peraluminous trondhjemitic composition and their chemical compositions are similar to Barberton 3.2 Ga trondhjemite, and more broadly match the chemical properties of HP-type Archaean TTG, defined by Moyen (2011), in terms of most major, trace and RE elements. Therefore, melt generation via high pressure water-present melting of an eclogitic source appears to be a viable petrogenetic model for the formation of the high pressure (HP)-type trondhjemites which constitute a component of the Paleo- to Meso-Archaean sodic continental crust. We propose that this mechanism of TTG formation involves the upper surface of the subducting slab acting as an anatectic capture site for metamorphic fluid evolved from cooler domains slightly deeper within the hydrated upper portion of the slab which may explain the lack of water-induced mantle melts (andesite or diorites) being produced concurrently with HP-type Archaean TTG magmatism during the Paleo- to Meso-Archaean Eon.

## Acknowledgements

This research was supported by NRF funding to G. Stevens as part of the SARCHI program. J.D. Clemens provided the DSE4 starting material and J-F Moyen provided the Barberton TTG database. R. Rossouw assisted with the trace element analyses.

## Appendix A

Accuracy and precision of EDS and WDS analyses from the University of Stellenbosch SEM configuration.

Cert. Std	Obsidian <sup>a</sup>				Almandine				Plagioclase An65			
	N = 10	Actual	Measured ave.	$\sigma$	$r$	Actual	Measured ave.	$\sigma$	$r$	Actual	Measured Ave.	$\sigma$
SiO <sub>2</sub>	73.9	74.5	0.1	0.4	39.2	39.1	0.3	0.0	54.2	53.3	0.8	0.8
TiO <sub>2</sub>	0.1	0.1	0.0	0.0								
Ti <sup>b</sup>	0.06	0.05	0.0	0.0								
Al <sub>2</sub> O <sub>3</sub>	13.1	12.9	0.1	0.0	22.1	22.3	0.4	0.1	28.5	29.0	0.7	0.2
FeO	1.7	1.8	0.1	0.0	23.3	22.9	0.1	0.1	0.4	0.5	0.0	0.0
MnO					0.6	0.4	0.0	0.1				
MgO	0.1	0.1	0.0	0.0	10.7	11.2	0.1	0.3				
Mg <sup>b</sup>	0.04	0.03	0.0	0.0								
CaO	0.8	0.8	0.0	0.0	4.2	4.2	0.0	0.0	11.8	12.0	0.1	0.0
Na <sub>2</sub> O	4.1	4.1	0.1	0.0					4.4	4.6	0.7	0.0
K <sub>2</sub> O	5.0	5.4	0.0	0.1					0.4	0.4	0.0	0.0
Sr <sup>b</sup>									0.08	0.11	0.0	0.0
H <sub>2</sub> O <sup>c</sup>	0.8	0.8	0.3	0.0								
Cl	0.4	0.4	0.0	0.0								
Total	99.9	100.0			100.0	100.1			100.0	99.8		

$\sigma$ —standard deviation;  $r$ —residual difference between the actual certified composition of the certified standard (Cert. Std) (Internal Astimex Scientific Mineral) and the measured average composition.

<sup>a</sup> Cryostage was used during analysis.

<sup>b</sup> Elements which were measured using WDS.

<sup>c</sup> Deduced from the difference between the measured total and 100 wt.%.

## References

- Alt, J.C., Teagle, D.A.H., 2000. Hydrothermal alteration and fluid fluxes in ophiolites and oceanic crust. In: Dilek, Y., et al. (Ed.), *Ophiolites and Oceanic Crust: New Insights from Field Studies and Ocean Drilling Program*. Geological Society of America Special Paper 349, 273–282.
- Ayres, M., Harris, N., Vance, D., 1997. Possible constraints on anatectic melt residence times from accessory mineral dissolution rates; an example from Himalayan leucogranites. *Mineralogical Magazine* 61 (1), 29–36.
- Barker, F., 1979. Trondhjemite: definition, environment and hypotheses of origin. In: Barker, F. (Ed.), *Trondhjemites, Dacites and Related Rocks*. Elsevier, Amsterdam, pp. 1–12.
- Barker, F., Arth, J.G., 1976. Generation of trondhjemitic–tonalitic liquids and Archaean bimodal trondhjemite–basalt suites. *Geology* 4, 596–600.
- Bédard, J.H., 2006. A catalytic delamination-driven model for coupled genesis of Archaean crust and sub-continental lithospheric mantle. *Geochimica et Cosmochimica Acta* 70, 1188–1214.
- Carbno, G.B., Canil, D., 2001. Mantle structure beneath the SW Slave craton, Canada: constraints from garnet geochemistry in the Drybones Bay Kimberlite. *Journal of Petrology* 43 (1), 129–142.
- Carlson, W.D., 2006. Rates of Fe, Mg, Mn, and Ca diffusion in garnet. *American Mineralogist* 91 (1), 1–11.
- Chakraborty, S., Dingwell, D.B., Rubie, D.C., 1995. Multicomponent diffusion in ternary silicate melts in the system K<sub>2</sub>O–Al<sub>2</sub>O<sub>3</sub>–SiO<sub>2</sub>: I. Experimental measurements. *Geochimica et Cosmochimica Acta* 59 (2), 255–264.
- Clemens, J.D., 1984. Water contents of silicic to intermediate magmas. *Lithos* 17, 273–287.
- Clemens, J.D., Yearron, L.M., Stevens, G., 2006. Barberton (South Africa) TTG magmas: geochemical and experimental constraints on source-rock petrology, pressure of formation and tectonic setting. *Precambrian Research* 151, 53–78.
- Condie, K.C., 1981. *Archaean Greenstone Belts*. Elsevier, Amsterdam, p. 434.
- Connolly, J.A.D., Pettrini, K., 2002. An automated strategy for calculation of phase diagram sections and retrieval of rock properties as a function of physical conditions. *Journal of Metamorphic Geology* 20, 697–708.
- Davies, G.F., 1992. On the emergence of plate tectonics. *Geology* 20 (11), 963–966.
- Deer, W.A., Howie, R.A., Zussman, J., 1997. *Rock Forming Minerals*. The Geological Society, London, p. 570.
- Dick, H.J.B., 2000. A long in situ section of the lower oceanic crust: Results of ODP Leg 176 drilling at the Southwest Indian Ridge. *Earth and Planetary Science Letters* 179, 31–51.
- Diener, J., Stevens, G., Kisters, A.F.M., Poujol, M., 2005. Metamorphism and exhumation of the basal parts of the Barberton greenstone belt, South Africa: constraining the rates of mid-Archaean tectonism. *Precambrian Research* 143, 87–112.
- Droop, G.T.R., 1987. A general equation for estimating the Fe<sup>3+</sup> concentration in ferromagnesian silicates and oxides from microprobe analysis, using stoichiometric criteria. *Mineralogical Magazine* 51, 431–435.
- Drummond, M.S., Defant, M.J., 1990. A model from trondhjemite–tonalite–dacite genesis and crustal growth via slab melting: Archaean to modern comparisons. *Journal of Geophysical Research* 95, 21503–21521.
- Foley, S.F., Tiepolo, M., Vannucci, R., 2002. Growth of early continental crust controlled by melting of amphibolite in subduction zones. *Nature* 417, 837–840.
- Grove, T.L., Chatterjee, N., Parman, S.W., Médard, E., 2006. The influence of H<sub>2</sub>O on mantle wedge melting. *Earth and Planetary Science Letters* 249, 74–89.
- Hermann, J., Spandler, C., Hack, A., Korsakov, A.V., 2006. Aqueous fluids and hydrous melts in high-pressure and ultra-high pressure rocks: implications for element transfer in subduction zones. *Lithos* 92, 399–417.
- Hofmann, A.W., 1988. Chemical differentiation of the Earth – the relationship between mantle, continental-crust, and oceanic-crust. *Earth and Planetary Science Letters* 90 (3), 297–314.
- Kisters, A.F.M., Belcher, R., Poujol, M., Dziggel, A., 2010. Continental growth and convergence-related arc plutonism in the Mesoarchaean: evidence from the Barberton granitoid–greenstone terrain, South Africa. *Precambrian Research* 178, 15–26.
- Kretz, 1983. Symbols for rock-forming minerals. *American Mineralogist* 68, 277–279.
- Longerich, H.P., Jackson, S.E., Günther, D., 1996. Laser ablation inductively coupled plasma mass spectrometric transient signal data acquisition and analyte concentration calculation. *Journal of Analytical Atomic Spectrometry* 11 (9), 899–904.
- Martin, H., 1994. In: Condie, K.C. (Ed.), *The Archaean Grey Gneisses and the Genesis of the Continental Crust in Archaean Crustal Evolution*. Elsevier, Amsterdam, pp. 205–259.
- Martin, H., 1999. The adakitic magmas: modern analogues of Archaean granitoids. *Lithos* 46 (3), 411–429.
- Martin, H., Moyen, J.-F., 2002. Secular changes in TTG composition as markers of the progressive cooling of the Earth. *Geology* 30 (4), 319–322.
- Martin, E., Sigmarsson, O., 2007. Crustal thermal state and origin of silicic magma in Iceland: the case of Torfajökull, Ljósufjöll and Snæfellsjökull volcanoes. *Contributions to Mineralogy and Petrology* 153, 593–605.
- Médard, E., McCammon, C.A., Barr, J.A., Grove, T., 2008. Oxygen fugacity, temperature reproducibility, and H<sub>2</sub>O contents of nominally anhydrous piston–cylinder experiments using graphite capsules. *American Mineralogist* 93 (11–12), 1838–1844.
- Moyen, J.-F., 2011. The composite Archaean grey gneisses: petrological significance, and evidence for a non-unique tectonic setting for Archaean crustal growth. *Lithos* 123, 21–36.
- Moyen, J.-F., Stevens, G., 2006. Experimental constraints on TTG petrogenesis: implications for Archaean geodynamics. In: Benn, K., et al. (Ed.), *Archaean Geodynamics and Environments*, 164. American Geophysical Union Geophysical Monograph, pp. 149–175.
- Moyen, J.-F., Stevens, G., Kisters, A., 2006. Record of mid-Archaean subduction from metamorphism in the Barberton terrain, South Africa. *Nature* 442, 559–562.
- Mysen, B.O., Wheeler, K., 2000. Solubility behaviour of water in haploandesitic melts at high pressure and high temperature. *American Mineralogist* 85 (9), 1128–1142.
- O'Connor, A.C., 1965. A classification for quartz-rich igneous rocks based on feldspar ratios. *United States Geological Survey. Professional Paper* 525B, 79–84.
- Peacock, S.M., van Keken, P.E., Holloway, S.D., Hacker, B.R., Abers, G.A., Fergason, R.L., 2005. Thermal structure of the Costa Rica–Nicaragua subduction zone. *Physics of the Earth and Planetary Interiors* 149, 187–200.
- Rapp, R.P., Shimizu, N., Norman, M.D., 2003. Growth of early continental crust by partial melting of eclogite. *Nature* 425, 605–609.
- Rapp, R.P., Norman, M.D., Laporte, D., Xaxley, G.M., Martin, H., Foley, S.F., 2010. Continental Formation in the Archaean and Chemical Evolution of the Cratonic

- Lithosphere: Melt-Rock Reaction Experiments at 3–4GPa and Petrogenesis of Archean Mg-Diorites (Sanukitoids). *Journal of Petrology* 51 (6), 1237–1266.
- Rudnick, R.L., 1995. Making continental crust. *Nature* 378, 571–578.
- Schmidt, M.W., Poli, S., 1998. Experimentally based water budgets for dehydrating slabs and consequences for arc magma generation. *Earth and Planetary Science Letters* 163, 361–379.
- Schmidt, M.W., Dardon, A., Chazot, G., Vannucci, R., 2004. The dependence of Nb and Ta rutile-melt partitioning on melt composition and Nb/Ta fractionation during subduction processes. *Earth and Planetary Science Letters* 226, 415–432.
- Shand, S.J., 1943. *Eruptive Rocks. Their Genesis, Composition, Classification, and Their Relation to Ore-Deposits with a Chapter on Meteorite*. John Wiley & Sons, New York.
- Shaw, D.M., 1970. Trace element fractionation during anatexis. *Geochim. Cosmochim. Acta* 34, 237–243.
- Skora, S., Baumgartner, L.P., Mahlen, N.J., Johnson, C.M., Pilet, S., Hellebrand, E., 2006. Diffusion-limited REE uptake by eclogite garnets and its consequences for Lu–Hf and Sm–Nd geochronology. *Contributions to Mineralogy and Petrology* 152 (6), 703–720.
- Smithies, R.H., Champion, D.C., 2000. The Archean high-Mg diorite suite: links to tonalite–trondhjemite–granodiorite magmatism and implications for early Archean crustal growth. *Journal of Petrology* 41, 1653–1671.
- Smithies, R.H., Champion, D.C., Cassidy, K.F., 2003. Formation of Earth's early Archean continental crust. *Precambrian Research* 127 (1–3), 89–101.
- Smithies, R.H., Champion, D.C., Van Kranendonk, M., 2009. Formation of Paleoproterozoic continental crust: intracrustal melting of enriched basalt. *Earth and Planetary Science Letters* 281 (3–4), 298–306.
- Spicer, E.M., Stevens, G., Buick, I., 2004. The low-pressure partial melting behaviour of natural boron-bearing metapelites from the Mt. Stafford area, central Australia. *Contributions to Mineralogy and Petrology* 148, 160–179.
- Sykes, D., Sato, R., Luth, R.W., Milln, P., Poet, B., 1992. Water solubility mechanisms in KAlSi<sub>3</sub>O<sub>8</sub> melts at high pressure. *Geochimica et Cosmochimica Acta* 57, 3575–3584.
- Tepley III, F.J., Davidson, J.P., Tilling, R.I., Arth, J.G., 2000. Magma mixing, recharge and eruption histories recorded in plagioclase phenocrysts from El Chichón Volcano, Mexico. *Journal of Petrology* 41 (9), 1397–1411.
- Tuttle, O.F., Bowen, N.L., 1958. Origin of granite in the light of experimental studies in the system NaAlSi<sub>3</sub>O<sub>8</sub>–KAlSi<sub>3</sub>O<sub>8</sub>–SiO<sub>2</sub>–H<sub>2</sub>O. *Geological Society of America Memoirs* 74.
- van Keken, P.E., Kiefer, B., Peacock, S.M., 2002. High-resolution models of subduction zones: implications for mineral dehydration reactions and the transport of water into the deep mantle. *Geochemistry, Geophysics, Geosystems* 3 (10), 1056.
- Vielzeuf, D., Clemens, J.D., 1992. Fluid-absent melting of phlogopite + quartz: experiments and models. *American Mineralogist* 77, 1206–1222.
- Winter, J.D., 2001. In: Lynch, Patrick (Ed.), *An Introduction to Igneous and Metamorphic Petrology*, p. 248.
- Wyllie, P.J., Tuttle, O.F., 1961. Experimental Investigation of silicate systems containing two volatile components, Part II. The effects of NH<sub>3</sub> and HF, in addition to H<sub>2</sub>O, on the melting temperatures of albite and granite. *American Journal of Science* 259, 128–143.

## CHAPTER 3

### **The end of continental growth by TTG magmatism**

#### *A presentation of the research paper*

This research paper is published in *Terra Nova*. I am the first author and Prof. Gary Stevens and Dr Jeroen van Hunen are the co-authors of the paper.

This research paper evaluates the viability of fluid-present eclogite melting to produce HP-type trondhjemites within likely Archaean subduction scenarios and uses numerical and metamorphic models to predict the temperatures and the release of water-rich fluids within the subducting slab. This research paper demonstrates that, for reasonable Archaean mantle wedge temperatures, the bulk of the water produced by metamorphic reactions within the slab is captured by an anatectic zone near the slab surface, which produces melts with compositions very similar to Archaean trondhjemites.

I led all aspects of the metamorphic modelling, calculations and data interpretation under the supervision of Prof. Gary Stevens. I did all of the written work and I created all the diagrams. Prof. Gary Stevens participated in the writing as a typical second author. The numerical modelling was done by Dr Jeroen van Hunen.

# The end of continental growth by TTG magmatism

Angelique Laurie,<sup>1</sup> Gary Stevens<sup>1</sup> and Jeroen van Hunen<sup>2</sup>

<sup>1</sup>Department of Earth Sciences, Centre for Crustal Petrology, Stellenbosch University, Matieland 7602, South Africa; <sup>2</sup>Department of Earth Sciences, Science Laboratories, Durham University, Durham DH1 3LE, UK

## ABSTRACT

High- $\text{Al}_2\text{O}_3$  tonalite, trondhjemite and granodiorite (TTG) magmas characterise felsic Archaean crust, yet are uncommon in the post-Archaean rock record. Consequently, understanding the petrogenesis of these rocks provides valuable insights into early Earth processes. Fluid-absent slab melting represents the dominant hypothesis for the origin of these rocks; however, the absence of voluminous magmas of intermediate composition formed concurrently with these TTGs is incompatible with expectations of slab water loss prior to slab melting. This study demonstrates that for reasonable Archaean mantle

temperatures, slab-derived water is captured by an anatectic zone near the slab surface, which melts via reactions that consume quartz, clinopyroxene and water to produce high- $\text{Al}_2\text{O}_3$  Archaean trondhjemite. Late in the Archaean, the mantle cooled sufficiently to prevent wet melting of the slab, allowing slab water to migrate into the wedge and produce intermediate composition magmatism, which has since been associated with subduction zones.

Terra Nova, 00, 1–7, 2012

## Introduction

The Palaeo- to Meso-Archaean felsic crust is dominated by tonalite, trondhjemite and granodiorite (TTG) series rocks (Jahn *et al.*, 1981; Martin *et al.*, 1983), and in particular, the ‘high- $\text{Al}_2\text{O}_3$ ’ type of TTG (i.e.  $\text{Al}_2\text{O}_3 > 15$  wt% at  $\text{SiO}_2 = 70$  wt%) (Barker and Arth, 1976). The bulk of Earth’s old cratonic crust formed around nuclei of TTG composition, thus these rocks probably formed Earth’s oldest continental crust. Consequently, studies focused on the petrogenesis of these granitoids form the basis for our understanding of the creation and early evolution of Earth’s continental crust. TTG granitoids are uncommon in the post-Archaean rock record. This suggests that a fundamental change occurred on Earth towards the end of the Archaean Eon, which changed the composition of new magma additions to the continental crust from sodic, leucocratic TTG magma to magmas of intermediate composition (andesites and diorites) (*e.g.* Shirey and Hanson, 1984).

Archaean TTG granitoids are characterised by high Na : Ca and Na : K ratios (*e.g.* Moyen, 2011) and are therefore distinct from the calcalkaline magmas, which typify post-

Archaean arcs (Martin, 1994). This study focuses on the high-pressure (HP) variety (Moyen, 2011) of the high- $\text{Al}_2\text{O}_3$ -type TTGs. These rocks are characterised by high Sr content, as well as high La/Yb and low Nb/Ta ratios, which are, respectively, interpreted to indicate the absence of plagioclase, a substantial fraction of garnet (> 15%), and the presence of rutile, in the residuum from which magmas separated (Martin and Moyen, 2002; Rapp *et al.*, 2003; Schmidt *et al.*, 2004; Moyen and Stevens, 2006). Consequently, these magmas are interpreted to arise by partial melting of an eclogite facies metabasalt (Rapp *et al.*, 2003; Moyen, 2011).

Various different geodynamic scenarios have been proposed for the formation of Archaean TTG magmas (*e.g.* Zegers and van Keken, 2001; Foley *et al.*, 2003; Bédard, 2006); however, the required high pressure of partial melting has been interpreted to indicate their formation via anatexis of the upper portions of slabs within Archaean subduction zones (Condie, 1981; Martin, 1994, 1999; Smithies and Champion, 2000; Rapp *et al.*, 2003; Smithies *et al.*, 2003) as a consequence of higher Archaean mantle temperatures (Rudnick, 1995; Albarède, 1998; Prelevic and Foley, 2007).

Melting has generally been considered to occur through fluid-absent processes (*e.g.* Foley *et al.*, 2002; Rapp *et al.*, 2003; Moyen and Stevens, 2006). However, in contrast with the Phanerozoic rock record, there is little

evidence to suggest that slab fluids metasomatise the overlying mantle wedge during the Archaean, as no significant volume of andesites or diorites are commonly produced concurrently with Palaeo- to Meso-Archaean TTGs. Thus, fluid-absent melting fails to account for the substantial amount of water likely to be lost from the subducting slab prior to the conditions for fluid-absent anatexis being attained (Schmidt and Poli, 1998). A potential solution to this problem is to consider the possibility of TTG production by fluid-present melting, as proposed by Drummond and Defant (1990). This notion is supported by recent experimental findings: Laurie and Stevens (2012) produced trondhjemitic melts via water-present melting of an eclogite facies metabasalt, which are very similar in trace and major element composition to the HP-type TTG (Fig. 1). Melting in these experiments occurred via the reaction:  $\text{Qtz} + \text{Cpx}_1 + \text{Grt}_1 + \text{H}_2\text{O} = \text{Melt} + \text{Cpx}_2 + \text{Grt}_2$ , with the involvement of omphacitic clinopyroxene as a reactant being important in shaping both the characteristic major and trace element signature.

This study evaluates the viability of water-fluxed eclogite melting to produce HP-type trondhjemites within likely Archaean subduction scenarios using numeric and metamorphic models to predict the pressure–temperature evolution of different layers within the subducting slab as well as water release from within the slab.

Correspondence: Angelique Laurie, Department of Earth Sciences, Centre for Crustal Petrology, Stellenbosch University, Matieland 7602, South Africa. Tel.: +27 21 808 3127; fax: +27 21 808 3129; e-mail: alaurie@sun.ac.za

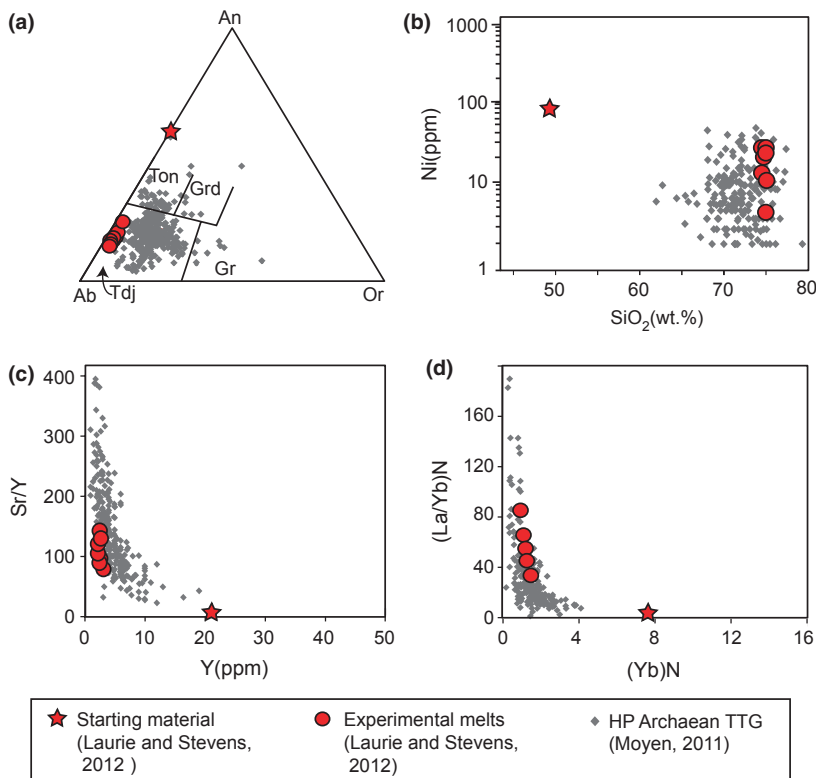


**Fig. 1** The major and trace element chemistry of experimental glasses (red circles) produced via water-present melting of eclogite facies metabasalt (red star) from Laurie and Stevens (2012), compared with the compositions of high-pressure (HP)-type Archaean tonalite, trondhjemite and granodiorite (TTG) defined by Moyen (2011) (grey diamonds). (a) The Ab(albite)-An(anorthite)-Or(orthoclase) ternary feldspar diagram (O'Connor, 1965) with the granitoid fields defined by Barker (1979). Gr-granite; Tdj-trondhjemite; Ton-tonalite; Grd-granodiorite; (b) Ni (p.p.m.) vs. SiO<sub>2</sub> (wt.%); (c) Sr/Y vs. Y (p.p.m.); (d) La/Yb vs. Yb. La and Yb are normalised to chondrite (Thompson, 1982). The experimental melt compositions are trondhjemitic and are characterised by light rare earth element (LREE) enrichment; heavy rare earth element (HREE) and Y depletion; and have high Ni contents for a leucocratic melt; they are very similar in composition to the natural TTGs.

### Modelling

Given the significant uncertainty in many of the parameters that govern the dynamics and thermal structure of assumed Archaean subduction systems (including slab age, subduction velocity, mantle wedge temperature, thermal structure of the overriding plate, latent heat from thermodynamic reactions, and the composition and volume of the magmas produced), a simple modelling approach using first order parameters for a hypothetical Archaean subduction scenario was applied to test the viability and implications of water-fluxed slab melting. The  $P$ - $T$  profiles of the upper portions of subducting slabs were modelled as a function of mantle

temperature [from assumed present-day mantle temperature of 1350 °C (e.g. van Hunen and Moyen, 2012) to 1650 °C], age of the subducting crust and subduction rate. These parameters are considered the primary factors, which control the  $P$ - $T$  paths followed by subducted crust (Peacock *et al.*, 1994).

### Modelling setup

Citcom (Moresi and Gurnis, 1996; Zhong *et al.*, 2000) was used to produce a model of the thermal structure within the subduction zone, using a setup similar to that of model 1a in van Keken *et al.* (2008) and the results are benchmarked against those produced by the van Keken *et al.*'s (2008)

study. Thus, the study uses an analytical corner flow mantle and slab flow model, which is coupled to a numerical temperature advection-diffusion solver; however, the thermal structure of the inflowing slab on the left-hand size boundary was rotated to the slab dip angle. The model resolution used was 2.5-km finite element size. Modelled slab temperatures using this simple scenario are lower than those produced using similar flow models with kinematically prescribed slab motion, but with more complex mantle wedge rheology (e.g. van Keken *et al.*, 2002; Syracuse *et al.*, 2010). Fully dynamic slab models, such as Arcay *et al.* (2007), on the other hand, show similarly cooler slab temperatures to those produced in this study. We adopt this simple mantle rheology model and note that slab temperatures should be considered as lower estimates of possible values. Furthermore, the profiles of present-day subduction zones, which have been modelled using more complex mantle wedge rheology by Syracuse *et al.* (2010) and van Keken *et al.* (2011), are illustrated in Fig. 2bi for comparison.

### Results

The results of the modelling (Fig. 2ai) indicate that the  $P$ - $T$  profiles followed by the upper portions of subducting slabs are dependent on both the age of the slab and the speed of subduction. Younger crust is always warmer and the speed of subduction strongly controls the shape of the  $P$ - $T$  paths. Fast subduction produces a strong temperature inflection of the slab-surface paths towards higher temperatures, whereas the paths of slab interiors show only moderate temperature increase. The temperatures of slow subducting slabs increase approximately consistently over the entire pressure range, with only a very small temperature inflection of the slab surface. Disregarding differences in model parameters, the modelling results are essentially similar to those by Peacock *et al.* (1994) and cooler yet similar in shape to those of Syracuse *et al.* (2010) and van Keken *et al.* (2011) (Fig. 2bi).

Within reasonably young and fast subduction zones, the upper slab surface undergoes near-isobaric heating on progression past the wedge tip and



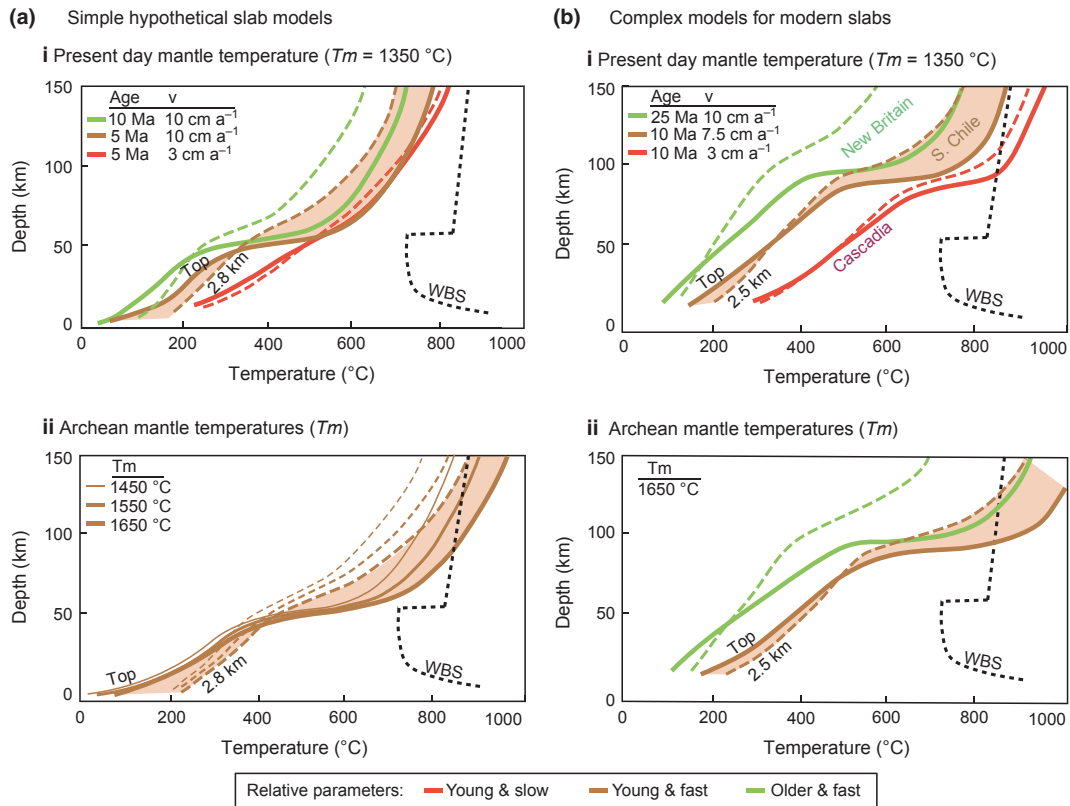


**Fig. 2** Modelled  $P$ – $T$  paths followed by the upper portion of subducting slabs. Bold lines represent the upper slab interface surface and dashed lines represent the slab at a depth of 2.5–2.8 km below the slab surface. (a) Upper slab  $P$ – $T$  paths within hypothetical Archaean subduction zones modelled by applying a simple mantle rheology model and an overriding lithospheric thickness of 50 km (this study). (b) Upper slab  $P$ – $T$  paths modelled by applying a complex mantle rheology model and a slab mantle decoupling until the depth of 80 km (Syracuse *et al.*, 2010; van Keken *et al.*, 2011). (i) Mantle temperature is maintained at modern approximate temperatures (1350 °C) (Moyen and van Hunen, 2012) and slab age and subduction speed ( $v$ ) are varied while all other parameters are kept constant. Disregarding different model parameters, the models in (a) and (b) are similar and indicate that the profiles of young slabs are hotter than those of older slabs (e.g. brown vs. green profiles); slow subduction rates produce hot upper slab profiles with weak internal temperature gradients (red profiles); and fast subduction rates produce upper slab profiles with prominent temperature inflections and strong internal thermal gradients in the upper portion of the slab (green and brown profiles). (ii) The  $P$ – $T$  paths of upper slabs from reasonably young and fast subduction zones modelled for increased mantle temperatures. This is proposed to be the configuration which would satisfy water-fluxed slab melting during the Archaean Eon to produce high-pressure-type trondhjemite. WBS–Wet basalt solidus within plagioclase stability limits represents the haplotonalitic solidus (an = ~50) (Johannes and Holtz, 1996) and at pressures above plagioclase stability, the wet (fluid-present) K-free metamorphic solidus is extrapolated from Kessel *et al.* (2005).

remains the hottest portion of the slab, whilst the underlying slab interiors remain cool. This may provide the most appropriate subduction profile for water-fluxed melting of the upper slab, as the cool hydrated slab interiors may release fluid to flux melting within the hot upper slab due to a warmer Archaean mantle wedge. Although young and slow subduction produces the hottest slabs, this configuration will not satisfy water-fluxed slab melting as slab interiors will dehydrate shortly after the upper slab and when the upper slab reaches temperatures

sufficient for water-present melting, there will be no water to flux slab melting. Consequently, the  $P$ – $T$  paths for young and fast subduction were modelled for increased mantle temperatures and the resultant slab  $P$ – $T$  path shift to higher temperatures (Fig. 2ii).

### Slab dehydration

Water-present melting processes have been argued against on the grounds of the very low porosity of high-grade metamorphic rocks (Peacock *et al.*, 2005). In essence, this follows conven-

tional thinking on the fluid-state during anatexis of the continental crust; however, during the Archaean, fast subduction would create pronounced temperature inversion within the upper portions of slabs on progression past the wedge tip (Fig. 2ii). Oceanic crust is known to be hydrated to considerable depths (2–3 km with 3–5 wt% H<sub>2</sub>O) (Bickle *et al.*, 1994; Alt and Teagle, 2000; Dick, 2000) and the likely degree of hydration for an Archaean subducting slab is proposed to be similar to that of modern crust (e.g. Kusky *et al.*, 2001; Furnes *et al.*,

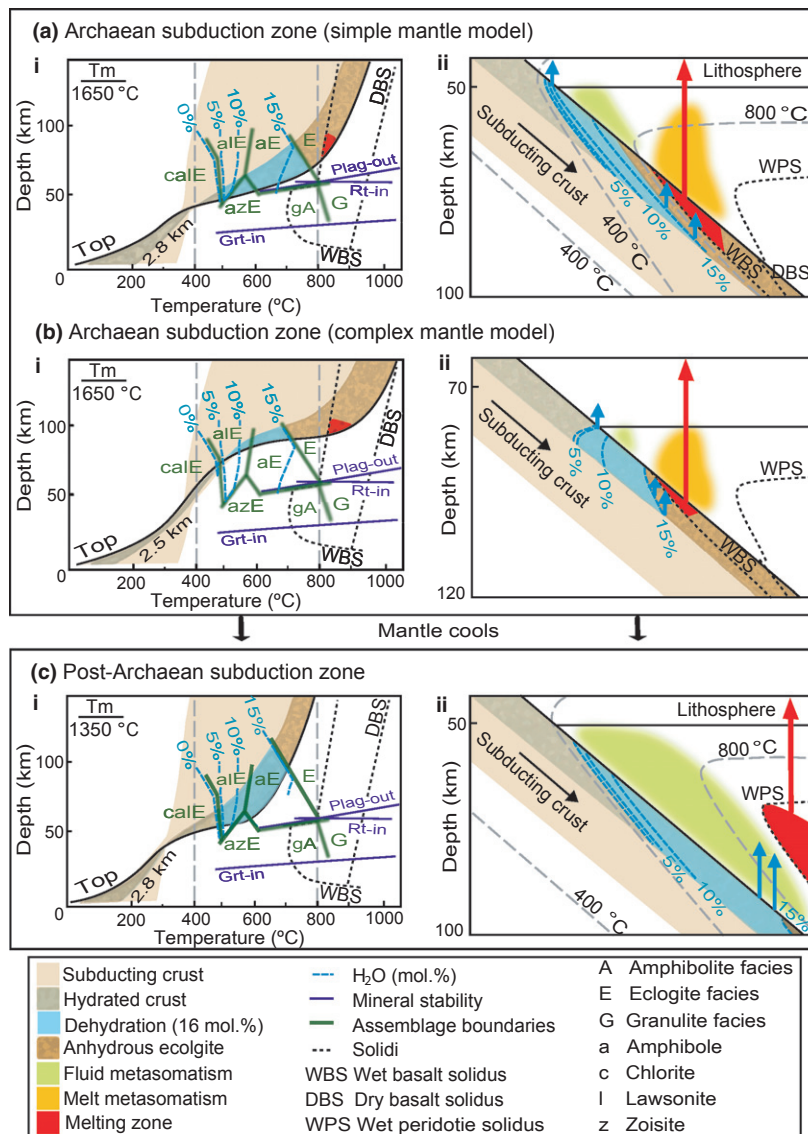


**Fig. 3** A comparison between Archaean and present-day fast subduction of young slabs. (a) Modelled young (5 Ma) and fast (10 cm a<sup>-1</sup>) subducting Archaean slab assuming a 1650 °C mantle with a simple mantle wedge rheology. (b) Modelled young (10 Ma) and fast (7.5 cm a<sup>-1</sup>) Archaean subducting slab assuming a 1650 °C mantle with a complex mantle rheology. (c) Modelled young (5 Ma) and fast (10 cm a<sup>-1</sup>) subducting slab with proposed present-day mantle temperature (1350 °C). (i) The *P–T* paths of the slab surface and the slab at 2.8 km below the slab for each of the three examples (a, b and c). (ii) The thermal structure model of the subduction zone for each of the three examples (grey, dashed lines). Strong temperature gradients exist in the upper portions of the slab, near the slab interface (black line) and produces hot anhydrous upper slab portions that overlie cooler hydrated slab portions beyond the base of the lithosphere of the overriding plate (horizontal black line). In both the Archaean examples (hotter mantle), the upper portions of the slab are above the relevant water-present solidus whilst the underlying slab portions dehydrate. This metamorphic water rises and fluxes melting of the upper slab. In the present-day mantle scenario, the slab is cooler and does not reach temperatures sufficient for water-present or water-absent melting to occur within reasonable depths. Slab dehydration occurs at deeper levels and is more sparsely distributed within the subduction zone compared with within Archaean slabs. Consequently, slab fluids interact with mantle rocks deeper within the wedge that are above their water-present solidus and induce water-fluxed mantle melting. The metamorphic facies boundaries (green lines) and water isopleths (blue dashed lines) are extracted from a Na-Ca-Fe-Mg-Al-Si-H-Ti-O pseudosection (metamorphic equilibrium phase diagram), which was constructed for a basaltic composition (Laurie and Stevens, 2012). The pseudosection was calculated using the software program PERPLEX (Connolly, 1990, 2005; Connolly and Pettrini, 2002), which used the Holland and Powell (1998) thermodynamic dataset. Solid solution models: Gt(HP), Cpx(HP), Opx(HP), TiBio(HP), Am(DHP), feldspar, Ep(HP), Chl(HP) and IlGkPy. 5 wt% water was assumed in the bulk composition and 5% of iron as Fe<sub>2</sub>O<sub>3</sub>, to allow for epidote stability at lower *P–T* conditions. g, garnet. Grt-in (Green, 1982). Rt-in (Zamora, 2000). Plag-out (Holland, 1980). DBS-Green (1982). WPS-Wyllie (1979).

2007). Thus, anatexis of the hottest portions of fast Archaean slabs may indeed be driven by ascending water that is derived from dehydration reactions in deeper slab rocks.

Information on water release by the slab, extracted from a pseudosection (modelled metamorphic phase diagram), predicts that all mineral-bound water (16 mol.% or 5 wt%) within the upper 2.8 km of the slab is released as the slab is heated between 450 and 700 °C (Fig. 3). Details of the pseudosection modelling are provided in the caption to Fig. 3. Dehydration reactions produced within the slab are temperature-dependent, due to near-isobaric upper slab heating, and include the breakdown of chlorite, lawsonite, zoisite and amphibole, which release 5 mol.%, 5 mol.%, 2 mol.% and 4 mol.% water, respectively, as they leave the assemblage.

### Discussion

The results of the thermal and metamorphic modelling suggest that during the Archaean, when Earth's mantle was significantly hotter (e.g.  $T_m = 1650$  °C), fast subducting slabs were characterised by a hot and anhydrous upper portion, which was above the temperature of the relevant water-present eclogite solidus (Kessel *et al.*, 2005) and that this zone was underlain by cooler hydrous metamorphic rocks capable of undergoing substantial dehydration (blue-shaded area Fig. 3a). Consequently, interaction of the metamorphic fluid with the overlying eclogitised slab triggered water-present melting via reactions of the type investigated by Laurie and Stevens (2012) (red-shaded area Fig. 3a) to produce HP-type Archaean TTG. The same conclusions can be drawn from slab models created using more complex mantle wedge rheology (Fig. 3b).

This mechanism provides a regenerating configuration for water-present slab melting that may result in large integrated melt volumes. This is due to the continual supply of new hydrated crust overlain by a new fertile anatectic zone, by the subduction process and allows zones of slab anatexis to function as capture sites for water, which is released from the slab. This accounts for the lack of evidence for Archaean water-induced mantle wedge magmatic products (e.g.

andesites or diorites) forming concurrently with Palaeo- to Meso-Archaean HP-type TTG granitoids. The slab dehydrates (blue-shaded area in Fig. 3) at shallow levels within Archaean subduction zones as a consequence of hotter mantle temperatures and thus only metasomatises a limited portion of the mantle wedge at shallow levels in the subduction zone (green-shaded area Fig. 3). This portion of the mantle is not hot enough for the water to induce mantle wedge melting. Dehydration curves (blue-dashed curves in Fig. 3) are at shallow angles to the slab surface, which promotes water-fluxed melting as ascending slab fluid must traverse the hotter portions of the slab that are above their water-saturated solidus.

The model predicts that fluid-absent melting of amphibole, as proposed by many previous studies, is impossible in this scenario as amphibole reacts out of the assemblage prior to anatectic temperatures being reached. This is consistent with experimental findings on amphibole melting behaviour in metabasalts (e.g. Wyllie and Wolf, 1993). Consequently, if the slab is to melt at attainable temperatures, it must melt by water-present reactions. In addition, the upper portions of the slab are likely to become quartz-depleted, as a consequence of fluid-present melting, making the slab unable to produce further felsic melts via dry-melting at greater depths.

Within the scenario modelled in this study, melting is limited by quartz and mineral modes derived from the pseudosection modelling suggest that the source is capable of producing  $\pm 20$  wt% ( $\pm 35$  vol.%) trondhjemitic melt. This is consistent with melt production estimated from quartz-free mantle eclogite xenoliths considered to be the counterparts to melting in late Archaean subduction zones (Jacob and Foley, 1999; Barth *et al.*, 2001) and with the results of experiments investigating the water-present melting of eclogite at relevant pressures (Laurie and Stevens, 2012). If the anatectic zone is assumed to extend 0.5 km below the slab surface and the subduction rate is  $10 \text{ cm a}^{-1}$  ( $100 \text{ km Ma}^{-1}$ ), then the volume of trondhjemitic melt which can be produced per km of arc length is  $17.5 \text{ km}^3 \text{ Ma}^{-1}$ . These production rates appear consistent with the volume of

the arc-derived Meso-Archaean trondhjemitic, which were emplaced over 60 Ma within the Barberton granitoid-greenstone terrain in South Africa at *c.* 3.23 Ga (Moyen *et al.*, 2006; Kisters *et al.*, 2010). This suggests that the melting mechanism proposed by this study provides a viable explanation for voluminous Archaean HP-type TTG production.

### Implications

The geometries of  $P$ – $T$  paths of the upper portions of fast subducting slabs and the water-present metabasaltic solidus are similar as they both deflect towards higher temperatures at pressures coincident with the wedge tip (Fig. 3). This suggests that a reasonably small decrease in the temperature of the mantle wedge towards the end of the Archaean, which causes the isobaric heating of the slab surface, will induce the abrupt shift away from Archaean TTG magmatism. On cooling of the mantle, slab melting, which formerly acted as a capture mechanism for metamorphic slab fluid, no longer occurred as slabs seldom reached temperatures sufficient for water-present melting. For the first time, slab dehydration fluids, which were now produced deeper within the subduction zone (Fig. 3cii), migrated into the mantle wedge. This mantle material had previously been metasomatised by slab melts, which had not managed to traverse the wedge (orange-shaded area Figs. 3a<sub>ii</sub> and b<sub>ii</sub>). Interaction of this metasomatised mantle with slab water acted to spawn an initial pulse of water-induced melting, which produced enriched mantle melts (sanukitoids) (e.g. Martin *et al.*, 2009; Rapp *et al.*, 2010) and from this time frame onwards, arc-related intermediate calcalkaline magmatism characterised arc settings and arc-related continental growth products (Fig. 3c).

### Acknowledgements

This research was supported by NRF funding to Gary Stevens as part of the SARCHI program. JvH was supported by the European Research Council (ERC StG 279828). We thank P.E. van Keken for providing access to models for various model subduction scenarios. S.F. Foley and P.E. van Keken are thanked for providing constructive reviews that were helpful in improving the manuscript.

## References

- Albarède, F., 1998. The growth of continental crust. *Tectonophysics*, **196**, 1–14.
- Alt, J.C. and Teagle, D.A.H., 2000. Hydrothermal alteration and fluid fluxes in ophiolites and oceanic crust. In: *Ophiolites and Oceanic Crust: New Insights from Field Studies and Ocean Drilling Program* (Y. Dilek, E. Moores, D. Elthon and A. Nicolas, eds). *Spec. Pap.- Geol. Soc. Am.*, **349**, 273–282.
- Arcay, D., Tric, E. and Doin, M.P., 2007. Slab surface temperature in subduction zones: influence of the interplate decoupling depth and upper plate thinning processes. *Earth Planet. Sci. Lett.*, **255**, 324–338.
- Barker, F., 1979. Trondhjemite: definition, environment and hypothesis of origin. In: *Trondhjemites, Dacites and Related Rocks* (F. Barker, ed), pp. 1–12. Elsevier, Amsterdam.
- Barker, F. and Arth, J.G., 1976. Generation of trondhjemitic-tonalitic liquids and Archaean bimodal trondhjemite-basalt suites. *Geology*, **4**, 596–600.
- Barth, M.G., Rudnick, R.L., Horn, I., McDonough, W.F., Spicuzza, M.J., Valley, J.V. and Haggerty, S.E., 2001. Geochemistry of xenolithic eclogites from West Africa, Part I: A link between low MgO eclogites and Archaean crust formation. *Geochim. Cosmochim. Acta*, **65**, 1499–1527.
- Bédard, J.H., 2006. A catalytic delamination-driven model for coupled genesis of Archaean crust and sub-continental lithospheric mantle. *Geochim. Cosmochim. Acta*, **70**, 1188–1214.
- Bickle, M.J., Nisbet, E.G. and Martin, A., 1994. Archaean greenstone belts are not oceanic crust. *J. Geol.*, **102**, 121–138.
- Condie, K.C., 1981. *Archaean Greenstone Belts*. Elsevier, Amsterdam, 434.
- Connolly, J.A.D., 1990. Multivariable phase diagrams: an algorithm based on generalized thermodynamics. *Am. J. Sci.*, **290**, 666–718.
- Connolly, J.A.D., 2005. Computation of phase equilibria by linear programming: a tool for geodynamic modeling and its application to subduction zone decarbonation. *Earth Planet. Sci. Lett.*, **236**, 524–541.
- Connolly, J.A.D. and Petrini, K., 2002. An automated strategy for calculation of phase diagram sections and retrieval of rock properties as a function of physical conditions. *J. Metamorph. Geol.*, **20**, 697–708.
- Dick, H.J.B., 2000. A long in situ section of the lower oceanic crust: results of ODP Leg 176 drilling at the Southwest Indian Ridge. *Earth Planet. Sci. Lett.*, **179**, 31–51.
- Drummond, M.S. and Defant, M.J., 1990. A model from trondhjemite-tonalite-dacite genesis and crustal growth via slab melting: Archean to modern comparisons. *J. Geophys. Res.*, **95**, 21503–21521.
- Foley, S.F., Tiepolo, M. and Vannucci, R., 2002. Growth of early continental crust controlled by melting of amphibolite in subduction zones. *Nature*, **417**, 837–840.
- Foley, S.F., Buhre, S. and Jacob, D., 2003. Evolution of the Archaean crust by delamination and shallow subduction. *Nature*, **421**, 249–252.
- Furnes, H., de Wit, M., Staudigel, H., Rosing, M. and Muehlenbachs, K., 2007. A vestige of Earth's oldest ophiolite. *Science*, **315**, 1704.
- Green, T.H., 1982. Anatexis of mafic crust and high pressure crystallisation of andesite. In: *Andesites* (R. Thorpe, ed), pp. 465–486. J. Wiley and sons, New-York.
- Holland, T., 1980. The reaction albite = jadeite + quartz determined experimentally in the range 600–1200°C. *Am. Mineral.*, **65**, 129–134.
- Holland, T. and Powell, R., 1998. An internally consistent thermodynamic dataset for phases of petrological interest. *J. Metamorph. Geol.*, **16**, 309.
- van Hunen, J. and Moyen, J.-F., 2012. Archaean Subduction: Fact or Fiction? *Annu. Rev. Earth Planet. Sci.*, **40**, 195.
- Jacob, D. and Foley, S., 1999. Evidence for Archaean ocean crust with low high field strength element signature from diamondiferous eclogite xenoliths. *Lithos*, **48**, 317–336.
- Jahn, B.M., Glikson, A.Y., Peucat, J.J. and Hickman, A.H., 1981. REE geochemistry and isotopic data of Archaean silicic volcanics and granitoids from the Pilbara Block, western Australia: implications for the early crustal evolution. *Geochim. Cosmochim. Acta*, **45**, 1633–1652.
- Johannes, W. and Holtz, F., 1996. Petrogenesis and experimental petrology of granitic rocks. In: *Minerals and Rocks Series*, Vol. 22 (P.J. Wyllie, A. El Goresy, W. von Engelhardt and T. Hahn, eds), pp. 335. Springer-Verlag, Berlin.
- van Keken, P.E., Kiefer, B. and Peacock, S.M., 2002. High-resolution models of subduction zones: implications for mineral dehydration reactions and the transport of water into the deep mantle. *Geochem. Geophys. Geosys.*, **3**, 1056.
- van Keken, P.E., Currie, C., King, S.D., Behn, M.D., Cagnioncle, A., He, J.H., Katz, R.F., Lin, S.C., Parmentier, E.M., Spiegelman, M. and Wang, K.L., 2008. A community benchmark for subduction zone modeling. *Phys. Earth Planet. In.*, **171**, 187–197.
- van Keken, P.E., Hacker, B.R., Syracuse, E.M. and Abers, G.A., 2011. Subduction factory: 4. depth-dependent flux of H<sub>2</sub>O from subducting slabs worldwide. *J. Geophys. Res.*, **116**, B01401.
- Kessel, R., Ulmer, P., Pettke, T., Schmidt, M.W. and Thompson, A.B., 2005. The water-basalt system at 4 to 6 GPa: phase relations and second critical endpoint in a K-free eclogite at 700 to 1400°C. *Earth Planet. Sci. Lett.*, **237**, 873–892.
- Kisters, A.F.M., Belcher, R., Poujol, M. and Dziggel, A., 2010. Continental growth and convergence-related arc plutonism in the Mesoarchaean: evidence from the Barberton granitoid-greenstone terrain, South Africa. *Precambrian Res.*, **178**, 15–26.
- Kusky, T.M., Li, J.H. and Tucker, R.T., 2001. The Archaean Dongwanzi ophiolite complex, North China craton: 2.505 billion year old oceanic crust and mantle. *Science*, **292**, 1142–1145.
- Laurie, A. and Stevens, G., 2012. Water-present eclogite melting to produce Earth's early felsic crust. *Chem. Geol.*, **314–317**, 83–95.
- Martin, H., 1994. The Archaean grey gneisses and the genesis of the continental crust in Archaean crustal evolution. In: *Archaean Crustal Evolution* (K.C. Condie, ed), pp. 205–259. Elsevier, Amsterdam.
- Martin, H., 1999. The adakitic magmas: modern analogues of Archaean granitoids. *Lithos*, **46**, 411–429.
- Martin, H. and Moyen, J.-F., 2002. Secular changes in TTG composition as markers of the progressive cooling of the Earth. *Geology*, **30**, 319–322.
- Martin, H., Chauvel, C. and Jahn, B.M., 1983. Major and trace element geochemistry and crustal evolution of Archaean granodioritic rocks from eastern Finland. *Precambrian Res.*, **21**, 159–180.
- Martin, H., Moyen, J.-F. and Rapp, R., 2009. The sanukitoid series: magmatism at the Archaean-Proterozoic transition. *Earth Env. Sci. T. R. So.*, **100**, 15–33.
- Moresi, L.N. and Gurnis, M., 1996. Constraints on the lateral strength of slabs from three dimensional dynamic flow models. *Earth Planet. Sci. Lett.*, **138**, 15–28.
- Moyen, J.-F., 2011. The composite Archaean grey gneisses: petrological significance, and evidence for a non-unique tectonic setting for Archaean crustal growth. *Lithos*, **123**, 21–36.
- Moyen, J.-F. and Stevens, G., 2006. Experimental constraints on TTG petrogenesis: implications for Archaean geodynamics. In: *Archaean Geodynamics and Environments* (K. Benn, J.-C. Mareschal and K.C. Condie, eds). *AGU Geophys. Monogr. Ser.*, **164**, 149–175. AGU, Washington, DC.
- Moyen, J.-F. and van Hunen, J., 2012. Short-term episodicity of Archaean plate tectonics. *Geology*, **40**, 451–454.
- Moyen, J.-F., Stevens, G. and Kisters, A., 2006. Record of mid-Archaean subduction from metamorphism in the Barber-

- ton terrain, South Africa. *Nature*, **442**, 559–562.
- O'Connor, A.C., 1965. A classification for quartz-rich igneous rocks based on feldspar ratios. *U.S. Geol. Surv. Prof. Pap.*, **525B**, 79–84.
- Peacock, S.M., Rushmer, T. and Thompson, A.B., 1994. Partial melting of subducting oceanic crust. *Earth Planet. Sci. Lett.*, **121**, 227–244.
- Peacock, S.M., van Keken, P.E., Holloway, S.D., Hacker, B.R., Abers, G.A. and Ferguson, R.L., 2005. Thermal structure of the Costa Rica–Nicaragua subduction zone. *Phys. Earth Planet In.*, **149**, 187–200.
- Prelevic, D. and Foley, S.F., 2007. Accretion of arc-oceanic lithospheric mantle in the Mediterranean: evidence from extremely high-Mg olivines and Cr-rich spinel inclusions in lamproites. *Earth Planet. Sci. Lett.*, **256**, 120–135.
- Rapp, R.P., Shimizu, N. and Norman, M.D., 2003. Growth of early continental crust by partial melting of eclogite. *Nature*, **425**, 605–609.
- Rapp, R.P., Norman, M.D., Laporte, D., Yaxley, G.M., Martin, H. and Foley, S.F., 2010. Continent formation in the Archaean and chemical evolution of the Cratonic lithosphere: melt-rock reaction experiments at 3–4 GPa and petrogenesis of Archean Mg-Diorites (Sanukitoids). *J. Petrol.*, **51**, 1237–1266.
- Rudnick, R.L., 1995. Making continental crust. *Nature*, **378**, 571–578.
- Schmidt, M.W. and Poli, S., 1998. Experimentally based water budgets for dehydrating slabs and consequences for arc magma generation. *Earth Planet. Sci. Lett.*, **163**, 361–379.
- Schmidt, M.W., Dardon, A., Chazot, G. and Vannucci, R., 2004. The dependence of Nb and Ta rutile-melt partitioning on melt composition and Nb/Ta fractionation during subduction processes. *Earth Planet. Sci. Lett.*, **226**, 415–432.
- Shirey, S.B. and Hanson, G.N., 1984. Mantle-derived Archaean monzodiorites and trachyandesites. *Nature*, **310**, 222–224.
- Smithies, R.H. and Champion, D.C., 2000. The Archaean high-Mg diorite suite: links to tonalite–trondhjemite–granodiorite magmatism and implications for early Archaean crustal growth. *J. Petrol.*, **41**, 1653–1671.
- Smithies, R.H., Champion, D.C. and Cassidy, K.F., 2003. Formation of Earth's early Archaean continental crust. *Precambrian Res.*, **127**, 89–101.
- Syracuse, E.M., van Keken, P.E. and Abers, G.A., 2010. The global range of subduction zone thermal models. *Phys. Earth Planet. In.*, **183**, 73–90.
- Thompson, R.N., 1982. Magmatism of the British Tertiary province. *Scottish J. Geol.*, **18**, 49–107.
- Wyllie, P.J., 1979. Magmas and volatile components. *Am. Mineral.*, **654**, 469–500.
- Wyllie, P.J. and Wolf, M.B., 1993. Amphibolite dehydration-melting: sorting out the solidus. In: *Magmatic Processes and Plate Tectonics* (H. M. Prichard, T. Alabaster, N.B.W. Harris and C. R. Neary, eds). *Geol. Soc. Spec. Publ.*, **76**, 405–416.
- Zamora, D., 2000. *Fusion de la croûte océanique subductée: approche expérimentale et géochimique*. Thèse d'université thesis, Université Blaise-Pascal, Clermont-Ferrand.
- Zegers, T. and van Keken, P.E., 2001. Middle Archaean continent formation by crustal delamination. *Geology*, **29**, 1083–1086.
- Zhong, S.J., Zuber, M.T., Moresi, L. and Gurnis, M., 2000. Role of temperature-dependent viscosity and surface plates in spherical shell models of mantle convection. *J. Geophys. Res.-Sol. Ea.*, **105**, 11063–11082.

Received 21 June 2012; revised version accepted 16 October 2012

## CHAPTER 4

### **The water-saturated low-K<sub>2</sub>O eclogite solidus: Implications for the generation of Earth's early felsic continental crust**

#### *A presentation of the research paper*

This research paper is submitted to *Contributions to Mineralogy and Petrology*. I am the first author and Prof. Gary Stevens is the co-author.

This research paper has experimentally investigated partial melting of eclogite via the reaction  $\text{H}_2\text{O} + \text{Cpx} + \text{Quartz} \pm \text{Grt}$  between 1.6 and 3.0 GPa, and 700 and 900 °C. Three different starting materials were used, a natural low-K<sub>2</sub>O eclogite, a gel of similar composition to the eclogite, as well a synthetic eclogite formed by subsolidus crystallisation from the gel. This research paper experimentally defines the fluid-present low-K<sub>2</sub>O metabasaltic solidus at eclogite-facies pressures (1.8 – 3.0 GPa). The partial melting behaviour of the natural and synthetic eclogite samples demonstrate that the solidus shifts to higher temperatures at pressures above the plagioclase-out reaction. Experiments using the gel starting material undergo metastable melting at a temperature below the wet eclogite solidus and consequently do not resolve the solidus accurately.

All aspects of the sample preparation, experiments, data acquisitions and calculations were lead by me under the supervision of Prof. Gary Stevens. I did all of the written work and I created all the diagrams. Prof. Gary Stevens conceptualized the research idea and participated in the writing as a typical second author. Dr Esme Spicer analysed the whole rock composition of the starting material using XRF.

## The water-saturated low-K<sub>2</sub>O eclogite solidus: Implications for the generation of Earth's early felsic continental crust.

Angelique Laurie · Gary Stevens

**Abstract** In contrast to post-Archaean calc-alkaline arc-related granitoids, the Tonalite-Trondhjemite-Granodiorite (TTG) granitoids, which dominate Paleo- and Meso-Archaean felsic continental crust, are Na-rich and relatively Ca- and K-poor. The high-pressure-subtype of TTG, which forms a substantial fraction of this Archean crust, has been interpreted to arise via the melting of basaltic rocks at eclogite-facies pressures within subduction zones. The absence of rocks of intermediate composition formed in association with these TTGs suggests that TTG magma formation was likely to have consumed fluid produced by slab devolatilisation. Consequently, this study has experimentally investigated partial melting of eclogite via the reaction  $\text{H}_2\text{O} + \text{Cpx} + \text{Quartz} \pm \text{Grt}$  between 1.6 and 3.0 GPa, and 700 and 900 °C. Three different starting materials were used, a natural low-K<sub>2</sub>O (< 0.01 wt.% K<sub>2</sub>O) eclogite, a gel of similar composition to the eclogite, as well as a synthetic eclogite formed by subsolidus crystallisation from the gel. The experimental melt compositions above 1.8 GPa are trondhjemitic and similar in major and trace element composition to high-pressure-type TTG. The partial melting behaviour of the natural and synthetic

eclogite samples demonstrate that the solidus shifts to higher temperatures at pressures above the plagioclase-out reaction. Experiments using the gel starting material undergo metastable melting at a temperature below the wet eclogite solidus and consequently do not resolve the solidus accurately. Likely *P-T* paths followed by the upper portion of Archaean subducting slabs intersect the solidus at pressures consistent with the geochemical signature of these TTG rocks. Modelling suggests that a relatively small decrease in mantle wedge temperature results in the upper slab not intersecting the solidus. Consequently, the wet low-K<sub>2</sub>O eclogite solidus has important implications for understanding the shift from TTG to calc-alkaline granitoid compositions that is recorded in several areas during the late Archaean.

### Introduction

For all of Earth's post-Archaean history, the reactions that have produced and continue to produce granitoid magmas in arc settings typically consume plagioclase as a major reactant. The resultant magmas contain Na and Ca in proportions that define the calc-alkaline compositional trend. This process is considered to begin with H<sub>2</sub>O-saturated partial melting of peridotite in the mantle wedge that is induced by the ascent of slab derived water-rich fluids or melts (Grove *et al.* 2006). The resultant initially near water-saturated

---

A. Laurie (✉) · G. Stevens

Department of Earth Sciences, Centre for Crustal Petrology, Stellenbosch University, Matieland 7602, South Africa.  
e-mail: [alaurie@sun.ac.za](mailto:alaurie@sun.ac.za)

mantle melts rise through the mantle wedge, equilibrating with hotter and dryer mantle, to ultimately produce the basalts and andesites that characterise this setting (Grove *et al.* 2006). The re-melting of juvenile continental crust of intermediate average composition, consisting largely of andesite and related volcanoclastic sedimentary material, produces the calc-alkaline I-type series granitoids associated with arcs (e.g. Clemens *et al.* 2011; Gill 1981; Hildreth *et al.* 1987; Miller and Harris 1989). Pressure in the source areas for these granites is typically within the stability limits of plagioclase ( $< 1.8$  GPa at the high temperatures involved).

In contrast with calc-alkaline I-type granitoids, the tonalite, trondhjemite and granodiorite (TTG) rock compositions, which dominate Paleo- and Meso-Archaean felsic continental crust, are Na-rich and relatively Ca-poor (Jahn *et al.* 1981; Martin *et al.* 1987). Thus, they depart markedly from the calc-alkaline trend (Fig. 1) (Martin 1994). Thus, despite the fact that substantial evidence exists in favour of their genesis in association with arcs, their petrogenesis must be fundamentally different to the calc-alkaline I-type granites.

Archaean TTG granitoids are proposed to arise through the partial melting of an a metabasaltic

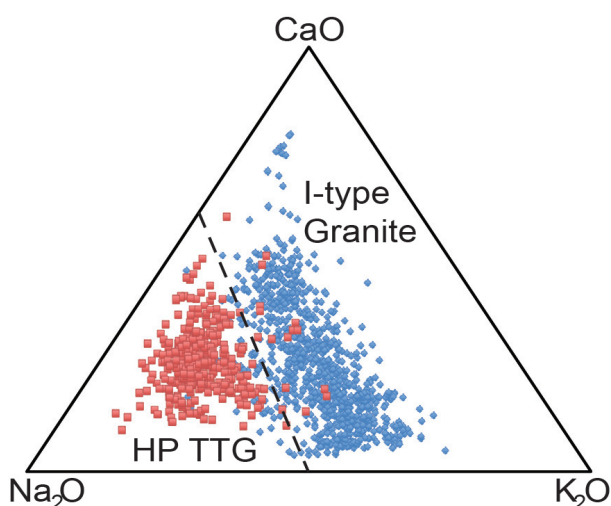


**Fig. 1**  $Na_2O$ - $K_2O$ - $CaO$  ternary diagram comparing sodic Archaean high-pressure(HP)-type Tonalite-Trondhjemite-Granodiorite (TTG) granitoids (red squares) (Moyen 2011) which characterised Archaean continental growth products with more calcic calc-alkaline I-type granitoids which characterise post-Archaean arc-related continental growth products (blue diamonds).

source (e.g. Moyen and Stevens 2006) and can be classified on the basis of their geochemistry according to the pressure at which the magmas arose (Moyen 2011). The High Pressure (HP) ( $>1.8$  GPa) variety (Moyen 2011) are predominantly trondhjemitic and are characterised by high Sr content (typically  $> 300$  ppm), high La/Yb ratios (Ave. 56) and low Nb concentration (typically  $< 7$  ppm), which are respectively interpreted to indicate the absence of plagioclase, a substantial fraction of garnet ( $>15\%$ ), and the presence of rutile in the residuum from which the magmas separated (Martin and Moyen 2002; Rapp *et al.* 2003; Schmidt *et al.* 2004; Moyen and Stevens 2006). Consequently, these magmas are interpreted to arise by partial melting of a metabasaltic source under eclogite-facies conditions (Rapp *et al.* 2003; Moyen 2011), particularly within the pressure range of 1.8 and 3.0 GPa, suggesting their formation by the anatexis of the upper portions of slabs within Archaean subduction zones (e.g. Condie 1981; Martin 1994; Smithies and Champion 2000; Rapp *et al.* 2003). Slab melting has been proposed as a generally viable process during Archaean times, as a consequence of higher Archaean mantle temperatures (Rudnick 1995; Albarède 1998; Prelevic and Foley 2007). As eclogite contains insignificant amounts of mineral-bound  $H_2O$ , the fluid-absent fertility of such sources for producing granite magma is very limited (e.g. Stevens and Clemens 1993). Consequently,  $H_2O$ -present melting is necessary to produce HP-type TTG magmas. Laurie *et al.* (2012b) demonstrated that within potential Archaean subduction zones, slab-derived metamorphic water is likely to have induced fluid-present anatexis of the upper eclogite layers of the slab and hence provide a viable genetic model for HP-type Archaean TTG, as was first proposed by Drummond and Defant (1990).

The water-present melting of metabasaltic sources at pressures in excess of plagioclase stability, is likely to have important implications for both solidus temperature and melt composition. Under eclogite-facies conditions Na will reside in the jadeite component of Cpx. Thus, in the absence of significant  $K_2O$  in the source, fluid-present partial melting must occur via a reaction that consumes water, quartz or coesite and clinopyroxene (Kessel *et al.* 2005). In a recent experimental study investigating the major and trace element compositions of the melts produced by



this process, Laurie and Stevens (2012a) documented the relevant reaction to be  $H_2O + Cpx + Grt + Quartz = Melt + Grt_2 + Cpx_2$  (mineral abbreviations throughout this work are as recommended by Kretz (1983)), and demonstrated that the melt compositions produced are trondhjemitic and are very similar to Archaean HP-type TTG granitoid compositions. The entropy of clinopyroxene is significantly lower than that of plagioclase which is the dominant pre-anatectic Na-bearing phase at pressures below 1.8 GPa (Holland 1989). Consequently, low- $K_2O$  eclogites should undergo partial melting at higher temperatures than chemically equivalent plagioclase-bearing assemblages (Nichols *et al.* 1994). This behaviour will be less apparent in relatively  $K_2O$ -rich rocks, where initial melting will occur by similar reactions under eclogite facies conditions and at lower pressures, due to K always residing in high entropy micas (typically biotite or phengite) (Holland 1989). Evaluation of the magnitude of the solidus shift that must occur in low- $K_2O$  metamafic rocks on entering the eclogite facies is difficult to evaluate because the location of the fluid-present solidus for such rocks has not been experimentally described at pressures within the lower pressure portion of the eclogite-facies, that is important for HP-type TTG genesis (1.8-3.0 GPa). However, the contrasting experimental results of Johannes and Holtz (1996), which located the water-present low- $K_2O$  haplotonalitic solidus ( $Qtz + Pl + H_2O$ ) between 690 °C and 750 °C in the 0.5 GPa to 1.5 GPa pressure interval, and the study of Kessel *et al.* (2005) (Fig. 2), which located the water-present low- $K_2O$  eclogite solidus at 4.0 GPa to lie between 850 °C and 900 °C, suggest an increase in the water saturated solidus temperature on entering the eclogite facies. Understanding the partial melting of mafic rocks within the lower pressure portion of the eclogite facies is crucial to understanding the petrogenesis of the high-pressure variety of Archaean TTG magmas, this study experimentally investigates the partial melting of the assemblage  $Omph + Grt + Qtz + H_2O$  between 1.6 and 3 GPa.

### Experimental and analytical techniques

Water-present partial melting experiments were con-

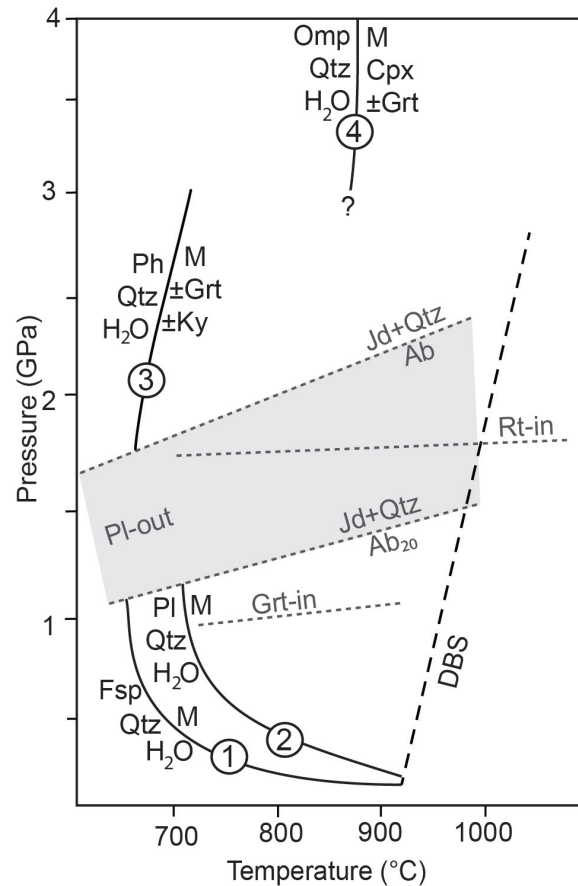


**Fig. 2:** *P-T* diagram illustrating previously defined solidi. The water-present haplogranitic ( $Fsp + Qtz + H_2O = Melt$ ) (solidus 1) and haplotonalitic ( $Pl + Qtz + H_2O = Melt$ ) (solidus 2) solidi at pressures within plagioclase stability (Johannes and Holtz 1996) and the water-present phengite (solidus 3) (Nichols *et al.* 1994) and low- $K_2O$  (<0.1 wt.%  $K_2O$ ) metabasaltic solidi (solidus 4) (Kessel *et al.* 2005). Solid black lines indicate solidi. Mineral stabilities are indicated by dashed grey lines. The grey shaded area represents the pressure range of the plagioclase-out reaction (albite-jadeite transition) which depends on the plagioclase compositions ( $Ab = Jd + Qtz$ ; and  $Ab_{20} = Jd + Qtz$ ) (Helgeson *et al.* 1978). M-Melt, Ph-Phengite, Omp-Omphacite, Cpx-Clinopyroxene, Px-Pyroxene, Grt-garnet, Qtz-Quartz, Pl-Plagioclase, Fsp-Feldspar including orthoclase and plagioclase. The black dashed line represents the dry (fluid-absent) basalt solidus (DBS) of (Green 1982).

ducted between 1.5 GPa and 3.0 GPa and 700 °C and 900 °C (Table 1). The experimental results reported in this study include those reported in the study by Laurie and Stevens (2012a), which investigated the compositions of melts produced by water-present eclogite melting between 870 °C and 900 °C within the pressure interval 1.9 GPa to 3.0 GPa.

**Table 1:** Experimental run conditions and experimental products.

Exp. Run	Starting material	P (GPa)	dev.	T (°C)	dev.	Duration (days)	H <sub>2</sub> O <sup>a</sup> (wt.%)	Assemblage <sup>b</sup>
	DSE4 (SM)							Grt, Cpx, Rt, (Ilm), (Am), (Plag), Qtz
	B-gel(SM)							Gel
10	SE-1(SM)	2.0	0.1	700	1	14	10	Grt, Cpx, Rt, Am, Qtz, Vapour
1	DSE4	1.5	0.4	850	1	7	31	Grt, Cpx, (Rt), Ilm, Melt, Vapour
2	DSE4	1.6	0.4	700	2	10	22	Grt, Cpx, (Rt), Ilm, Am, Plag, Qtz, Vapour
3	DSE4	1.6	0.3	750	1	10	22	Grt, Cpx, (Rt), Ilm, Am, Melt, Vapour
4	DSE4	1.7	0.3	800	1	10	30	Grt, Cpx, (Rt), Ilm, Am, Melt, Vapour
5	DSE4	1.9	0.4	750	1	10	25	Grt, Cpx, Rt, Qtz, Am, Vapour, precipitate from fluid
6	DSE4	1.9	0.4	850	2	7	29	Grt, Cpx, Rt, Qtz, Vapour
7	DSE4	1.9	0.4	870	1	7	21	Grt, Cpx, Rt, Melt, Vapour
8	SE-1	1.9	0.2	870	1	14	10	Grt, Cpx, Rt, Melt, Vapour
9	DSE4	1.9	0.4	900	1	7	20	Grt, Cpx, Rt, Melt, Vapour
10 <sup>c</sup>	B-gel	2.0	0.2	700	1	14	10	Grt, Cpx, Rt, Am, Qtz, Vapour
11	SE-1	2.0	0.3	800	1	14	10	Grt, Cpx, Rt, Qtz, Vapour
12	B-gel	2.0	0.1	800	1	14	10	Grt, Cpx, Rt, Melt, Vapour
13	DSE4	2.2	0.2	800	1	14	7	Grt, Cpx, Rt, Qtz, Vapour, precipitate from fluid
14	SE-1	2.2	0.3	800	1	14	10	Grt, Cpx, Rt, Qtz, Vapour
15	B-gel	2.2	0.4	800	1	14	10	Grt, Cpx, Rt, Melt, Vapour
16	SE-1	2.2	0.2	870	1	14	10	Grt, Cpx, Rt, Melt, Vapour
17	DSE4	2.2	0.4	880	1	7	19	Grt, Cpx, Rt, Melt, Vapour
18	DSE4	2.3	0.4	850	1	7	34	Grt, Cpx, Rt, Qtz, Vapour, precipitate from fluid
19	DSE4	2.6	0.1	850	1	10	10	Grt, Cpx, Rt, Qtz, Vapour
20	DSE4	2.6	0.4	870	1	7	25	Grt, Cpx, Rt, Melt, Vapour
21	DSE4	2.9	0.4	870	1	7	29	Grt, Cpx, Rt, Melt, Vapour
22	DSE4	3.0	0.4	870	1	7	32	Grt, Cpx, Rt, Melt, Vapour

<sup>a</sup>H<sub>2</sub>O represents the weight percentage of distilled water added to the experimental capsule before the capsule was sealed. Therefore the values are maximum concentrations. <sup>b</sup>Phases in brackets occur as relict phases. <sup>c</sup>Experiment 10 was the preconditioning run which produced the synthetic eclogite starting material which was used in the runs 8, 11, 14 and 16. SM-starting material. DSE4-Dabie Shan Eclogite; B-gel-gel with a basaltic composition; SE-1-synthetic eclogite. Grt-garnet; Cpx-clinopyroxene; Rt-rutile; Ilm-ilmenite; Am-amphibole; Plag-plagioclase; Qtz-quartz.

### The starting materials

These experiments set-out to investigate the nature of the water-saturated solidus under low-pressure eclogite-facies conditions of a metabasaltic composition with a K<sub>2</sub>O content less than that required to produce phengite in the subsolidus assemblage. As omphacite is the only mineral in such rocks other than phengite which may contain more than trace quantities of K<sub>2</sub>O, this concentration is determined by the solubility of K<sub>2</sub>O in omphacite and the amount of omphacite in the pre-anatectic assemblage. The solubility of K<sub>2</sub>O in omphacite may be up to 0.08 wt.% K<sub>2</sub>O in high pressure, type-II crustal eclogite xenoliths (> 4.5 GPa) (McCandless and Gurney 1989; Jacob and Foley 1999). Therefore, with at least 30 wt.% ompha-

cite in the subsolidus assemblage at lower eclogite facies conditions, the bulk composition may contain up to 0.024 wt.% K<sub>2</sub>O without stabilising phengite. However, this value is a maximum constraint as K<sub>2</sub>O solubility increases at higher pressure and the pressure range relevant to this study (1.9 - 3.0 GPa) is lower than the pressure range for which this value for K<sub>2</sub>O solubility in clinopyroxene was determined (> 4.5 GPa). Preliminary reconnaissance experiments, at pressures above 1.8 GPa (i.e. above plagioclase stability), using a gel of approximate MORB composition, and less than 0.01 wt.% K<sub>2</sub>O, produced melt at temperatures only slightly above those of the projected metastable extension of the Qtz + Pl + H<sub>2</sub>O solidus of Johannes and Holtz (1996). This result was considered to represent metastable melting and con-

sequently, three different starting materials were used in this study (Table 2): 1) A natural low- $K_2O$  ( $\pm 0.01$  wt.%  $K_2O$ ) basaltic eclogite (DSE4); 2) a gel of similar composition similar to DSE4; and 3) a synthetic eclogite which was produced by conditioning the gel at 2.0 GPa and 700 °C i.e. below the projected metastable extension of the Qtz + Pl +  $H_2O$  solidus. This approach enables comparison between the solidi encountered using the different starting materials. Mineral proportions for the crystalline starting materials were calculated using the least squared regression method in combination with the measured bulk and mineral compositions (Table 2 and Table 3-4). The resultant mineral proportions are consistent with visual estimates from SEM BSE images.

#### *The natural eclogite starting material*

DSE4 is an eclogite-facies rock of MORB composition from the Dabie Shan region in central China and is characterised by the peak metamorphic mineral assemblage: ( $\sim 40$  %) Omp + ( $\sim 44$  %) Grt + ( $\sim 12$  %) Qtz + ( $\sim 2$  %) Rt + ( $\sim 1$  %) Aln + ( $\sim 1$  %) Ap. The clinopyroxene is omphacitic and the garnet composition is almandine-rich (60-61 % alm; 18 %

prp; 22-23 % grs; and 1 % sps) (Table 3). Retrograde ilmenite growth occurs around relict rutile grains. Minor retrograde symplectitic coronas of amphibole and clinopyroxene intergrowths, with subordinate albitic plagioclase have formed at the expense of garnet and omphacite during decompression. The clinopyroxene crystals of the intergrowths are less sodic and less aluminium rich (4.0-2.5 wt.%  $Na_2O$ ) than the peak metamorphic omphacite. These retrograde intergrowths constitute only a small fraction of the rock ( $\sim 5$  %), thus, these minerals are present in negligible amounts. The advantages of using a natural eclogite starting material are that the likelihood of metastable melting of Pl + Qtz +  $H_2O$  will be avoided during heating of the experiment at pressures above that of plagioclase stability ( $> \pm 1.8$  GPa) and that the experiment will not need to grow a large garnet fraction in order to equilibrate.

#### *The basaltic composition gel starting material*

Due to the fact that an eclogite constitutes an unusual choice as starting material in a partial melting study, a NCFMASHTO laboratory prepared gel (B-gel) with a composition very similar to DSE4 was used for comparison with the melting behaviour of DSE4. B-gel and DSE4 are similar in composition, however, DSE4 contains minor amounts of  $P_2O_5$  and MnO, which are absent in the gel, and it is higher in MgO and has lower CaO concentration compared to B-gel. The gel starting material was prepared according to the Hamilton and Henderson (1968) technique with the following modifications: The FeO and  $TiO_2$  components were added to the dried gel after the gel making process was complete. The source for FeO was a combination of  $Fe^{2+}$  sponge and  $Fe^{3+}$  powder added in stoichiometric proportions after the FeO content of the Fe sponge had been determined by measuring the weight gain produced by complete oxidation at 1000 °C. A small amount of natural garnet crystals were added to the powder prior to final grinding to act as nucleation seeds. The composition of the garnet seed is provided in Table 3. The gel was used as a starting material for experiments conducted at 2.0 and 2.2 GPa and at 800 °C which are compared to the results of experiments conducted at the same conditions using the natural eclogite starting material.

**Table 2:** Major element bulk rock geochemistry of the starting materials: a natural eclogite (DSE4) and a gel (B-gel). The compositions of average global MORB (Winter 2001 (BVTP Table 1.2.5.2)), the experimental starting composition used by Kessel et al. 2005 (Kessel TB-1) are provided for comparison. Bulk rock analysis for DSE4 and B-gel was done via XRF.

wt. %	DSE4	B-gel	Ave. MORB	Kessel TB-1
SiO <sub>2</sub>	50.0	50.3	50.5	51.6
TiO <sub>2</sub>	2.5	2.5	1.6	1.5
Al <sub>2</sub> O <sub>3</sub>	12.8	13.0	15.3	16.7
FeO <sup>a</sup>	16.2	16.2	10.5	10.3
MgO	5.7	4.3	7.5	7.0
MnO	0.3	0.0	0.0	0.0
CaO	9.6	10.5	11.5	9.9
Na <sub>2</sub> O	2.0	2.0	2.6	3.2
K <sub>2</sub> O	0.0	0.0	0.2	0.0
P <sub>2</sub> O <sub>5</sub>	0.3	0.0	0.1	0.0
<b>Total</b>	<b>99.5</b>	<b>98.9</b>	<b>99.8</b>	<b>99.2</b>
Na <sub>2</sub> O/CaO	0.2	0.2	0.2	0.3
K <sub>2</sub> O/Na <sub>2</sub> O	0.0	0.0	0.1	0.0
Ferro <sup>b</sup>	24.7	23.0	19.6	18.8
Mg# <sup>c</sup>	38.5	32.1	56.0	54.8

<sup>a</sup>All Fe is expressed as FeO. <sup>b</sup>Ferro =  $TiO_2 + FeO + MgO + MnO$ . <sup>c</sup>Mg# =  $100 * Mg / (Mg + Fe^{2+} + Fe^{3+})$ .



Table 3 continued.

Experimental run products		Supersolidus		DSE4		DSE4		SE-1		DSE4		DSE4		SE-1		DSE4		DSE4							
wt.%		DSE4	DSE4	DSE4	DSE4	DSE4	DSE4	DSE4	DSE4	DSE4	DSE4	DSE4	DSE4	DSE4	DSE4	DSE4	DSE4	DSE4	DSE4						
SM	P (GPa)	1.5	1.6	1.7	1.9	1.9	1.9	2.2	2.2	2.2	2.2	2.2	2.2	2.2	2.2	2.2	2.2	2.2	2.2						
T (°C)	850	750	800	870	900	870	870	800	800	800	800	800	800	800	870	870	870	870	870						
N = 3	Ave.	σ	Ave.	σ	Ave.	σ	Ave.	σ	Ave.	σ	Ave.	σ	Ave.	σ	Ave.	σ	Ave.	σ	Ave.						
SiO <sub>2</sub>	38.3	0.6	37.7	0.2	38.2	1.1	38.7	0.2	36.8	0.7	39.1	1.0	38.0	0.4	37.6	0.4	37.4	0.7	39.0	0.1	39.0	0.6	38.5	1.1	
TiO <sub>2</sub>	0.0	0.0	0.0	0.1	0.0	0.0	0.0	0.1	1.5	1.0	0.0	0.0	1.9	0.1	1.9	0.1	1.6	1.0	0.0	0.0	0.0	0.0	0.0	0.0	
Al <sub>2</sub> O <sub>3</sub>	21.5	0.6	20.8	0.1	21.7	0.7	21.4	0.1	21.7	0.4	21.6	0.4	21.0	0.3	20.8	0.3	20.9	0.4	22.0	0.3	22.4	0.1	21.8	0.6	21.8
Cr <sub>2</sub> O <sub>3</sub>	0.0	0.0	0.0	0.0	0.0	0.0	0.0	0.0	0.0	0.0	0.0	0.0	0.0	0.0	0.0	0.0	0.0	0.0	0.0	0.0	0.0	0.0	0.0	0.0	
Fe <sub>2</sub> O <sub>3</sub>	0.6	0.8	1.5	0.0	0.0	0.0	2.2	0.0	0.0	0.0	1.3	1.3	0.0	0.0	0.0	0.0	0.0	0.0	0.0	0.0	0.0	0.0	0.0	0.0	
FeO	27.5	0.8	27.3	0.2	26.9	1.7	25.8	0.2	27.7	0.4	26.4	0.8	26.4	0.5	25.9	0.5	27.7	0.4	27.1	0.0	25.3	0.3	26.2	0.8	25.4
MnO	0.5	0.1	0.4	0.0	0.4	0.3	0.6	0.0	0.0	0.0	0.5	0.1	0.0	0.0	0.0	0.0	0.0	0.0	0.0	0.0	0.0	0.0	0.0	0.0	
MgO	4.6	0.3	4.2	0.1	4.8	0.5	5.8	0.1	2.5	0.0	5.8	0.7	3.3	0.2	3.4	0.2	2.8	0.0	5.0	0.1	5.0	0.2	5.1	0.3	5.7
CaO	7.5	0.2	7.7	0.1	7.6	0.4	7.5	0.1	11.1	0.2	7.3	0.4	11.2	0.3	11.2	0.3	11.3	0.2	7.7	0.1	7.8	0.3	7.9	0.2	7.5
Na <sub>2</sub> O	0.0	0.0	0.0	0.0	0.0	0.0	0.0	0.0	0.0	0.0	0.0	0.0	0.0	0.0	0.0	0.0	0.0	0.0	0.0	0.0	0.0	0.0	0.0	0.0	
K <sub>2</sub> O	0.0	0.0	0.0	0.0	0.0	0.0	0.0	0.0	0.0	0.0	0.0	0.0	0.0	0.0	0.0	0.0	0.0	0.0	0.0	0.0	0.0	0.0	0.0	0.0	
Totals	100.5	3.4	99.6	0.8	99.6	7.6	102.0	0.8	101.3	2.7	102.0	4.7	101.8	1.9	100.8	1.9	101.7	2.7	101.4	1.0	100.0	1.1	101.1	3.4	101.0
Si	3.0	0.0	3.0	0.1	3.0	0.1	3.0	0.1	3.0	0.1	3.0	0.0	3.0	0.1	3.0	0.1	3.0	0.1	3.0	0.0	3.0	0.0	3.0	0.0	3.0
Ti	0.0	0.0	0.0	0.0	0.0	0.0	0.0	0.0	0.1	0.0	0.0	0.0	0.1	0.0	0.1	0.0	0.1	0.0	0.0	0.0	0.0	0.0	0.0	0.0	0.0
Al	2.0	0.0	1.9	0.1	2.0	0.1	1.9	0.1	2.0	0.1	1.9	0.0	2.0	0.1	2.0	0.1	2.0	0.1	2.0	0.0	2.0	0.0	2.0	0.0	2.0
Cr	0.0	0.0	0.0	0.0	0.0	0.0	0.0	0.0	0.0	0.0	0.0	0.0	0.0	0.0	0.0	0.0	0.0	0.0	0.0	0.0	0.0	0.0	0.0	0.0	0.0
Fe <sup>3+</sup> a	0.0	0.0	0.1	0.1	0.0	0.2	0.1	0.1	0.1	0.1	0.1	0.1	0.1	0.1	0.1	0.1	0.1	0.1	0.1	0.0	0.0	0.0	0.0	0.0	0.0
Fe <sup>2+</sup>	1.8	0.0	1.8	0.1	1.8	0.1	1.7	0.1	1.8	0.1	1.7	0.1	1.7	0.1	1.7	0.1	1.7	0.1	1.7	0.0	1.6	0.0	1.7	0.0	1.6
Mn	0.0	0.0	0.0	0.0	0.0	0.0	0.0	0.0	0.0	0.0	0.0	0.0	0.0	0.0	0.0	0.0	0.0	0.0	0.0	0.0	0.0	0.0	0.0	0.0	0.0
Mg	0.5	0.0	0.5	0.0	0.6	0.1	0.7	0.0	0.2	0.0	0.7	0.1	0.4	0.0	0.4	0.0	0.2	0.0	0.6	0.0	0.6	0.0	0.6	0.0	0.7
Ca	0.6	0.0	0.7	0.1	0.6	0.0	0.6	0.1	0.9	0.1	0.6	0.0	0.9	0.1	0.9	0.1	0.9	0.1	0.6	0.0	0.7	0.0	0.7	0.0	0.6
Na	0.0	0.0	0.0	0.0	0.0	0.0	0.0	0.0	0.0	0.0	0.0	0.0	0.0	0.0	0.0	0.0	0.0	0.0	0.0	0.0	0.0	0.0	0.0	0.0	0.0
K	0.0	0.0	0.0	0.0	0.0	0.0	0.0	0.0	0.0	0.0	0.0	0.0	0.0	0.0	0.0	0.0	0.0	0.0	0.0	0.0	0.0	0.0	0.0	0.0	0.0
Sum	8.0	0.0	8.0	0.0	8.0	8.0	8.0	8.0	8.0	8.0	8.0	8.0	8.0	8.0	8.0	8.0	8.0	8.0	8.0	8.0	8.0	8.0	8.0	8.0	8.0
Mg <sup>#b</sup>	22.8	21.1	21.1	21.1	21.1	24.1	27.8	27.8	13.9	27.7	27.7	18.3	19.0	19.0	19.0	15.3	15.3	24.7	26.0	26.0	25.6	25.6	27.9	27.9	
Alm <sup>c</sup>	60.7	61.1	61.1	61.1	61.1	59.5	56.4	56.4	59.8	57.3	57.3	56.6	55.9	55.9	55.9	58.8	58.8	59.1	57.3	57.3	57.7	57.7	56.3	56.3	
Pyr <sup>d</sup>	18.1	16.8	16.8	16.8	16.8	18.9	22.6	22.6	9.6	22.4	22.4	12.6	13.1	13.1	10.6	10.6	19.4	20.2	20.2	20.0	20.0	22.4	22.4		
Grs <sup>e</sup>	21.9	22.8	22.8	22.8	22.8	22.3	21.9	21.9	31.2	21.2	21.2	31.5	31.7	31.7	31.2	31.2	22.3	23.5	23.5	23.1	23.1	22.2	22.2		

<sup>a</sup>Fe<sup>3+</sup> calculated using method from Droop (1987). <sup>b</sup>Mg# = 100 \* Mg / (Mg + Fe<sup>2+</sup> + Fe<sup>3+</sup>). <sup>c</sup>Alm = 100 \* Mg / (Ca + Fe + Mn + Mg). <sup>d</sup>Pyr = 100 \* Mg / (Ca + Fe + Mn + Mg). <sup>e</sup>Grs = 100 \* Ca / (Ca + Fe + Mn + Mg). SM-starting material. σ - standard deviation.

**Table 4:** Clinopyroxene compositions from DSE4 starting materials and experimental run products. Clinopyroxene formulas calculated to 6 oxygens.

wt.%	Starting material					Experimental run products											
	DSE4		SE-1			Subsolidus				SE-1				DSE4			
	core	rim	$\sigma$	ave.	$\sigma$	DSE4	B-gel	SE-1	DSE4	SE-1	DSE4	SE-1	DSE4	SE-1	DSE4	SE-1	DSE4
SM				2			2										
P (GPa)				700			700										
T (°C)				700			700										
N = 5				Ave.	$\sigma$		Ave.	$\sigma$									
SiO <sub>2</sub>	55.3	54.2	0.0	54.9	0.4	54.6	0.4	53.8	0.2	53.7	0.6	53.8	0.4	53.4	0.8	53.8	0.4
TiO <sub>2</sub>	0.0	0.0	0.0	0.3	0.1	0.0	0.2	0.0	0.1	0.0	0.1	0.3	0.2	0.0	0.0	0.3	0.2
Al <sub>2</sub> O <sub>3</sub>	7.5	5.1	0.0	9.6	0.2	5.2	0.2	4.7	0.3	4.4	1.0	7.6	0.2	5.0	1.0	7.6	0.2
Cr <sub>2</sub> O <sub>3</sub>	0.0	0.0	0.0	0.0	0.0	0.0	0.0	0.0	0.0	0.0	0.0	0.0	0.0	0.0	0.0	0.0	0.0
Fe <sub>2</sub> O <sub>3</sub>	0.0	0.3	0.0	2.3	0.0	0.0	0.5	0.0	0.0	0.0	0.0	0.0	0.0	0.0	0.0	0.0	0.0
FeO	8.0	9.4	0.1	6.9	0.2	8.0	0.4	7.8	0.2	9.5	0.8	8.9	0.4	8.4	0.5	8.5	0.4
MnO	0.0	0.0	0.0	0.0	0.0	0.0	0.0	0.0	0.0	0.0	0.0	0.0	0.0	0.0	0.0	0.0	0.0
MgO	8.9	9.8	0.0	8.2	0.3	10.1	0.5	9.9	0.3	10.0	0.3	8.9	0.5	11.5	0.3	8.8	0.5
CaO	13.6	17.8	0.1	16.0	0.3	18.1	0.3	18.3	0.2	18.7	0.3	15.8	0.3	18.2	0.3	16.0	0.3
Na <sub>2</sub> O	6.3	3.6	0.1	3.6	0.0	3.8	0.2	4.1	0.2	3.8	0.3	4.5	0.2	3.3	0.3	4.6	0.2
Totals	99.6	99.9	0.6	99.9	0.2	99.8	0.9	99.0	0.6	100.1	1.2	99.7	1.3	99.8	1.2	99.5	0.6
Si	2.0	2.0	0.0	2.0	0.0	2.0	0.0	2.0	0.0	2.0	0.0	2.0	0.0	2.0	0.0	2.0	0.0
Ti	0.0	0.0	0.0	0.0	0.0	0.0	0.0	0.0	0.0	0.0	0.0	0.0	0.0	0.0	0.0	0.0	0.0
Al	0.3	0.2	0.0	0.4	0.0	0.1	0.0	0.1	0.0	0.1	0.0	0.3	0.0	0.1	0.0	0.3	0.0
Cr	0.0	0.0	0.0	0.0	0.0	0.0	0.0	0.0	0.0	0.0	0.0	0.0	0.0	0.0	0.0	0.0	0.0
Fe <sup>3+*</sup>	0.2	0.1	0.0	0.0	0.0	0.1	0.0	0.0	0.0	0.0	0.0	0.0	0.0	0.1	0.0	0.0	0.0
Fe <sup>2+</sup>	0.1	0.2	0.0	0.2	0.0	0.2	0.0	0.3	0.0	0.3	0.0	0.2	0.0	0.2	0.0	0.2	0.0
Mn	0.0	0.0	0.0	0.0	0.0	0.0	0.0	0.0	0.0	0.0	0.0	0.0	0.0	0.0	0.0	0.0	0.0
Mg	0.5	0.5	0.0	0.4	0.0	0.6	0.0	0.6	0.0	0.6	0.0	0.5	0.0	0.6	0.0	0.5	0.0
Ca	0.5	0.7	0.0	0.7	0.0	0.8	0.0	0.7	0.0	0.8	0.0	0.6	0.0	0.8	0.0	0.6	0.0
Na	0.4	0.3	0.0	0.3	0.0	0.2	0.0	0.3	0.0	0.2	0.0	0.3	0.0	0.2	0.0	0.3	0.0
Sum	4.0	4.0	0.0	4.0	0.0	4.0	0.0	4.0	0.0	4.0	0.0	4.0	0.0	4.0	0.0	4.0	0.0
Mg# <sup>b</sup>	66.4	64.9		67.7		69.3		68.9		65.2		64.2		71.0		65.0	

<sup>a</sup>Fe<sup>3+</sup> calculated using method from Droop (1987). <sup>b</sup>Mg# = 100 \* Mg / (Mg + Fe<sup>2+</sup> + Fe<sup>3+</sup>). SM-starting material.  $\sigma$  - standard deviation.

Table 4 continued.

wt%		Experimental run products																														
		Supersolidus																														
SM	DSE4	DSE4	DSE4	DSE4	SE-1	DSE4	B-gel	B-gel	SE-1	DSE4	DSE4	DSE4	DSE4	DSE4																		
P	1.5	1.6	1.7	1.9	1.9	1.9	2.0	2.0	2.2	2.2	2.2	2.2	2.2	2.2																		
T (°C)	850	750	800	870	870	900	800	800	870	880	870	870	870	870																		
N = 5	Ave.	$\sigma$	Ave.	$\sigma$	Ave.	$\sigma$	Ave.	$\sigma$	Ave.	$\sigma$	Ave.	$\sigma$	Ave.	$\sigma$																		
SiO <sub>2</sub>	53.4	0.4	54.6	0.4	53.1	0.2	53.6	0.0	54.8	0.2	53.5	0.1	52.7	0.6	52.1	0.6	54.8	0.2	53.2	0.4	52.5	0.1	54.8	0.2	53.5	0.1						
TiO <sub>2</sub>	0.0	0.2	0.7	0.2	0.0	0.1	0.3	0.0	0.2	0.1	0.2	0.1	0.3	0.1	0.3	0.1	0.3	0.1	0.3	0.1	0.4	0.2	0.1	0.0	0.1	0.0	0.0	0.0				
Al <sub>2</sub> O <sub>3</sub>	2.1	0.2	2.6	0.2	2.6	0.3	2.0	0.0	4.6	0.3	1.9	0.0	3.1	1.0	3.6	1.0	4.7	0.3	2.7	0.2	2.3	0.0	2.1	0.3	1.9	0.0	0.0					
Cr <sub>2</sub> O <sub>3</sub>	0.0	0.0	0.0	0.0	0.0	0.0	0.0	0.0	0.0	0.0	0.0	0.0	0.0	0.0	0.0	0.0	0.0	0.0	0.0	0.0	0.0	0.0	0.0	0.0	0.0	0.0	0.0	0.0	0.0			
Fe <sub>2</sub> O <sub>3</sub>	0.0	0.0	0.0	0.0	0.0	0.0	0.0	0.0	0.0	0.0	0.0	0.0	0.0	0.0	0.0	0.0	0.0	0.0	0.0	0.0	0.0	0.0	0.0	0.0	0.0	0.0	0.0	0.0	0.0	0.0		
FeO	11.1	0.4	9.8	0.4	11.7	0.2	11.0	0.0	9.2	0.2	11.5	1.0	12.3	0.8	11.9	0.8	9.0	0.2	12.6	0.4	12.7	0.4	9.7	0.2	11.5	1.0	0.0	0.0	0.0	0.0		
MnO	0.0	0.0	0.0	0.0	0.0	0.0	0.0	0.0	0.0	0.0	0.0	0.0	0.0	0.0	0.0	0.0	0.0	0.0	0.0	0.0	0.0	0.0	0.0	0.0	0.0	0.0	0.0	0.0	0.0	0.0		
MgO	12.0	0.5	12.1	0.5	11.8	0.3	13.1	1.0	11.6	0.3	12.9	0.0	11.7	0.3	11.2	0.3	11.6	0.3	11.0	0.5	12.1	0.2	12.3	0.3	12.9	0.0	0.0	0.0	0.0	0.0	0.0	0.0
CaO	19.6	0.3	19.2	0.3	19.7	0.2	18.8	0.8	17.3	0.2	19.3	0.1	18.1	0.3	18.5	0.3	17.1	0.2	18.3	0.3	18.6	0.0	20.0	0.2	19.3	0.1	0.0	0.0	0.0	0.0	0.0	0.0
Na <sub>2</sub> O	1.5	0.2	1.4	0.2	1.1	0.2	1.0	0.0	2.1	0.2	0.8	0.0	1.5	0.1	1.9	0.1	2.3	0.2	1.6	0.2	1.2	0.0	1.7	0.2	1.1	0.0	0.0	0.0	0.0	0.0	0.0	
Totals	99.7	1.2	100.4	0.6	100.0	0.8	99.8	1.3	99.8	1.3	100.1	0.973	99.7	0.6	99.5	0.3	99.8	0.3	99.8	0.8	99.6	0.5	100.6	1.0	100.2	0.8	0.0	0.0	0.0	0.0	0.0	0.0
Si	2.0	0.0	2.0	0.0	2.0	0.0	2.0	0.0	2.0	0.0	2.0	0.0	2.0	0.0	2.0	0.0	2.0	0.0	2.0	0.0	2.0	0.0	2.0	0.0	2.0	0.0	0.0	0.0	0.0	0.0	0.0	0.0
Ti	0.0	0.0	0.0	0.0	0.0	0.0	0.0	0.0	0.0	0.0	0.0	0.0	0.0	0.0	0.0	0.0	0.0	0.0	0.0	0.0	0.0	0.0	0.0	0.0	0.0	0.0	0.0	0.0	0.0	0.0	0.0	0.0
Al	0.1	0.0	0.1	0.0	0.1	0.0	0.1	0.0	0.2	0.0	0.1	0.0	0.1	0.0	0.1	0.0	0.2	0.0	0.1	0.0	0.1	0.0	0.1	0.0	0.1	0.0	0.0	0.0	0.0	0.0	0.0	0.0
Cr	0.0	0.0	0.0	0.0	0.0	0.0	0.0	0.0	0.0	0.0	0.0	0.0	0.0	0.0	0.0	0.0	0.0	0.0	0.0	0.0	0.0	0.0	0.0	0.0	0.0	0.0	0.0	0.0	0.0	0.0	0.0	0.0
Fe <sup>3+</sup>	0.0	0.0	0.0	0.0	0.0	0.0	0.0	0.0	0.0	0.0	0.0	0.0	0.0	0.0	0.0	0.0	0.0	0.0	0.0	0.0	0.0	0.0	0.0	0.0	0.0	0.0	0.0	0.0	0.0	0.0	0.0	0.0
Fe <sup>2+</sup>	0.3	0.0	0.3	0.0	0.4	0.0	0.3	0.0	0.3	0.0	0.4	0.0	0.4	0.0	0.4	0.0	0.3	0.0	0.5	0.0	0.5	0.0	0.3	0.0	0.4	0.0	0.0	0.0	0.0	0.0	0.0	0.0
Mn	0.0	0.0	0.0	0.0	0.0	0.0	0.0	0.0	0.0	0.0	0.0	0.0	0.0	0.0	0.0	0.0	0.0	0.0	0.0	0.0	0.0	0.0	0.0	0.0	0.0	0.0	0.0	0.0	0.0	0.0	0.0	0.0
Mg	0.6	0.0	0.6	0.0	0.6	0.0	0.6	0.0	0.6	0.0	0.7	0.0	0.7	0.0	0.7	0.0	0.6	0.0	0.6	0.0	0.6	0.0	0.7	0.0	0.7	0.0	0.0	0.0	0.0	0.0	0.0	0.0
Ca	0.8	0.0	0.8	0.0	0.8	0.0	0.8	0.0	0.7	0.0	0.8	0.0	0.7	0.0	0.7	0.0	0.7	0.0	0.7	0.0	0.7	0.0	0.8	0.0	0.8	0.0	0.0	0.0	0.0	0.0	0.0	0.0
Na	0.1	0.0	0.1	0.0	0.1	0.0	0.1	0.0	0.2	0.0	0.0	0.0	0.1	0.0	0.1	0.0	0.2	0.0	0.1	0.0	0.1	0.0	0.1	0.0	0.1	0.0	0.0	0.0	0.0	0.0	0.0	0.0
Sum	4.0	0.0	4.0	0.0	4.0	0.0	4.0	0.0	4.0	0.0	4.0	0.0	4.0	0.0	4.0	0.0	4.0	0.0	4.0	0.0	4.0	0.0	4.0	0.0	4.0	0.0	0.0	0.0	0.0	0.0	0.0	0.0
Mg <sup>#b</sup>	65.9	68.8	68.8	64.3	68.0	69.7	66.7	63.0	62.7	69.7	60.9	63.0	69.4	66.7	62.7	69.7	60.9	63.0	69.4	66.7	63.0	69.4	66.7	63.0	69.4	66.7	0.0	0.0	0.0	0.0	0.0	

<sup>a</sup>Fe<sup>3+</sup> calculated using method from Droop (1987). <sup>b</sup>Mg# = 100 \* Mg / (Mg + Fe<sup>2+</sup> + Fe<sup>3+</sup>). SM-starting material.  $\sigma$  - standard deviation

### ***The synthetic eclogite starting material***

A synthetic eclogite starting material (SE-1) was produced by conditioning the B-gel starting material at 2.0 GPa and 700 °C for 14 days. This is within eclogite-facies pressure and is at a lower temperature than the metastable extension of the Qtz + Pl + H<sub>2</sub>O solidus. On conditioning under these conditions an eclogite facies assemblage crystallised, consisting of (~ 39 %) Cpx + (~ 42 %) Grt + (~ 7 %) Amph + (~ 12 %) Qtz + (~ 2 %) Rt. New almandine-rich garnet (62 % alm, 9 % prp and 30 % grs) crystallises around large garnet seed crystals. The clinopyroxene is omphacitic (3.6 wt.% Na<sub>2</sub>O and 9.6 wt.% Al<sub>2</sub>O<sub>3</sub>) and forms smaller elongated euhedral crystals. The amphibole occurs as even smaller needle-like crystals. The synthetic eclogite was used as a starting material for experiments conducted between 1.9 and 2.2 GPa and at 800 °C and 870 °C which are compared with the results of experiments conducted using the natural eclogite under the same conditions.

### **Experimental set-up and procedure**

The experiments were conducted using a Holloway design, non-end-loaded, 12.5 mm piston cylinder apparatus for experiments below 2.2 GPa and above this pressure a 10 mm diameter pressure vessel was used. Temperature was controlled using a Depths of the Earth controller and a type-K (chromel-alumel) thermocouple. Pressure was measured with a Heise gauge (0–5 GPa). In this configuration, the apparatus has an accuracy of approximately ± 5 °C and ± 0.01 GPa (Schilling and Wunder 2004). The final starting material powders were prepared for use by grinding the natural rock or dried Fe- and Ti-bearing gel to a powder with an average grain size of 5 µm, using an agate mortar and pestle under acetone. Tube-shaped gold capsules (3–4 mm in width and 10–12 mm in length) were constructed from 0.2 mm thick pure gold sheet. In all cases, sufficient water was added to the capsule to ensure water saturation of the experiment (7–32 wt.% H<sub>2</sub>O or 14–53 mol% H<sub>2</sub>O) (Table 1). Typical water solubility in rhyolitic melts is 25 mol% H<sub>2</sub>O at a pressure of 2.0 GPa and 1500°C (Sykes *et al.* 1992) and water solubility increases by 16–18 mol% / 1.0 GPa, at a constant temperature in haplo-andesitic melts (Mysen and Wheeler, 2000). Thus, water solu-

bility in the melts is expected to be high under the conditions of these experiments. The capsules were sealed with an arc welder whilst the lower end of the capsule was kept cool in a water bath to prevent water loss from the capsule. The capsules were tested for leaks in a vacuum water bath and folded to fit into the graphite furnace. Capsules were placed so that the sample powder was separated from the thermocouple by only the capsule wall and a 0.5 mm thick sapphire disc. Two different arrangements were used for packing the capsule into the furnace: 1) where the open spaces between the folds of the capsule and around the capsule were filled by crushed ceramic powder; or 2) the capsule was pressed into a preformed plug of boron nitride with a diameter equivalent to the internal diameter of the graphite furnace. This method was adopted during the experimental programme to limit thermocouple failures considered to arise due to differential compressibility of components inside the furnace. However, as boron nitride is known to efficiently restrict hydrogen diffusion, this did have the benefit of allowing for comparison between the behaviour of hydrogen in the two situations. Experiments at 870 °C used only a salt sleeve around the furnace; those at higher temperature used both an inner Pyrex sleeve around the furnace and an outer salt sleeve. The hot piston-out method was employed in setting up each run. The experiments were quenched isobarically, with a quench rate of greater than 30 °C / second, for the high temperature portion of the quench (to below the solidus). Following each experiment, the capsules were pierced and weighed immediately, and then placed in an oven at 100 °C for 24 hours, and then weighed again. Mass loss occurred in all cases and was interpreted to indicate the presence of excess water vapour and thus water saturation during the experiment. Diffusive loss of hydrogen from the capsules during the experiments, which has implications for the water content of the capsule, was monitored by measuring the hematite component in ilmenite. This was low and constant in all experiments where ilmenite was produced.

### **Analytical techniques**

The minerals in the starting material, as well as the minerals and glasses in the experimental run prod-



ucts, were analysed by quantitative energy-dispersive X-ray spectroscopy (EDS) and wavelength-dispersive X-ray spectroscopy (WDS) using a Zeiss EVO MA 15 Scanning Electron Microscope (SEM) fitted with an Oxford Instrument® Wave Dispersive X-ray Spectrometer and Oxford INCA software. Major elements were determined via EDS using an Oxford Instruments® X-Max 20 mm<sup>2</sup> detector and Oxford INCA software. Cl concentration in the glasses and precipitate formed from the fluid phase was selectively quantified via WDS. Beam conditions during the quantitative analyses were 20 kV and approximately 1.0 A, with a working distance of 8.5 mm and a specimen beam current of ~20.00 nA. For mineral and glass analyses counting time was 15 seconds live-time. Natural mineral standards were used for standardisation and verification of the analyses. The system is designed to perform high-resolution imaging concurrently with quantitative analysis, with errors ranging from ± 0.6 to 0.1 wt.% on the major elements using EDS and ± 0.01 to 0.03 wt.% on major and trace elements using WDS (Laurie and Stevens 2012a). During analyses of the glasses a cryogenic stage was used to cool the sample to below -180 °C. This counteracts the migration-related counting losses on the light elements, especially Na<sub>2</sub>O, that make quantitative analyses of hydrous aluminous silicate glasses problematic (e.g. Vielzeuf and Clemens 1992). Further details of the techniques used for the mineral analyses are described by Diener *et al.* (2005) and Moyen and Stevens (2006), and for the glass analyses by Spicer *et al.* (2004).

### Experimental results

Table 1 summarises the experimental run conditions and the experimental results. Representative mineral and glass compositions from the experimental run products are provided in Tables 3-5. Phase proportions in the run products were calculated using the measured compositions of the minerals and glass and the relevant bulk rock (Table 2) in combination with an iterative mixing calculation which solved for minimum residuals and are consistent with visual estimates from back scatter electron (BSE) images.

### Detection of Melt

In general, the presence of melt at high temperature was easily identified by the conchoidal fracture of the quenched glass; its occurrence as an interstitial phase; the typical low dihedral angles which formed between the glass and residual crystals (Holness *et al.* 2005); as well as its characteristic vesicles and silica- and aluminium-rich ED x-ray spectrum (Table 5, Fig. 3). The subsolidus run products contain domains that are almost quartz-free and domains that contain abundant quartz (Fig. 3). Thus, these experiments are characterised by significant quartz redistribution which is interpreted to reflect quartz dissolution and precipitation by the fluid phase. In experiments where this occurred, an amorphous phase was produced, typically in proximity with large, newly crystallised, blocky quartz crystals (Fig. 3). The amorphous phase is volumetrically subordinate to the quartz and also occurs as inclusions in quartz. This phase is interpreted to reflect a precipitate from the fluid phase on cooling and as detailed below, it differs substantially in composition from the quenched melt and is much more compositionally variable than the melt.

### Results of the experiments using a natural eclogite starting material

Fifteen experiments were conducted using DSE4 starting material between 1.5 GPa and 3.0 GPa and 700 °C and 900 °C. In the pressure interval 1.5 to 1.7 GPa, partial melting occurred between 700 °C and 750 °C; and between 1.9 and 3.0 GPa, partial melting occurred between 850 °C and 870 °C (Fig. 4).

In subsolidus experimental run products clinopyroxene, garnet and quartz are the dominant mineral phases. The stable titaniferous phase is pressure dependent and rutile is stable above 1.8 GPa and ilmenite below 1.8 GPa. Where ilmenite is stable, remnant rutile cores from the starting material persist within new ilmenite crystals. Small crystals of amphibole occur in subsolidus experiments below 800 °C and small amounts of plagioclase occur in the subsolidus run at 1.6 GPa. Extensive new clinopyroxene (2.8-4.1 wt.% Na<sub>2</sub>O) has grown around remnant cores of pyroxene from the starting material. New garnet growth produced straight grain boundaries which are distinct

**Table 5:** Averaged normalised anhydrous experimental glass and precipitate major element compositions. The average composition for high pressure-type Archaean TTG (Moyen 2011) is provided for comparison the experimental glass compositions. The glass analyses were done using SEM-EDS with a cryostage. The experimental glass compositions are anhydrous equivalent compositions normalized to 100 wt.% total.

SM	Ave. glass compositions												Precipitate				HP -ty Archaean TTG															
	DSE 4	DSE4	DSE 4	SE-1	DSE 4	B- gel	B- gel	SE-1	DSE 4	DSE4	DSE 4	DSE 4	DSE 4	DSE 4	DSE 4	DSE 4		DSE 4	DSE 4													
P (GPa)	15	16	17	1.9	1.9	2.0	2.2	2.2	2.2	2.2	2.2	2.2	2.2	2.6	2.9	2.9	2.9	2.9														
T (°C)	850	750	800	870	900	800	800	870	880	870	870	870	870	870	870	870	870	870														
N	3	3	4	5	3	5	5	5	3	3	3	3	3	3	3	3	3	3														
wt.%																																
SiO <sub>2</sub>	75.5	1.2	75.9	0.0	75.4	3.6	74.7	0.9	75.3	1.2	74.4	0.7	76.3	0.9	76.7	0.9	76.2	0.2	75.2	0.6	75.3	0.2	75.3	0.8	75.1	0.4	80.9	3.0	70.9			
TiO <sub>2</sub>	0.3	0.0	0.3	0.0	0.5	0.1	0.1	0.0	0.5	0.0	0.3	0.5	0.3	0.0	0.3	0.0	0.4	0.1	0.5	0.1	0.4	0.1	0.4	0.2	0.2	0.3	0.0	0.0	0.3			
Al <sub>2</sub> O <sub>3</sub>	15.1	0.0	14.1	0.0	15.3	0.0	14.7	0.6	13.3	0.0	14.7	0.6	14.0	0.7	13.9	0.7	13.0	0.7	14.6	0.5	14.1	0.7	14.0	0.2	14.1	0.3	11.6	0.6	15.5			
FeO <sup>a</sup>	1.9	0.8	1.9	0.0	2.0	0.0	2.0	0.6	2.9	0.4	2.4	0.7	2.3	0.6	1.9	0.6	2.5	0.0	2.2	0.1	2.4	0.0	2.3	0.2	2.1	0.2	1.3	0.7	1.9			
MgO	0.5	0.0	0.3	0.0	0.3	0.2	0.4	0.4	0.5	0.0	0.5	0.6	0.4	0.4	0.3	0.4	0.3	0.3	0.3	0.3	0.1	0.2	0.3	0.2	0.1	0.3	0.4	0.2	0.6	0.8		
MnO	0.0	0.0	0.0	0.0	0.0	0.0	0.1	0.4	0.0	0.0	0.0	0.0	0.0	0.0	0.0	0.0	0.0	0.0	0.0	0.0	0.0	0.0	0.0	0.0	0.0	0.0	0.0	0.0	0.0			
CaO	2.7	0.0	3.0	0.0	2.3	0.1	2.4	0.1	2.6	0.0	2.7	0.4	2.3	0.1	2.2	0.1	2.4	0.1	2.2	0.1	2.3	0.1	2.2	0.1	2.2	0.4	2.3	0.6	0.7	0.2	2.8	
Na <sub>2</sub> O	3.9	0.1	4.4	0.0	4.1	0.1	5.4	0.8	4.8	0.1	4.9	1.5	3.9	0.8	4.3	0.5	5.0	0.1	4.9	0.1	5.3	0.1	5.4	0.1	5.4	0.7	5.9	0.9	2.6	6.6	5.2	
K <sub>2</sub> O	0.1	0.0	0.1	0.0	0.1	0.0	0.1	0.0	0.1	0.0	0.1	0.2	0.2	0.0	0.1	0.0	0.1	0.0	0.1	0.0	0.2	0.0	0.1	0.2	0.1	0.2	0.1	0.2	1.8	2.0	1.6	
P <sub>2</sub> O <sub>5</sub>	0.0	0.0	0.0	0.0	0.0	0.0	0.0	0.0	0.0	0.0	0.0	0.0	0.0	0.0	0.0	0.0	0.0	0.0	0.0	0.0	0.0	0.0	0.0	0.0	0.0	0.0	0.0	0.0	0.0	0.1	0.0	0.1
Cl <sup>b</sup>	0.0	0.0	0.0	0.0	0.0	0.0	0.0	0.0	-	-	-	-	-	-	-	-	-	-	-	-	-	-	-	-	-	-	-	-	-	-	-	
Total	100.	0	100.0	100.	100.	100.	100.	100.	100.	100.	100.	100.	100.	100.	100.	100.	100.	100.	100.	100.	100.	100.	100.	100.	100.	100.0	100.	100.	100.	99.2		
H <sub>2</sub> O <sup>c</sup>	9.7	1.4	10.3	0.9	13.7	1.6	15.9	2.1	15.7	0.5	15.9	0.6	15.6	0.7	16.2	0.6	15.9	0.4	16.1	0.5	16.9	0.8	18.9	1.1	18.6	0.9	18.9	0.5				
Na <sub>2</sub> O/Ca O	1.4	1.5	1.8	2.3	1.8	1.8	2.3	1.7	1.9	1.8	1.8	1.7	1.7	1.9	1.9	2.0	2.0	2.2	2.2	2.2	2.3	2.3	2.5	2.5	2.6	3.7	3.7	1.9				
K <sub>2</sub> O/ Na <sub>2</sub> O	0.0	0.0	0.0	0.0	0.0	0.0	0.0	0.0	0.0	0.0	0.0	0.0	0.0	0.0	0.0	0.0	0.0	0.0	0.0	0.0	0.0	0.0	0.0	0.0	0.0	0.0	0.7	0.3				
Ferro <sup>d</sup>	2.7	2.5	2.8	2.6	2.6	2.6	2.6	3.0	3.9	3.2	3.2	3.0	3.0	2.5	2.5	3.2	3.2	3.0	3.0	3.0	3.0	3.0	2.9	2.9	2.6	1.5	3.0					
Mg <sup>e</sup>	31.9	22.0	21.1	26.3	21.1	26.3	22.0	22.0	22.1	27.1	27.1	22.0	22.0	22.0	22.0	19.1	19.1	19.6	19.6	19.6	12.9	13.4	13.4	13.4	20.3	18.9	42.9					
Alkali <sup>f</sup>	4.0	4.5	4.2	5.5	4.2	5.5	4.1	4.1	5.1	5.0	5.0	4.1	4.1	4.4	4.4	5.1	5.1	5.0	5.0	5.0	5.5	5.5	5.5	5.5	6.0	4.4	6.9					

<sup>a</sup>All Fe is expressed as FeO. <sup>b</sup>Cl was analysed using SEM-WDS with a cryostage. <sup>c</sup>H<sub>2</sub>O contents deduced from totals. <sup>d</sup>Ferro = TiO<sub>2</sub> + FeO + MgO + MnO. <sup>e</sup>Mg# = 100 \* Mg / (Mg + Fe<sup>2+</sup> + Fe<sup>3+</sup>). <sup>f</sup>Alkali = Na<sub>2</sub>O + K<sub>2</sub>O. SM-starting material standard deviation. Precipitate – precipitate from fluid phase. HP-type Archaean TTG-High-pressure (> 1.8 GPa) type Archaean Tonalite-Trondhjemite-Granodiorite global average composition from Moyen (2011).

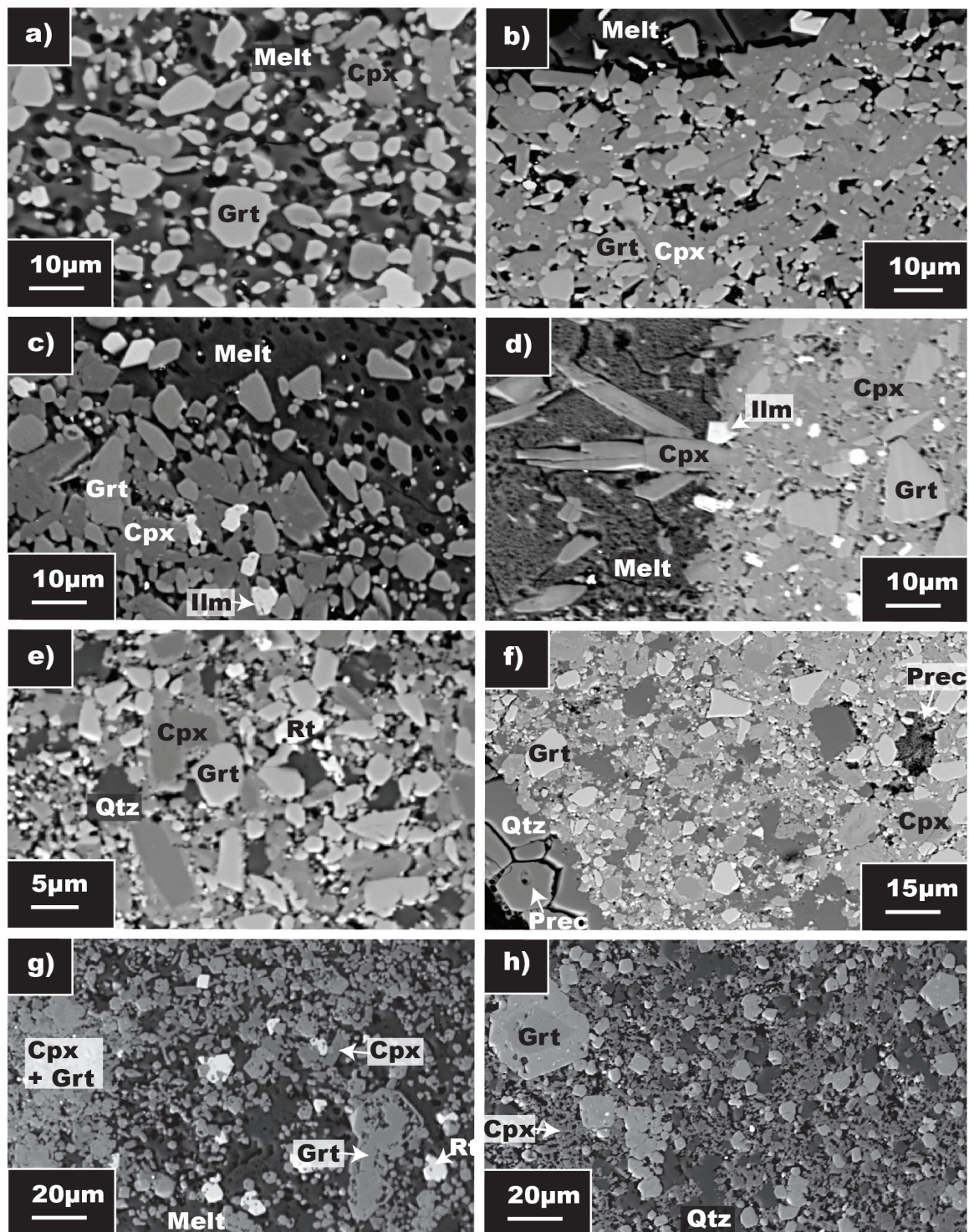


**Fig. 3:** Back scatter electron (BSE) images of experimental run products. a)-d) Representative partially melted run products from the DSE4 experimental runs. The mineral assemblages consist of Grt + Cpx + Rt/Ilm + Melt  $\pm$  Amph. Typical partial melting textures, where melt is interstitial and significant crystal growth is evident from faceted crystals. Melt-crystal segregation textures, with crystal rich domain formed in conjunction with melt pools. Crystal-rich domains are dominated by garnet and clinopyroxene. Cpx is characterised by dark relict Na-rich cores surrounded by extensive newly crystallised lighter rims which are irregularly zoned, however mostly the BSE brightest (i.e. most Na-poor) Cpx is in contact with the melt. e-f) Representa-

tive subsolidus run products from the DSE4 experimental runs. The mineral assemblage consists of Grt + Cpx + Rt/Ilm + Qtz  $\pm$  Amph  $\pm$  Pl. f) Subsolidus run product (2.2 GPa and 800 °C) illustrating the textures that result from quartz remobilisation, as well as those formed by an amorphous precipitate from the fluid phase (which can be confused with quenched melt). g) The gel 2.2 GPa and 800 °C experimental run product which has partially melted. Garnet, clinopyroxene and rutile coexist with melt. h) The synthetic eclogite 2.2 GPa and 800°C experimental run product which has not partially melted. The mineral assemblage consists of Grt + Cpx + Rt + Qtz.

from irregular grain boundaries of the crushed garnet of the starting material. The new garnet growth is more difficult to visualise in BSE images than the clinopyroxene, because in most experiments it is very similar in composition to the garnet of the starting material. Quartz remobilisation has occurred in several subsolidus runs and large blocky quartz crystals have grown which coexist with a precipitate (as described in section 3.1) which has a spongy texture as a consequence of abundant small vesicles. The 2.2 GPa and 800 °C experimental run product, which can be compared to the synthetic eclogite and gel 800 °C and 2.2 GPa run products, has the following phase proportions: (~ 40 %) Cpx + (~ 46 %) Grt + (~ 11 %) Qtz + (~ 2 %) Rt + (~ 1 %) Ap.

In all experiments above the solidus, quartz was completely consumed and garnet and clinopyroxene were the dominant minerals that coexisted with melt (Fig. 3). Laurie and Stevens (2012a) present a detailed analysis of the major and trace element compositions of the melts produced between 1.9 and 3.0 GPa. The clinopyroxene produced by the partial melting reaction is less sodic (0.8-1.7 wt.%  $\text{Na}_2\text{O}$ ) and aluminous and more calcic and MgO-rich compared with the clinopyroxene in the subsolidus run products and the starting material. Small remnant cores of unreacted clinopyroxene (6.3 wt.%  $\text{Na}_2\text{O}$ ) make up a small proportion of the run products. In areas where melt pooled, small euhedral crystals of clinopyroxene appear within the experimental glass (Fig. 3). Euhedral facets of new garnet are formed on the crushed garnet crystals of the starting material. The Mg# of the new garnet increases with increasing pressure and temperature of the experimental runs. Additionally, small euhedral garnet crystals have formed within the experimental glass. Rutile was the stable titaniferous phase above 1.9 GPa. Where ilmenite was stable, small relict rutile cores were observed in a small fraction of the ilmenite crystals. Amphibole is a minor new phase in the 1.9 GPa and 750 °C run product. The 1.9 GPa and 870 °C experimental run product, which can be compared with the synthetic eclogite run product at the same conditions, has the following phase proportions: (~ 35 %) Cpx + (~ 41 %) Grt + (~ 19 %) Melt + (~ 2 %) Rt.

The experimental glasses have the compositions of leucocratic trondhjemites (1.4–2.6  $\text{Na}_2\text{O}$ : CaO;

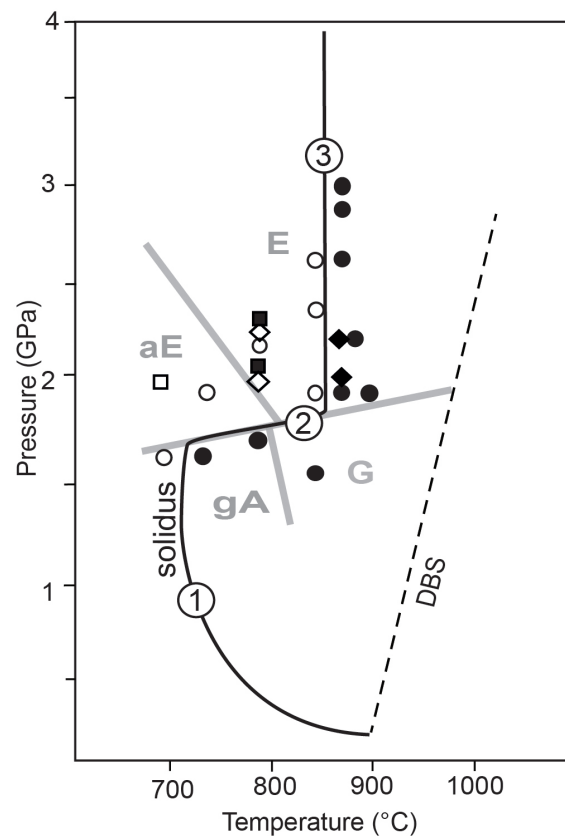


**Fig. 4:** A  $P$ - $T$  diagram which illustrates the experimental results and conditions of this study. The filled symbols represent experiments that underwent water-present partial melting and the open symbols represent experiments which did not. Circles represent experimental runs using the natural eclogite as the starting material (DSE4), diamonds represent experimental runs using the synthetic eclogite (SE-1) as the starting material, and squares represent experimental runs using the gel (B-gel) as the starting material. The low- $K_2O$  water-present metabasaltic solidus (thick black curve) consists of three portions (1, 2 and 3) which characterised by two different solidus reactions. In the simplest form these are: (1)  $\text{Pl} + \text{Qtz} + \text{H}_2\text{O} = \text{Melt}$ ; (2 and 3)  $\text{Omp} + \text{Qtz} + \text{H}_2\text{O} = \text{Melt} + \text{Cpx}$ . The high-pressure portion of the water-present metabasaltic solidus (2 and 3) has been redefined by this study. The low pressure portion of the water-present metabasaltic solidus (1) represents the haplo-tonalitic solidus ( $\text{an} = \sim 50$ ) (Johannes and Holtz 1996). The newly defined solidus is characterised by an inflection of  $\sim 100$  °C towards higher temperatures near the plagioclase-out curve (2) of the modelled metamorphic facies boundaries (thick grey lines) as calculated by Laurie *et al.* (2012b) for the DSE4 composition. Metamorphic facies: E-Eclogite, A-Amphibolite, G-Granulite. Mineral abbreviations: a-amphibole, g-garnet.

74.4–75.9 wt.%  $\text{SiO}_2$ ;  $\text{MgO} + \text{FeO} + \text{TiO}_2 + \text{MnO} < 3.3$  wt.%(Table 5). The glasses produced at lower pressures are progressively more calcic (Fig. 5). They

have very low  $K_2O$  (0.1–0.2 wt.%  $K_2O$ ) and  $MgO$  contents (0.2–0.5 wt.%  $MgO$ ) which reflects the composition of the starting material, which has a very low  $K_2O$  content (< 0.1 wt.%) and  $Mg\#$  ( $Mg\# = 38.5$ ). The water content in the experimental glass, as estimated from the wt.% total of the EDS analyses, increases with pressure from 9.7 wt.%  $H_2O$  at 1.5 GPa and 850 °C, to 19.9 wt.%  $H_2O$  at 3.0 GPa and 870 °C and is consistent with leucocratic melts at high pressure (Sykes *et al.* 1992). When compared with the amorphous phase precipitated from the fluid, the melt is poorer in silica and incompatible elements such as chlorine and potassium and it is relatively enriched in compatible elements such as titanium (Table 5).

The melts plot within the HP-type Archaean TTG field on a  $Na_2O - K_2O - CaO$  diagram (Fig. 5) and have major element chemistry that is within the range of HP-type Archaean TTG rocks (Table 5). Laurie and Stevens (2012a) measured a full spectrum of the trace

and Rare Earth Elements (REE) in the melts produced between 1.9 GPa and 3.0 GPa and demonstrate that the trace and REE geochemistry is also very similar to the compositions of HP-type Archaean TTG.

Results of the experiments using a gel starting material

Two experiments were conducted using a basaltic gel starting material (B-gel) between 2.0 GPa and 2.2 GPa and 800 °C. Both the experiments at 800 °C (2.0 GPa and 2.2 GPa) underwent partial melting (Fig. 4).

At 2.0 GPa and 2.2 GPa and 800 °C the mineral assemblages consisted of: (~ 34-35 %) Cpx + (~ 42-43 %) Grt + (~ 20 %) Melt + (~ 2 %) Rt (Fig. 3g). Garnet and clinopyroxene were the dominant minerals coexisting with melt and in both run products quartz was consumed. The clinopyroxene produced during the experimental runs forms small euhedral elongated

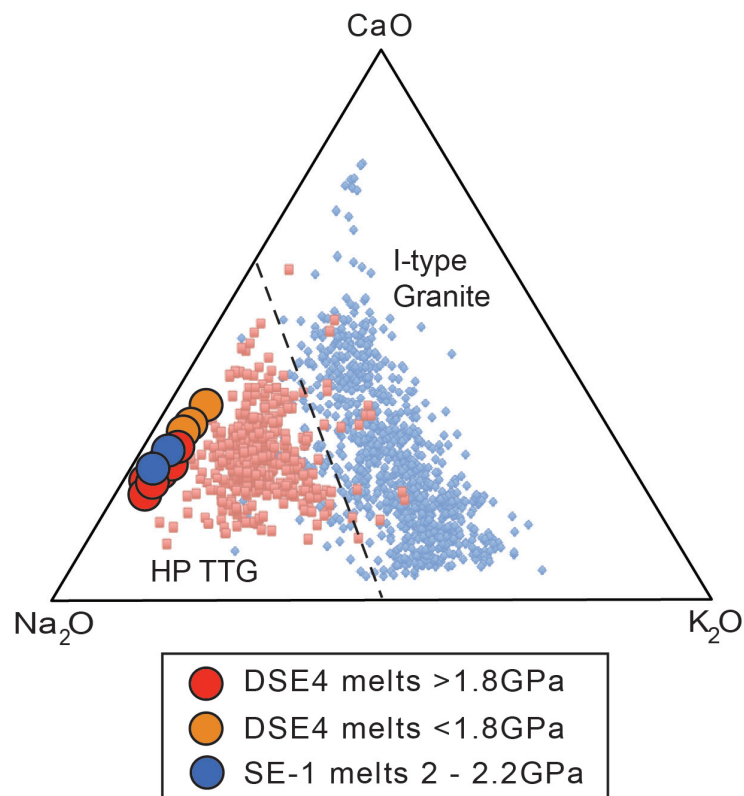


**Fig. 5:**  $Na_2O-K_2O-CaO$  ternary geochemical diagram representing the experimental melt compositions from the experiments using the natural eclogite (DSE4) and synthetic eclogite (SE-1) starting materials at 1.5 GPa to 1.8 GPa and 750 °C to 850 °C; and 1.9 GPa to 3.0 GPa and 870 °C to 900 °C. The experimental melts fall within the field of sodic

high-pressure (HP)-type Archaean Tonalite-Trondhjemite-Granodiorite (TTG) (Moyen 2011). The field of calc-alkaline I-type granitoids which characterise post-Archaean arc-related continental growth products is indicated for comparison.

crystals which have 1.3-1.9 wt.% Na<sub>2</sub>O and 3.1-3.6 wt.% Al<sub>2</sub>O<sub>3</sub>. In areas of abundant melt, small euhedral crystals of clinopyroxene appear within the experimental glass (quenched melt). New garnet forms around large garnet seeds and forms small euhedral garnet crystals within the melt. The garnet is almandine-rich (56-57 % alm, 13 % pyr, 32 % grs). Occasionally several very small garnet crystals appear to have merged to grow much larger garnet crystals.

The experimental glasses have the compositions of leucocratic trondhjemites (1.7-1.9 Na<sub>2</sub>O: CaO) (76.3-76.7 wt.% SiO<sub>2</sub>; 2.5-3.0 wt. % MgO + FeO + TiO<sub>2</sub> + MnO) (Table 5). They have very low K<sub>2</sub>O (0.1-0.2 wt.% K<sub>2</sub>O) and MgO contents (0.3-0.4 wt.% MgO). The water content in the experimental glass, as estimated from the pre-normalisation wt.% total of the analyses, is ± 16 wt.% H<sub>2</sub>O.

Results of experiments using a synthetic eclogite starting material

Four experiments were conducted using synthetic eclogite starting material (SE-1) at 2.0 GPa and 2.2 GPa at 800 °C; and at 1.9 GPa and 2.2 GPa at 870 °C. Neither of the lower temperature runs melted whilst both of the experiments at 870 °C did melt (Fig. 4).

At 2.0 GPa and 2.2 GPa and 800 °C the mineral assemblages consisted of: (~ 33-34 %) Cpx + (~ 50-51 %) Grt + (~ 14 %) Qtz + (~ 2 %) Rt. New almandine-rich garnet (± 58 % alm, 10-11 % prp and 32-33 % grs) crystallises around larger garnet seed crystals or forms small euhedral crystals (Fig. 3h). The clinopyroxene is omphacitic (4.5-4.6 wt.% Na<sub>2</sub>O and 7.6 wt.% Al<sub>2</sub>O<sub>3</sub>) and forms small elongated euhedral crystals.

At 1.9 GPa and 2.2 GPa and 870 °C the mineral assemblages consisted of: (~ 29-30 %) Cpx + (~ 45-46 %) Grt + (~ 23-24 %) Melt + (~ 2 %) Rt. Garnet and clinopyroxene were the dominant minerals coexisting with melt and in both run products quartz was consumed. The clinopyroxene produced during the experimental runs is less sodic (2.1-2.3 wt.% Na<sub>2</sub>O) and aluminous (4.6-4.7 wt.% Al<sub>2</sub>O<sub>3</sub>), and more Ca- and Mg- rich compared with the clinopyroxene in the subsolidus run products. New garnet forms around large garnet seeds and also around garnet which persists from the subsolidus preconditioning run; and

small euhedral garnet crystals grew within the melt. The garnet is almandine-rich (59-60 % alm, 10-11 % pyr, 31 % grs) and the Mg number is higher than that of the garnet in the subsolidus runs.

The experimental glasses have the compositions of leucocratic trondhjemites (1.9-2.0 Na<sub>2</sub>O: CaO) (75.3-76.2 wt.% SiO<sub>2</sub>; 3.2-3.9 wt. % MgO + FeO + TiO<sub>2</sub> + MnO) (Table 5)(Fig. 5). They have similar very low K<sub>2</sub>O (0.1 wt.% K<sub>2</sub>O) and MgO contents (0.3-0.5 wt.% MgO) to the glasses produced by the eclogite melting experiments. The water content in the experimental glass as estimated from the pre-normalisation wt.% total of the analyses is ± 17 wt.% H<sub>2</sub>O.

## Discussion

The experimental results necessitate a discussion on the implications for using different starting materials at eclogite facies conditions within a low-K<sub>2</sub>O mafic system. The behaviour of natural eclogite, gel and synthetic eclogite starting materials at eclogite conditions are consequently discussed.

Comparison of experimental results produced using gel and crystalline starting materials at ± 2.1 GPa

At eclogite pressures (>1.8 GPa), the water present solidus is encountered at different temperatures for the crystalline and gel starting materials. Both the synthetic and natural eclogite assemblages undergo partial melting at approximately 100 °C higher temperature than the onset of melting for the experiments using the gel starting material.

The temperature at which gel experiments begin to partially melt at ± 2.1 GPa is consistent with the temperature of melting in the well-defined haplotonalitic system (Qtz + Pl + H<sub>2</sub>O), where the solidus between 1.0 GPa and 1.8 GPa lies between 690 °C and 750 °C (Johannes and Holtz 1996), depending on the composition of the plagioclase (solidus portion 1 in Fig. 4) (Johannes 1985). At 1.6 GPa, partial melting in DSE4 also occurred within the 700 to 750 °C temperature interval which is consistent with the haplotonalitic wet solidus. The fact that both crystalline eclogite assemblages melted at a significantly higher

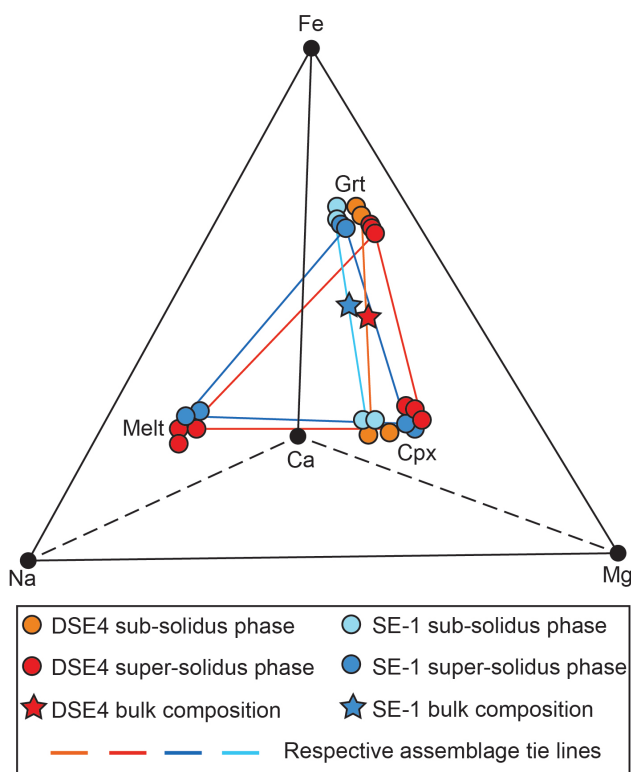


**Fig. 6:** Na-Ca-Mg-Fe tetrahedron geochemical diagram comparing experimental run products. The diagram compares the compositions of the phases within the sub-solidus and super-solidus experimental run product assemblages for experiments conducted using the natural eclogite (DSE4) and synthetic eclogite (SE-1) starting materials at 1.9 GPa to 2.2 GPa and 800 °C to 900 °C.

temperature than the gel above the plagioclase-out pressure, and the fact that the gel melted at temperatures consistent with the metastable extension of the hapltonalitic solidus, suggest that the gel starting material melted metastably.

Comparison of experimental results produced using crystalline starting materials at  $\pm 2.1$  GPa

The results of the synthetic eclogite experiments are compared to natural eclogite experiments which were conducted at similar conditions ( $\pm 2.0$  GPa and 800 °C; and  $\pm 2.0$  GPa and 870 °C). The bulk compositional difference between the two starting materials, as discussed in section 2.1., is reflected in the garnet compositions and can be visualised in Fig. 6. In both cases, at subsolidus conditions (800 °C) the experi-

mental run products consist of almandine-rich garnet, omphacitic pyroxene, rutile and quartz. The garnet produced using the synthetic eclogite starting material is slightly lower in MgO, and higher in CaO compared to the garnet produced using the natural eclogite starting material. Experiments using both starting materials encounter partial melting at 870 °C; and, at 870 °C the experimental run products consist of almandine-rich garnet, less sodic pyroxene, rutile and melt. At supersolidus conditions experiments using both starting materials produce clinopyroxene with a lower sodium and aluminium content in response to the production of leucocratic and sodic trondhjemitic melt, and produce garnet with a higher Mg number compared to their respective subsolidus compositions. The melting reaction for both starting materials at  $\pm 2.0$  GPa is characterised by the breakdown of the jadeite molecule in the clinopyroxene, together with quartz and water, to form melt in conjunction with a less sodic clinopyroxene. The experimental melt compositions have very similar major element, trace element and REE compositions to HP-type Archaean TTG (Table 5; Laurie and Stevens 2012a).

### Interpretation

Two different approaches have been followed in attempting to constrain this eclogite-facies portion of the low- $K_2O$  metabasaltic solidus. Experiments which used gel starting materials produce melt at lower temperatures than crystalline starting materials, provided that the pressure is above the plagioclase stability field, which is above 1.8 GPa for the composition used in this study. This study suggests that this may occur due to metastable melting being encountered when the temperature of the metastable extension of the  $Qtz + Pl + H_2O = Melt$  reaction is exceeded at a pressure above that of plagioclase stability. Therefore, we propose that at pressures above the plagioclase-out reaction, it does not appear possible to accurately constrain the position of the low- $K_2O$  water-present solidus using a gel-bearing starting material. This study predicts that plagioclase-bearing and glass starting materials would be similarly inappropriate and will behave similar to gel starting materials. Plagioclase-bearing starting materials may be

even more likely than gel starting materials to melt metastably due to the difficulty of converting plagioclase into omphacite more quickly than the melting reaction can proceed.

The results of this study demonstrate that the water-present solidus for low-K<sub>2</sub>O metabasaltic rocks above plagioclase stability is best defined using the crystalline eclogite starting materials. In such experiments the melting reaction is characterised by the breakdown of sodic pyroxene together with quartz and water to produce a trondhjemitic melt and less sodic clinopyroxene:  $Qtz + H_2O + Cpx_1 \pm Grt_1 = Melt + Cpx_2 \pm Grt_2$  and the solidus is located at a temperature between 850 °C and 870 °C (solidus portion 3 in Fig. 4). Kessel *et al.* (2005) determined the low-K<sub>2</sub>O metabasaltic wet solidus at 4.0 GPa to lie between 850 °C and 900 °C using an eclogite with 13-15 wt.% water added. This is consistent with the results of this study. Thus, the study of Kessel *et al.* (2005) is useful in extrapolating the findings of this work towards the 2nd critical endpoint, which is the point where silicate melt and aqueous fluid converge in composition and become indistinguishable from each other. This is located between 5.0 GPa and 6.0 GPa and 1000 °C and 1050 °C within the low-K<sub>2</sub>O basaltic system (Kessel *et al.* 2005).

The change in melting behaviour for water-saturated metamafic rocks due to plagioclase leaving the subsolidus assemblage, causes the solidus temperature to increase by approximately 100 °C. Thus, the solidus is defined by three distinctly different portions (Fig. 4). At pressures below 1.4 GPa, melting occurs via the simplified reaction  $Qtz + Pl + H_2O = Melt$  (portion 1 of Fig. 4) and the solidus is steep in *P-T* space. At pressures above 1.8 GPa, the melting reaction is displaced to significantly higher temperature (section 3 on Fig. 4) and becomes  $Qtz + H_2O + Cpx_1 \pm Grt_1 = Melt + Cpx_2 \pm Grt_2$ . This reaction is also steep. The two steep sections of the solidus are linked by a relatively flat portion (solidus portion 2 on Fig. 4) corresponding to the position of the plagioclase-out curve (Fig. 4). Within this pressure sensitive region of the solidus, melting on decompression reflects melting in response to clinopyroxene breakdown below the jadeite-albite transition (Helgeson *et al.* 1978).

## Implications

The eclogite-facies low-K<sub>2</sub>O water-present metabasaltic solidus defined in this study is useful in understanding the shift in continental growth products from Na-rich and TTG crust to more Ca-rich arc related calc-alkaline granitoids which occurred toward the end of the Archaean Eon. The pressure-temperature (*P-T*) paths followed by the upper portions of likely Archaean slabs were modelled by Laurie *et al.* (2012b) and they have a similar shape to the solidus defined in this study (Fig. 7a). Consequently, crust will follow a *P-T* path parallel to the solidus at subsolidus temperatures until reaching the mantle wedge tip. The temperature of the mantle wedge, in combination with potential shear heating, determines the temperature towards which the upper portions of the subducted crust will equilibrate (Laurie *et al.* 2012b). During the Archaean, the mantle wedge was sufficiently hot to heat the upper portion of basaltic slab, which are at eclogite-facies conditions, to temperatures above this water-present solidus. The slab was characterised by strong temperature gradients in the upper portions of the slab and the upper most hot anhydrous portions were underlain by cooler hydrated portions which release fluids during prograde metamorphism (Laurie *et al.* 2012b). These metamorphic fluids will rise buoyantly and interact with the upper eclogite portions of the slab which are above their water-present melting temperature. This will trigger water-present melting of the slab to produce HP-type trondhjemitic melts which may have characterised the Archaean felsic continental crust (Fig. 7a).

Throughout the Archaean Eon, mantle wedge temperatures gradually decreased (e.g. Albarède 1998; Prelevic and Foley 2007) and during the late Archaean the mantle had cooled sufficiently so that heating of the upper slab to above solidus temperatures became uncommon (Fig. 7b). Once the upper surface of subducting slabs were at a temperature below the water-saturated solidus, the upper portions of the slabs could no longer function as capture sites for the metamorphic water developed from deeper layers within the slab, thereby allowing interaction between slab water and the mantle wedge. From this point in Earth's evolution onwards, slab melting became a



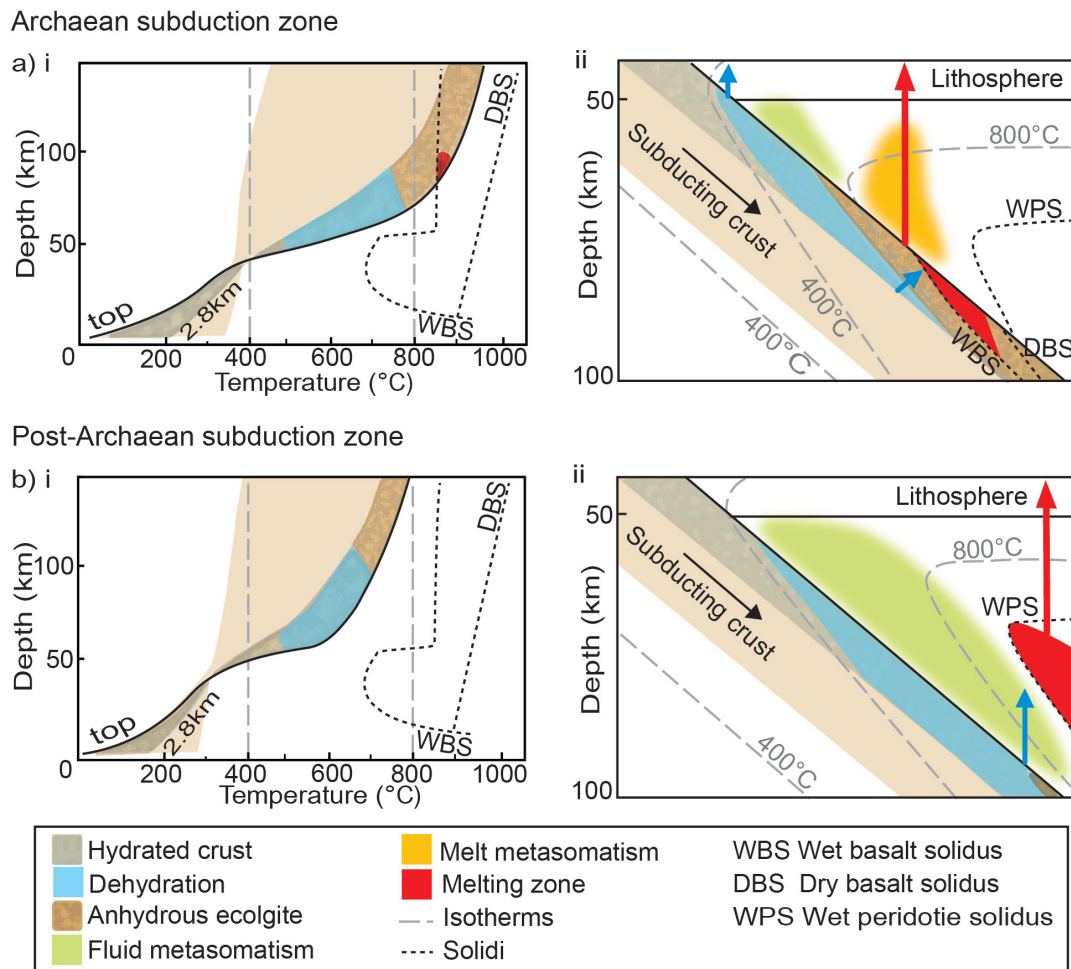


**Fig. 7:** Comparison of Archaean and present-day subduction scenarios. a) Modelled young (5 Myr) and fast (10 cm/yr) subducting slab within a proposed Archaean subduction zone defined by a 1650  $^{\circ}\text{C}$  mantle (Laurie *et al.* 2012b). b) Modelled young (5 Myr) and fast (10 cm/yr) subducting slab within a proposed present-day mantle conditions (1350  $^{\circ}\text{C}$  mantle) (Laurie *et al.* 2012b). i) The  $P$ - $T$  paths followed by the slab surface and the slab at 2.8 km below the slab surface for a) and b). ii) The thermal structure model of the subduction zone for a) and b). Both the  $P$ - $T$  paths of the upper slab and the water-present low- $K_2O$  (<0.1 wt.%  $K_2O$ ) metabasaltic solidus (WBS) have a shape which inflects to higher temperatures. During the Archaean, after progression of the slab past the wedge tip the slab is heated by the mantle and the temperature of the upper slab subsequently increases rapidly. The cooler portions of the

slab undergo dehydration and buoyantly rise and interact with the eclogitised upper portions of the slab which are by now above the low- $K_2O$  water-present metabasaltic solidus which produces high-pressure (HP)-type Archaean Tonalite-Trondhjemite-Granodiorite (TTG) which characterise Archaean felsic continental crust. In the present-day-mantle scenario  $P$ - $T$  paths of the slab are consequently cooler and the slab does not reach temperatures sufficient for water-present. The horizontal black line represents the mechanical bottom of the overriding plate. WBS- Wet basalt solidus within plagioclase stability limits represents the haplotonalitic solidus ( $an = \sim 50$ ) (Johannes and Holtz 1996) and at pressures above plagioclase stability, the wet (fluid-present) low- $K_2O$  metabasaltic solidus is from this study. DBS-Dry (fluid-absent) basalt solidus (Green 1982). WPS-Wet peridotite solidus (Wyllie 1979).

rare event and this resulted in a change in the type of granitoid magmas which are associated with arcs from TTG granitoids to the calc-alkaline I-type granitoids.

**Acknowledgements** This research was supported by NRF funding to GS as part of the SARChI program. J.D. Clemens provided the DSE4 starting material. J-F. Moyen provided the TTG database.

## References

- Albarède F (1998) The growth of continental crust. *Tectonophysics*, 196:1-14
- Clemens JD, Stevens G, Farina F (2011) The enigmatic sources of I-type granites: The peritectic connexion. *Lithos* 126(3-4):174-181, 14
- Condie KC (1981) *Archaean Greenstone Belts*. Elsevier, Amsterdam, pp 434
- Diener J, Stevens G, Kisters AFM, Poujol M (2005) Metamorphism and exhumation of the basal parts of the Barberton greenstone belt, South Africa: constraining the rates of mid-Archaean tectonism. *Precamb. Res.* 143:87–112
- Droop GTR (1987) A general equation for estimating the Fe<sup>3+</sup> concentration in ferromagnesian silicates and oxides from microprobe analysis, using stoichiometric criteria. *Min. Mag.* 51:431–435
- Drummond MS, Defant MJ (1990) A model from trondhjemitonalite-dacite genesis and crustal growth via slab melting: Archean to modern comparisons. *J. Geophys. Res.* 95:21503-21521
- Foley SF, Tiepolo M, Vannucci R (2002) Growth of early continental crust controlled by melting of amphibolite in subduction zones. *Nature* 417:837-840
- Gill JB (1981) *Orogenic Andesites and Plate Tectonics*. Springer-Verlag, Berlin, pp. 390
- Green TH (1982) Anatexis of mafic crust and high pressure crystallisation of andesite, in *Andesites*, edited by R. Thorpe, pp. 465-486, J. Wiley and sons, New-York, 1982
- Grove TL, Chatterjee N, Parman SW, Médard E (2006) The influence of H<sub>2</sub>O on mantle wedge melting. *Earth and Planetary Science Letters* 249:74–89
- Hamilton DL, Henderson CMB (1968) The Preparation of Silicate Compositions by a Gelling Method. *Mineralogical Magazine Miner. Mag.* 36(282):832-838. DOI: 10.1180/minmag.1968.036.282.11
- Harlow GE, Veblen DR (1991) Potassium in clinopyroxene inclusions from diamonds. *Science* 251(4994):652-5
- Helgeson HC, Delany JM, Nesbitt HW, Bird DK (1978) Summary and critique of the thermodynamic properties of rock-forming minerals. *Amer. J. Sci.* 278
- Hildreth W, Moorbath S (1987) Crustal contributions to arc magmatism in the Andes of Central Chile. *Contrib. Min. Pet.* 98(4):455-489
- Holland T (1989) Dependence of entropy on volume for silicate and oxide minerals: A review and a predictive model. *Am. Min.* 74,:5-13
- Holness MB, Cheadle MJ, McKenzie D (2005) On the use of changes in dihedral angle to decode Late-stage textural evolution in cumulates, *Journal of Petrology* 2005 46(8):1565-1583. doi:10.1093/petrology/egi026
- Jacob D, Foley S (1999) Evidence for Archean ocean crust with low high field strength element signature from diamondiferous eclogite xenoliths. *Lithos* 48:317-336
- Jahn BM, Glikson AY, Peucat JJ, Hickman AH (1981) REE geochemistry and isotopic data of Archean silicic volcanics and granitoids from the Pilbara Block, western Australia: implications for the early crustal evolution. *Geochim. Cosmochim. Acta.* 45:1633–1652
- Johannes W and Holtz J (1996) *Petrogenesis and experimental petrology of granitic rocks*. Minerals and Rocks Series Vol. 22.. Berlin: Springer-Verlag, pp335
- Johannes W (1985) The significance of experimental studies for the formation of migmatites. In ASHWORTJ. HR, ed *Migmatites*. Blackie, Glasgow, pp36-85
- Kessel R, Ulmer P, Pettke T, Schmidt MW, Thompson AB (2005) The water–basalt system at 4 to 6 GPa: Phase relations and second critical endpoint in a K-free eclogite at 700 to 1400°C. *Earth and Planetary Science Letters* 237:873-892
- Kretz (1983) Symbols for rock-forming minerals. *Am. Min.* 68:277-279
- Laurie A, Stevens G (2012) Water-present eclogite melting to produce Earth's early felsic crust. *Chem. Geol.* 314-317:83-95
- Laurie A, Stevens G, van Hunen J (in press) The end of continental growth by TTG magmatism. *Terra Nova*
- Martin H (1987) Petrogenesis of Archean trondhjemitites, tonalites and granodiorites from eastern Finland; major and trace element geochemistry. *J. Petrol.* 28(5):921-953
- Martin H (1994) The Archean grey gneisses and the genesis of the continental crust in Archean crustal evolution, in: *Condie, K. C. (Eds.), Elsevier, Amsterdam,*

- pp.205-259
- Martin H, Moyen J-F (2002) Secular changes in TTG composition as markers of the progressive cooling of the Earth. *Geology* 30(4):319-322
- McCandless TE, Gurney JJ (1989) Sodium in garnet and potassium in clinopyroxene; criteria for classifying mantle eclogites. in: Ross, J., Jaques, A.L., Ferguson, J., Green, D.H., O'Reilly, S.Y., Danchin, R.V., Janse, A.J.A. (Eds.), *Kimberlites and Related Rocks*. Special Publication—Geological Society of Australia, Perth vol. 14, pp. 827–832
- Miller JF, Harris NBW (1989) Evolution of continental crust in the Central Andes; constraints from Nd isotope systematics. *Geology* 17(7):615-617
- Moyen J-F (2011) The composite Archaean grey gneisses: petrological significance, and evidence for a non-unique tectonic setting for Archaean crustal growth. *Lithos* 123:21-36
- Moyen J-F, Stevens G (2006) Experimental constraints on TTG petrogenesis: Implications for Archean geodynamics, in: Benn, K., *et al.*, (Eds.), *Archean geodynamics and environments*. American Geophysical Union Geophysical Monograph 164:149–175
- Mysen BO, Wheeler K (2000) Solubility behaviour of water in haploandesitic melts at high pressure and high temperature. *Am. Min.* 85(9):1128-1142
- Nichols GT, Wyllie PJ, Stern CR (1994) Subduction zone melting of pelagic sediments constrained by melting experiments. *Nature* 371:785–788
- Prelevic D, Foley SF (2007) Accretion of arc-oceanic lithospheric mantle in the Mediterranean: Evidence from extremely high-Mg olivines and Cr-rich spinel inclusions in lamproites. *Earth and Planetary Sci. Lett.* 256(1-2):120-135
- Rapp RP, Shimizu N, Norman MD (2003) Growth of early continental crust by partial melting of eclogite. *Nature* 425:605-609
- Rudnick RL (1995) Making continental crust. *Nature* 378:571-578
- Schilling F, Wunder B (2004) Temperature distribution in piston-cylinder assemblies: Numerical simulations and laboratory experiments. *Eur. J. Mineral.* 16:7-14
- Schmidt MW, Dardon A, Chazot G, Vannucci R (2004) The dependence of Nb and Ta rutile-melt partitioning on melt composition and Nb/Ta fractionation during subduction processes. *Earth. Plan. Sci. Lett.* 226:415-432
- Smithies RH, Champion DC (2000) The Archaean high-Mg diorite suite: links to tonalite–trondhjemite–granodiorite magmatism and implications for early Archaean crustal growth. *J. Petrol.* 41:1653–1671
- Spicer EM, Stevens G, Buick I (2004) The low-pressure partial melting behaviour of natural boron-bearing metapelites from the Mt. Stafford area, central Australia. *Contrib. Mineral. Petrol.* 148:160-179
- Stevens G, Clemens JD (1993) Fluid absent melting and the roles of fluids in the lithosphere: A slanted summary? *Chem. Geol.* 108: 1-17
- Sykes D, Sato R, Luth RW, Milln P, Poet B (1992) Water solubility mechanisms in  $KAlSi_3O_8$  melts at high pressure. *Geochim. Cosmochim. Acta.* 57:3575-3584
- Vielzeuf D, Clemens JD (1992) Fluid-absent melting of phlogopite + quartz: experiments and models. *Am. Min.* 77:1206–1222
- Winter JD (2001) *An Introduction to Igneous and Metamorphic Petrology* In: Lynch, Patrick (Ed.), pp 248
- Wyllie PJ (1979) *Magma and volatile components*. *Am. Min.* 65:469-500
-

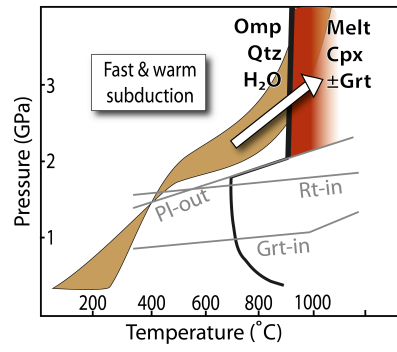
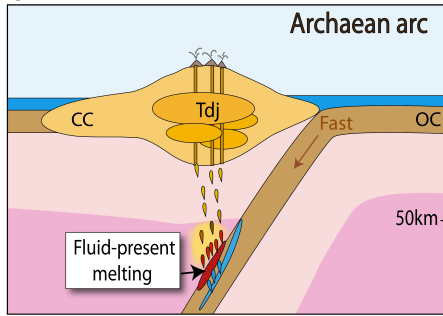
## CHAPTER 5

### Conclusions

This study has experimentally investigated the petrogenesis of high pressure (HP)-type Paleo- to Meso-Archaean tonalite, trondhjemite and granodiorite granitoids by the fluid-present partial melting of a low-K<sub>2</sub>O eclogite-facies metabasaltic source between 1.6 and 3.0 GPa, and 700 and 900 °C.

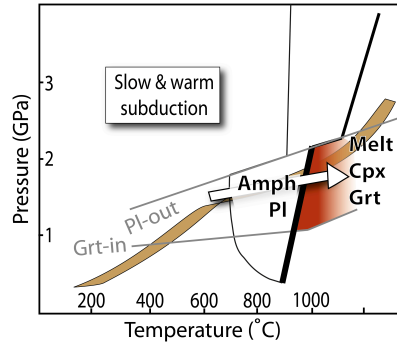
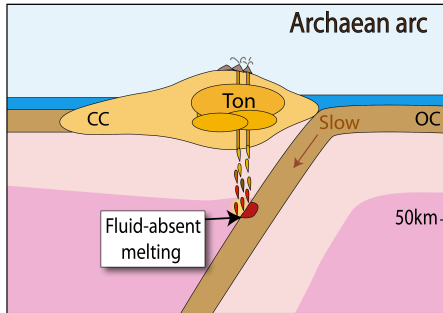
This study has accepted the popular notion of active plate tectonics during the Archaean, although it must be stated that the very existence of plate tectonics during the Archaean, particularly during the Paleo- to Meso-Archaean, remains a matter of debate (e.g. Bédard, 2006). Various tectonic scenarios for the genesis of the various types of TTG granitoids are proposed in Fig. 1. However, unlike the multiple plate-tectonic and non-plate-tectonic geodynamic scenarios that can be suggested for the formation of medium pressure (MP)- and low pressure (LP)-type TTG granitoids (Moyen, 2011) (Fig. 1), the requirements for the genesis of HP-type TTG are very difficult to be met without the existence of plate tectonics (Fig. 1). A subduction zone with specifically fast subducting crust is the only geodynamic scenario that can, firstly, enable the crust to remain cool enough for the transformation to eclogite-facies within a hotter Archaean Earth without undergoing partial melting at shallower depths. Secondly, a subduction zone enables fluid supply to the anatexis zone as sourced from underlying dehydrating crust. This is necessary for eclogite melting to occur within attainable temperatures. Lastly, the geochronology of Archaean HP-type trondhjemitic plutons indicate a protracted emplacement and accumulation history (e.g. the Meso-Archaean Badplaas trondhjemites, within the Barberton granitoid-greenstone terrain in South Africa,

A) High Pressure TTG

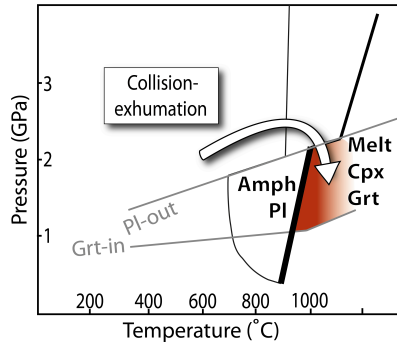
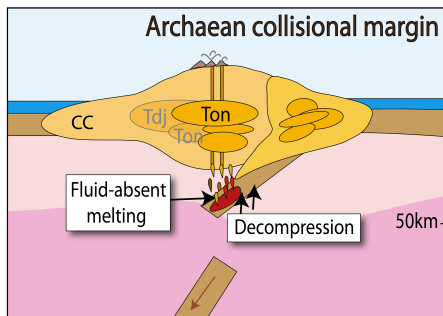


B) Medium Pressure TTG

1)

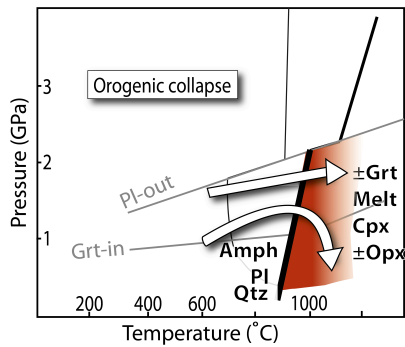
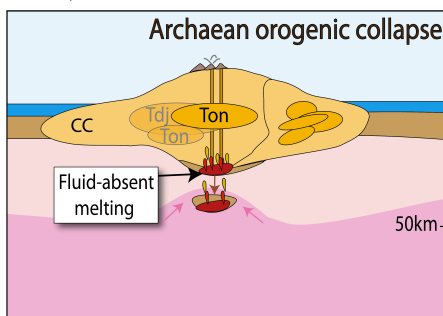


2)



C) Medium/Low Pressure TTG

1)



D) Low Pressure TTG

1)

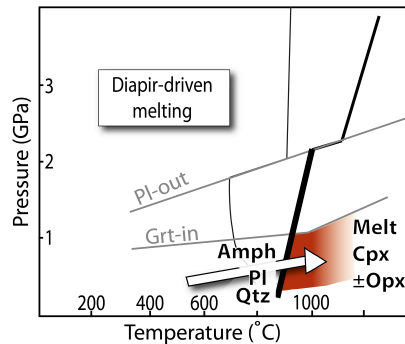
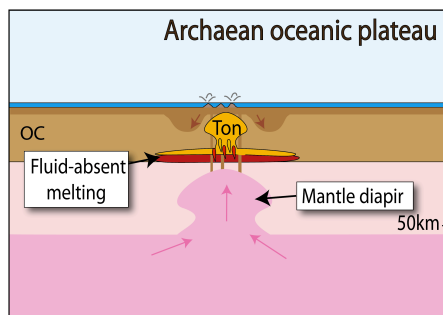


**Fig. 1:** Schematic diagrams depicting proposed geodynamic scenarios for the formation of high, medium and low-pressure TTG granitoids during the Archaean and  $P$ - $T$  diagrams indicating the  $P$ - $T$  evolution of the metamafic source rock during the corresponding geodynamic scenario. The wet solidus of amphibolites from experimental petrology and the stability limits of garnet, plagioclase and rutile in mafic compositions (Moyen and Stevens, 2006) are indicated. The red shaded regions correspond to the multivariant melting reactions that form TTG melts, amphibole breakdown reactions (MP- and LP-type TTG) below the plagioclase stability limit and eclogite breakdown reactions (high pressure type TTG granitoids) above this pressure. A) Illustrates the proposed setting for HP-type TTG, as outlined by this study. B) Illustrates the proposed setting for MP-type TTGs. B1) A young and slow subduction zone. This requires that the lithosphere-mantle decoupling (as discussed in Chapter 3 occur at depths below 50km within the subduction zone. B2) A collisional orogeny. Slab breakoff will result in the decompression-driven melting of the fertile slab. C) Illustrates the proposed setting for MP- or LP-type TTGs during orogenic collapse (Moyen, 2011). D) Illustrates the proposed setting for LP-type TTGs within an intra-plate situation such as the melting of the base of an oceanic plateau (Bédard, 2006).

were emplaced over a 60 Myr period (Kisters *et al.*, 2010)) and fast subduction is the only geodynamic scenario that can provide a rejuvenating configuration where fertile upper eclogite-facies crust and underlying hydrous crust are continually supplied for the duration of subduction.

The nature of the fluid-present low- $K_2O$  eclogite-facies metabasaltic rock solidus has been experimentally defined by this PhD study and lies between 850 and 870 °C between 1.9 and 3.0 GPa. It is characterised by a sharp inflection towards higher temperatures at the position of the plagioclase-out reaction. The results indicate that a crystalline eclogite-facies starting material is necessary to define this solidus to avoid metastable melting beyond temperatures of the  $Pl + H_2O + Qtz$  solidus at pressures above those of plagioclase stability.

Fluid-saturated partial melting of a crystalline low- $K_2O$  eclogite-facies metabasaltic rock between 1.9 and 3.0 GPa and 870 and 900 °C produced trondhjemitic melts by a melting reaction that is characterised by the breakdown of the jadeite molecule in the clinopyroxene, together with quartz and water, to form melt in conjunction with a less sodic clinopyroxene:  $Cpx_1 + Qtz + H_2O \pm Grt_1 = Melt + Cpx_2 \pm Grt_2$ . The experimental melts have major-, trace- and rare-earth-element compositions that are within the range of compositions displayed by

HP-type Archaean trondhjemites. Therefore, melt generation by high-pressure fluid-present melting of an eclogite-facies metabasaltic source appears to be a viable petrogenetic model for the formation of the HP-type TTG. This group of TTG granitoids constitutes an important component of the Paleo- to Meso-Archaean felsic continental crust associated with Archaean grey gneiss complexes.

This study has demonstrated from the results of numerical and metamorphic modelling that for reasonable Archaean mantle wedge temperatures within a hypothetical young and fast Archaean subduction zone, fluid-fluxed anatexis of the upper eclogite-facies basaltic slab may produce HP-type Archaean TTG. The anatectic zone near the slab surface captures water produced by metamorphic reactions within the underlying hydrated portion of the slab. Therefore, this geodynamic model may account for HP-type Archaean TTG production as well as the lack of fluid-fluxed mantle melts (andesite or diorites) being produced concurrently with HP-type Archaean TTG magmatism during the Paleo- and Meso-Archaean Eon (Fig. 2). Additionally, the results of the study provide constraints for likely Archaean subduction.

The geometries of  $P$ - $T$  paths of the upper portions of fast subducting slabs and the relevant low- $K_2O$  fluid-present solidus are similar as they both inflect towards higher temperatures. Therefore cooling of the upper mantle by only a small amount during the late Archaean ended fluid-present melting of the slab. This allowed slab water to migrate into the fluid- and melt-metasomatised wedge, which initially resulted in the formation of mantle enriched melts, such as sanukitoids, and thereafter produced fluid-fluxed mantle melts with dominantly intermediate composition that have since been associated with subduction zones (Fig. 1). This makes fluid-fluxed slab anatexis very dependant on the temperature in the mantle wedge.

Consequently, the wet low- $K_2O$  eclogite solidus has important implications for understanding the shift from TTG to calc-alkaline granitoid compositions that is recorded in several areas during the late Archaean and the existence of peculiar enriched-mantle-melts, such as sanukitoids, which characterise this temporal transition (Fig. 2).

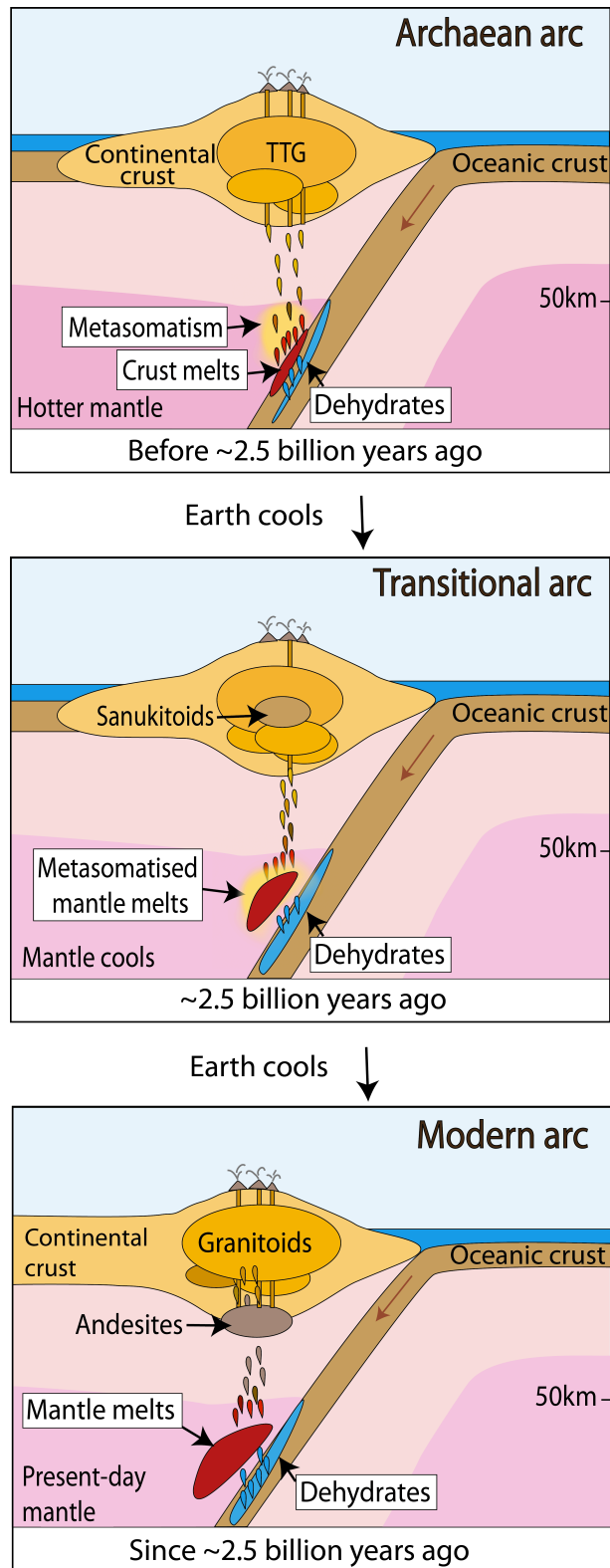


**Fig. 2:** A schematic diagram illustrating the tectonic model proposed by this study. A reasonably small decrease in the temperature of the mantle wedge towards the end of the Archaean, which causes the near-isobaric heating of the slab surface, will induce the abrupt shift away from Archaean TTG magmatism. On cooling of the mantle, slab melting, which formerly acted as a capture mechanism for metamorphic slab fluid, no longer occurred as slabs seldom reached temperatures sufficient for fluid-present melting. For the first time, slab dehydration fluids, which were now produced deeper within the subduction zone, migrated into the mantle wedge. This mantle material had previously been metasomatised by slab melts, which had not managed to traverse the wedge (yellow-shaded area). Interaction of this metasomatised mantle with slab water acted to spawn an initial pulse of fluid-induced melting, which produced enriched mantle melts such as sanukitoids. From this time frame onwards, arc-related magmas are produced by a process that begins with  $H_2O$ -saturated partial melting of peridotite in the mantle wedge that is induced by the ascent of slab derived water-rich fluids or melts. The resultant initially near fluid-saturated mantle melts rise through the mantle wedge, equilibrating with hotter and dryer mantle, to ultimately produce the basalts and andesites that characterise this setting characterized arc settings and arc-related continental growth products.



The results of this study indicate a possible consistency with the existence of Archaean plate tectonics. Furthermore, it may be possible to have generated the various types of TTG magmas within the context of a single uniform tectonic process. This may have occurred by melting different type of sources, or by melting the same source at different  $P$ - $T$  conditions, or by some combination of the two. Several TTG-types may originate within one prolonged geological event. For instance: The emplacement of HP- or MP-type TTG magmas by melting of a young and fast or slow slab, as depicted in Fig. 1A and 1C1, may be followed by the formation and emplacement of MP-type TTG granitoids within a collisional orogeny by slab decompression melting which is a consequence of slab breakoff (Fig. 1B2); furthermore, this may be followed by the formation and emplacement of MP- or LP- type TTGs during orogenic collapse (Fig. 1C), This is consistent with the global Archaean rock record where two or more types of TTG coexist within a particular grey gneiss terrain. Therefore, the potential tectonic model proposed by this study for the genesis of HP-type TTG granitoids is able to account for the spatial coexistence of more than one “type” of TTG found in several Archaean grey gneiss complexes, and it is able to explain a possible mechanism by which the shift in continental growth products from sodic TTG to intermediate compositions occurred towards the end of the Archaean Eon. Thus, the results of this thesis may have implications beyond HP-type TTG genesis, as the thesis makes an important contribution to the state of knowledge on early Earth processes and evolution, in general.

This study has produced various petrogenetic and potential geodynamic findings. The experimental results have provided excellent pressure constraints for the genesis of Archaean trondhjemites. The experimental results have therefore clearly and thoroughly demonstrated that fluid-present partial melting of a low  $K_2O$  metamafic eclogite between 1.9 and 3.0 GPa will produce a melt with nearly identical chemical compositions to Archaean trondhjemites

(HP-type TTG granitoid). The experimental investigation was; however, limited to a single source composition and the results are consequently source dependent. The geodynamic modelling results are dependent on many assumptions as the modeling was based on parameters that are unknown for the Archaean Eon. In spite of this, the modelling presented in this thesis allows the concept of fluid-fluxed eclogite melting within potential Archaean subduction zones to be evaluated and it represents the first study to numerically model a geodynamic scenario for the genesis of HP-type trondhjemite.

In conclusion, this PhD thesis has demonstrated a new viable petrogenetic model and a potential geodynamic model for the production of an important component of Earth's early felsic continental crust.

### **References:**

- Bédard, J., 2006. A catalytic delamination-driven model for coupled genesis of Archaean crust and sub-continental lithospheric mantle. *Geochimica Cosmochimica Acta* 70, 1188–1214.
- Kisters, A.F.M., Belcher, R., Poujol, M. and Dziggel, A., 2010. Continental growth and convergence-related arc plutonism in the Mesoarchaeon: evidence from the Barberton granitoid-greenstone terrain, South Africa. *Precambrian. Res.*, 178, 15-26.
- Moyen, J-F. and Stevens, G., 2006. Experimental constraints on TTG petrogenesis: Implications for Archean geodynamics. In: (Benn, K., et al. eds) *Archean geodynamics and environments*. AGU Geophys. Monogr., 164, 149–175.
- Moyen, J-F., 2011. The composite Archaean grey gneisses: petrological significance, and evidence for a non-unique tectonic setting for Archaean crustal growth. *Lithos*, 123, 21-36.